X-922-77-228

TMX 71395

GEODETIC AND ASTROMETIC MEASUREMENTS WITH VERY-LONG-BASELINE INTERFEROMETRY

DOUGLAS SCOTT ROBERTSON

AUGUST 1975

DEPARTMENT OF
EARTH AND PLANETARY SCIENCES
MASSACHUSETTS
INSTITUTE OF TECHNOLOGY
CAMBRIDGE, MASSACHUSETTS

GODDARD SPACE FLIGHT CENTER
GREENBELT, MARYLAND

X-922-77-228

GEODETIC AND ASTROMETIC MEASUREMENTS WITH VERY-LONG-BASELINE INTERFEROMETRY

DOUGLAS SCOTT ROBERTSON

AUGUST 1975

DEPARTMENT OF
EARTH AND PLANETARY SCIENCES
MASSACHUSETTS
INSTITUTE OF TECHNOLOGY
CAMBRIDGE, MASSACHUSETTS

GSFC

GODDARD SPACE FLIGHT CENTER
GREENBELT, MARYLAND

GEODETIC AND ASTROMETRIC MEASUREMENTS WITH VERY-LONG-BASELINE INTERFEROMETRY

by

Douglas S. Robertson

Submitted to the Department of Earth and Planetary Sciences in August, 1975, in partial fulfillment of the requirements for the degree of Doctor of Philosophy

ABSTRACT

The use of VLBI observations for the estimation of geodetic and astrometric parameters is discussed. Analytic models for the dependence of delay and delay rate on these parameters are developed and used for parameter estimation by the method of weighted least squares.

Results are presented from approximately 15,000 delay and delay-rate observations, obtained in a series of nineteen VLBI experiments involving a total of five stations on two continents. The rms scatter about the weighted mean in the estimates of baseline lengths can be summarized as follows [Haystack (Massachusetts) is the reference station]:

Scatter	Remote Site	Baseline Length	Number of Experiments
7 cm	Green Bank, (W. Va.)	845 km	5
26	Goldstone (California)	3900	16
40	Onsala (Sweden)	5600	8
79	Gilmore Creek (Alaska)	5040	3

GEODETIC AND ASTROMETIC MEASUREMENTS WITH VERY-LONG-BASELINE INTERFEROMETRY

by

Douglas Scott Robertson

B.S.

Principia College

(1968)

SUBMITTED IN PARTIAL FULFILLMENT
OF THE REQUIREMENTS FOR THE
DEGREE OF DOCTOR OF
PHILOSOPHY

at the

Massachusetts Institute of Technology

August 1975

Signature of Author: Douglas Scott Robertson
Department of Earth and Planetary Sciences, August 1975

Certified by: Irwin Shapiro
Thesis Supervisor

Accepted by: _____
Chairman, Departmental Graduate Committee

The station in Alaska had by far the poorest system sensitivity and that in Sweden the next poorest. The corresponding scatter in the source coordinate results is less than 0".1 for all coordinates except the declination of the low-declination sources, which have a scatter of the order of 0".2. The closure of baseline triangles is investigated and found to be consistent with the scatter of the various baseline-component results. Estimates are made of the wobble of the Earth's pole and of the irregularities in the Earth's rotation rate. The differences between our estimates of the pole position and the BIH estimates have a scatter of about 1 m in both the X and Y components, and the corresponding (A1-UT1) differences have a scatter of under 3ms. Estimates are also made of the precession constant and of the vertical Love number, h, for which a value of 0.55±0.05 was obtained.

Thesis Supervisor: Irwin I. Shapiro

Title: Professor of Geophysics and Physics

TABLE OF CONTENTS

FIGURE CAPTIONS

TABLES

ACKNOWLEDGEMENTS

The work reported in this thesis could not have been accomplished without the assistance and support of a large number of people. First, I am indebted to my thesis advisor, Prof. Irwin Shapiro, whose assistance and supervision were vital to every phase of the work reported in this thesis.

In addition, my work has depended upon our entire VLBI Group, not only for designing and operating the hardware required for VLBI observations, but also for writing the computer programs, VLBI1 and VLBI2, which are essential for the data processing. For this effort thanks are due to Dr. Alan E. E. Rogers, Dr. Alan R. Whitney, Dr. Curtis A. Knight, Dr. Hans F. Hinteregger, and Dr. Thomas A. Clark. Also Dr. Charles Counselman and Dr. Robert Reasenberg provided many helpful comments and suggestions concerning the preparation of this thesis. In addition, I would like to thank Dr. Michael E. Ash for his help with the programming of VLBI3.

The experiments reported in this thesis could not have been performed without the assistance of the staff at each station employed, that is, Haystack, Goldstone, NRAO, Onsala and NOAA (Gilmore Creek, Alaska). I would like to thank Drs. W. K. Klemperer and W. W. Warnock, B. O. Rönnäng, O. E. H. Rydbeck, A. E. Niell, D. J. Spitzmesser, L. Skjerve, N. Van-

denberg, G. E. Marandino, and L. K. Hutton.

For the typing of this thesis, I am indebted to Ms. Judith Ungermann.

Much of the work in this thesis was supported by the National Science Foundation, Grant 74-22712EAR.

CHAPTER 1

INTRODUCTION

One of the main themes of astronomical research throughout history has been the desire to construct instruments capable of increasingly finer angular resolution. In the field of radio astronomy this desire has culminated with the development of very-long-baseline interferometry (VLBI). A brief sketch of the history of radio astronomy should help to put this development into perspective.

The science of radio astronomy got its start in the 1930's with the discovery by Karl Jansky of extra-terrestrial radio signals. Jansky, who was then working at the Bell Telephone Laboratories, built a directional radio antenna for the purpose of locating sources of radio interference. This antenna had an angular resolution of about 30°. Even at this level of resolution Jansky was able to recognize that some of the sources of the signals he received were extra-terrestrial, and he was able to identify the newly discovered galactic center as the source of some of the signals.

It was obvious that if much progress were to be made in studying celestial radio sources, it would be necessary to improve the resolving power of the receiver systems. In particular, in order to compare radio observations with optical observations, it would be desirable to have a resolving power in the radio range comparable to optical telescope resolution. Increasing the resolving power of

radio antennas to this level was to prove a difficult task, for the angular resolution in radians of any receiver system is roughly equal to the ratio of the wavelength of the signals received to the diameter of the antenna system. The wavelengths of the radio signals being employed ranged from a few centimeters to several meters, whereas optical wavelengths are typically 5×10^{-7} m. Thus, in order to make a parabolic antenna to receive 3 cm radiation with the same resolving power achieved by a 15 cm diameter optical telescope, the radio antenna would have to be 10 km in diameter. Building such an antenna would be a herculean task, even if the antenna were to be fixed and not steerable. These difficulties were sufficiently obvious to make early researchers in radio astronomy turn to interferometry as the only practical way to achieve resolution performance comparable to that of optical telescopes.

With interferometry, angular resolution is achieved by comparing signals from widely separated antennas. The limiting factor on the resolution is then the distance between the antennas rather than simply the size of any single antenna. These early interferometers needed a real-time communication link to transmit signals from one antenna to the other. Technical problems with the communication link limited the antenna separations to tens of kilometers. The capabilities of these interferometers still provided a dramatic improvement over the capabilities of a single antenna, but it was clear that still better resolution could be attained if the communication

link restriction could be overcome.

The problem of eliminating the communication link was solved with the development of very-long-baseline interferometry (VLBI). With VLBI, the need to transmit signals from one station to the other in real time is bypassed by the use of highly stable atomic clocks at each station. The clocks are used to control the local oscillators which heterodyne the signals down to a frequency which can be sampled and recorded on a standard digital tape recorder system. (The clocks also control the sampling equipment and the tape recorders, but it is in the control of the local oscillators that the frequency stability of the clock is most important.) Thus instead of transmitting the radio signals from one antenna to the other in real time, it is only necessary to transport the tape recordings to a common location at leisure. With this development, the deployment of radio interferometer stations was limited only by the size and shape of the Earth.

There was an added, though not unexpected, bonus which resulted from the development of VLBI. The interferometer observations could be used to estimate the antenna separations as well as the positions of the radio sources observed. Antenna separation can be estimated from short-baseline interferometer data as well, but in the case of short-baseline interferometers, the accuracy of the antenna position determination is not substantially better than that obtainable with conventional survey techniques.

Over the longer baselines used in VLBI work, the conventional survey techniques are much less accurate than they are over shorter baselines. Thus the development of VLBI promised an improvement in the ability to determine both radio source positions and radio antenna locations. The purpose of this thesis is to report on a series of such determinations.

The work that led up to this thesis began in 1968 with a series of experiments involving stations in Tyngsboro, Massachusetts, and Green Bank, West Virginia. These earlier experiments are discussed in References 5, 6, and 21. The experiments reported on in this thesis were carried out between April 1972 and January 1975 under the sponsorship of the National Science Foundation, the Advanced Research Projects Agency of the Department of Defense, and the United States Geological Survey. The stations employed were located in Tyngsboro, Massachusetts; Goldstone, California; Green Bank, West Virginia; Gilmore Creek, Alaska; and Onsala, Sweden.

In the following Chapter, I will discuss the nature of the VLBI observables and the limitations of using them to estimate the astrometric and geodetic quantities of interest Chapter 3 will deal with the analytic models used to represent the VLBI observables in the computer programs used to analyze the VLBI data. Chapter 4 is concerned with the results of an analysis of a large body of VLBI observations spanning the period from April 1972 to January 1975. Finally, in Chapter 5, I will discuss briefly the prognosis for future progress in the development of VLBI.

CHAPTER 2

VLBI OBSERVABLES AND PARAMETER ESTIMATION

2.1 INTRODUCTION

As considered in this thesis, the fundamental VLBI observable is the measurement of the difference in arrival times at two stations of a radio signal from a distant radio source. This quantity is referred to as delay, and its time derivative is referred to as delay rate. Suitable combinations of such measurements can be used to estimate the locations of the stations and the radio sources. The nature and limitations of such estimates are the subjects of this chapter.

2.2 THE DELAY OBSERVABLE

In order to understand the delay observable, we construct the following idealized picture. Consider a point source of radio signals sufficiently distant that the signals arrive essentially as plane wave fronts, and consider two stationary receiving stations, capable of detecting and recording these signals. The stations are also equipped with accurate clocks capable of recording the arrival times of these signals (Figure 1). In the simplest case, with a non-rotating Earth, perfect clocks and receivers, and signals of arbitrary bandwidth, the difference in arrival times of the signals could in principle be determined by simply recording each signal on a strip chart recorder (also of arbitrary bandwidth) and then comparing the recordings to determine what shift of time origin will make the signals match.

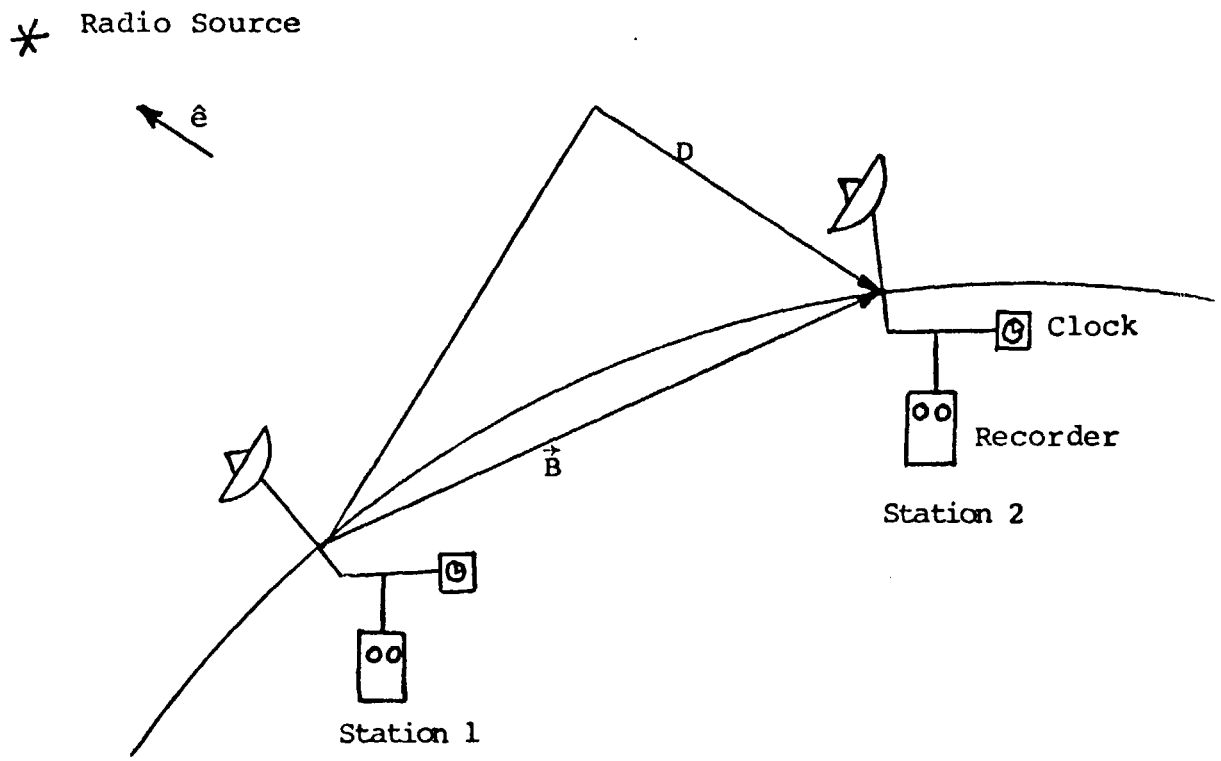

Figure 1

Basic VLBI Geometry

Real VLBI observations differ from this simple picture principally by having a limited receiver and recorder bandwidth, by having Doppler shifts in the signals due to the relative motions of the receiving sites, and by having imperfect clocks at each of the sites. Nevertheless, this picture is adequate for understanding much of the discussion which follows, and is a useful preliminary for understanding those situations where a more detailed model must be employed.

In the presence of a dispersive propagation medium (i.e. a medium in which the velocity of the incoming signal is a function of the frequency of the signal) there will be two characteristic velocities associated with the radio signals -- the group velocity and the phase velocity. There will therefore be two characteristic delays, the group delay and the phase delay. Our data-reduction programs are designed to estimate both the phase delay and the group delay, as well as the phase-delay rate. In theory, the difference between the phase delay and the group delay could be measured and used to estimate the magnitude of the effect of the dispersive medium. It has not been possible with the data being discussed in this thesis to resolve the closely spaced (~0.127 ns) ambiguities in the phase-delay data, and therefore the phase-delay information has not been used (see Reference 21, pps. 21-25).

There are also ambiguities in the group-delay data, but the group-delay ambiguities are much more widely spaced (typically $\frac{1}{3}$ μsec to 1 μsec -- see Table 2), and can be

eliminated from the data (see Chapter 4).

In the remainder of this chapter it will be assumed, unless specified otherwise, that the propagation medium is non-dispersive and that therefore no distinction need be made between phase delay and group delay.

2.3 THREE COMPONENTS OF DELAY

It is useful to think of VLBI delay observations as composed of three components. The first component is due to the geometry of the station locations and source location, as illustrated in Figure 1. This component contains all of the information about the geodetic and astrometric parameters that are of interest.* The second component is due to instrumental effects, principally clock errors. The third component is due to effects of the propagation medium (e.g. the atmosphere and the ionosphere). The detailed theory and computer algorithms required to deal with each of these components will be discussed in Chapter 3.

2.3.1 Geometric Delay

In order to understand the use of delay observations for the estimation of geodetic and astrometric quantities, we need to consider the geometric component of the delay observable.

---

*Many of the radio sources that we observe are known to have structure on the order of 10^{-3} arc-sec. Structure on this scale could affect the delays on transcontinental baselines by about 0.1 ns. The effects of source structure have not been considered in the discussions in this thesis since other uncertainties dominate our results.

From Figure 1, we see that the arrival time of a signal at Station 2 minus the corresponding arrival time at Station 1, i.e. the geometric delay, τ_g, can be written as

$$\tau_g = \frac{D}{c} = -\frac{\vec{B}}{c} \cdot \hat{e} \qquad (2\text{-}1)$$

where $\hat{e}$ is the unit vector in the direction of the radio source, $\vec{B}$ is the vector separation of the receiving stations, and c is the speed of light. (In the remainder of this thesis, the unit of time will be taken to be the second, and the unit of length will be the light-second. With these assumptions, $c \equiv 1$, and it will not appear explicitly in equations such as Equation (2-1). For a discussion of the specific coordinate system in which $\vec{B}$ and $\hat{e}$ are defined for this thesis, see Section 3.1.) Now for an inertial coordinate system we will assume that $\hat{e}$ is fixed, and that $\vec{B}$ will, to a very good approximation, rotate with a constant angular velocity $\vec{\Omega}$, the angular velocity of the Earth. τ_g is therefore a diurnal sinusoid:

$$\tau_g = K_1 \sin(\Omega t + \phi) + K_2 \qquad (2\text{-}2)$$

Because at present there is no available method for setting the clock epoch and rate (see Section 2.4) at each station to the accuracy required for VLBI observation, two additional terms must be added to Equation (2-2) to represent the differences in the clock epochs and rates at the two sites:

$$\tau_g = K_1 \sin(\Omega t + \phi) + K_2 + c_0 + c_1 t \qquad (2\text{-}3)$$

Thus delay observations on a single source can be used to determine only four independent parameters (e.g. K_1, ϕ, $(K_2 + c_0)$, and c_1; Ω is assumed to be known). The parameters

that we wish to determine from these observations are: three components of the baseline, two source coordinates (components of $\hat{e}$), and the two clock parameters, c_0 and c_1. Of these seven parameters, only six can be estimated, as the right ascension of the source cannot be separated from the hour angle of the baseline. There are still six parameters to be estimated, and only four independent observations. This is clearly an under-determined case. In other words, VLBI observation of a single radio source cannot serve to determine all of the baseline and source coordinates that we wish to estimate. However, if we observe more than one source, each source adds three new independent observations (K_1, K_2 and ϕ for that source; c_0 and c_1 are common to all sources) and only two new unknown parameters. It is thus easily shown (see Reference 17) that observations on a minimum of three sources are necessary to determine all of the parameters of interest (3 baseline parameters, 5 source parameters and 2 clock parameters, in that case). Furthermore, since there are ten unknown parameters, there must be at least ten observations in all, and each source must be observed at least three times. In actual practice these minimum numbers of sources and observations are generally greatly exceeded in order to provide redundancy and internal consistency checks on the data.

If the observations made are delay rates rather than delays, a slightly different situation emerges. If we resolve

$\vec{B}$ into equatorial and polar components in Equation (2-1),

$$\tau_g = -\vec{B}_{EQ} \cdot \hat{e} - \vec{B}_P \cdot \hat{e} \qquad (2\text{-}4)$$

and differentiate this equation, noting that $\vec{B}$ was assumed to be rotating with an angular velocity Ω parallel to $\vec{B}_P$, we see that

$$\dot{\vec{B}}_P = 0 \qquad (2\text{-}5)$$

and

$$\dot{\tau}_g = -\dot{\vec{B}}_{EQ} \cdot \hat{e} \qquad (2\text{-}6)$$

Thus delay-rate observations have no sensitivity to the polar component of the baseline.

If we differentiate Equation (2-3), we get

$$\dot{\tau}_g = \Omega K_1 \cos(\Omega t + \phi) + c_1 \qquad (2\text{-}7)$$

Following an analysis similar to that for delay observables, we note that there are four unknown quantities which we wish to estimate from observation of a single source (two baseline parameters, one source parameter and one clock parameter), and there are only three independent parameters in Equation (2-7). If we observe more than one source, each new source adds two unknowns, but only two independent observations (e.g. K_1 and ϕ; c_1 is common to all sources). Thus it is not possible with delay rates alone to estimate all of the parameters of geodetic and astrometric interest. The polar component of the baseline cannot be estimated, and, in addition, at least one of the baseline coordinates or source

coordinates must be determined by some other means.

If the observations made are a combination of delays and delay rates, one might expect that the minimum number of sources to be observed would be less than the number required for delay data alone. This is not the case, however. If there are enough delay observations to determine the delay vs. time sinusoid, then the delay rates are also determined, and measurements of delay rates do not then add independent information. (The situation is the same as for observations of delay beyond the minimum number required to determine the delay vs. time sinusoid.)

In all of the VLBI data that will be discussed in Chapter 4 the minimum criteria for the estimation of all the baseline coordinates and source coordinates will be more than met. In general, the data sets will include data which span a period of one to four days, involving two to four stations and ten to twenty radio sources. Also, both delay and delay-rate observations will generally be included simultaneously in the solutions.

There are other parameters which affect the geometric delay, besides the coordinates of the baselines and of the sources. These other parameters concern effects of the non-rigidity of the Earth and irregularities in the Earth's angular velocity vector, $\vec{\Omega}$. These parameters are of interest in geophysics. Because these effects modify the curve defined

by Equation (2-2), the arguments of the previous paragraphs concerning the information content of a set of delay observations on a single source need to be modified. That is to say, the delay vs. time curve for a given source contains information about the flexure of the Earth and the irregularities in $\vec{\Omega}$ in addition to information about the three geometric parameters discussed. The analytic expressions for these irregularities and their effects on delay and delay rate will be discussed in Chapter 3.

2.3.2 Instrumental Delay

The instrumental delay can be thought of as consisting of two components. The first component is the time required for the signals to travel from the antenna to the device which samples and records the signals. We will refer to this component of the instrumental delay as the "cable" delay, although the signal passes through amplifiers, mixers and other active components in addition to cables. The second component of the instrumental delay is caused by the error in the system clock at each station (VLBI is sensitive, of course, only to the differences between the clock errors at the various stations).

In an ideal VLBI station the cable delay should be carefully measured and eliminated from the data. However, since the equipment necessary to make such measurements was not available during nearly all of the experiments reported on in this thesis, the cable delay must be dealt with. The cable

delay could be either dispersive (frequency dependent) or non-dispersive, and it could be constant or time-varying. If it is non-dispersive, then its effects will be indistinguishable from the effects of the clock errors. If it is dispersive, then it could well affect the group delay and the phase-delay rate differently. In the absence of direct cable-delay measurements as a function of frequency, dispersive cable delays will have to be regarded as a possible source of systematic error.

We have attempted to model the errors in the system clock at each station in terms of a polynomial in time whose coefficients will be estimated from the VLBI data. If we refer to the clock error at Station i as ε_i, then*

$$\varepsilon_i = \alpha_i + \beta_i t + \alpha_i t^2 \ldots \qquad (2\text{-}8)$$

where the first term will

*In the remainder of this thesis it will be recognized that, in the absence of measurements of the cable delay, an unknown portion of the apparent clock error is caused by (non-dispersive) changes in cable delays.

be referred to as the clock-offset error, and the second term will be referred to as the clock-rate error. Higher order terms will be referred to as "second-order term", "third-order term", etc., as needed. (The reader should be aware that an n^{th} order polynomial generally contains n + 1 coefficients, and that, for example, the coefficient of the second-order term is actually the third coefficient in the polynomial.)

In the hydrogen-maser clocks generally employed in VLBI work, the clock error consists predominantly of the clock-offset and rate-error terms. If the hydrogen maser is operating close to its purported stability limit of one part in 10^{14}, then the effects of error terms of second-order and higher should be less than one nanosecond in a day. Therefore the total instrumental delay in a well designed and operated VLBI system should be able to be modeled to the level of a nanosecond per day by determining the coefficients of the offset and rate terms of the clock-error polynomial.

In the data to be discussed in this thesis there are many instances of clocks whose stability was no better than a part in 10^{12}. The common types of clock errors include discontinuities in both offset and rate, and long-term drifts in the clock error due to the presence of significant high-order derivatives. The problems caused by the high-order derivatives of the clock error could sometimes be handled by fitting high-order coefficients of the clock-error polynomial. The discontinuities were handled by fitting a separate clock-error polynomial to

the data on either side of the discontinuity. The epochs at which the VLBI theoretical model changes from one polynomial to the next will be referred to as "breaks" in the clock-error polynomials. There is now no provision for constraining clock error polynomials to be continuous in any derivative across a "break", although this feature could easily be added.

The selection of the clock parameters for a set of VLBI observations with very badly behaved clocks is a problem whose solution is entirely up to the discretion of the person processing the data. The judicious resolution of this question and the determination of clock models which accurately reflect the behavior of the real clocks is probably the thorniest problem in the entire process of analyzing the VLBI data reported here. This problem will be discussed at some length in Chapter 4.

There is a technique which can be used to eliminate clock problems altogether. If there is more than one antenna at each station, observations can be taken on more than one radio source simultaneously. If such observations are differenced the clock errors are eliminated from the observations. This type of experiment has been performed and described elsewhere (References 3 and 7). If there is only one

antenna at each station, then observations cannot be made simultaneously on different sources. However, if the antennas can be switched with sufficient rapidity from one source to another, then it is possible to form differences of pairs of observations which are nearly simultaneous. However, since the observations being differenced are not exactly simultaneous, the effects of short-term clock drifts (that is, clock drifts which build to a significant level during the time interval between the two observations which have been differenced) will still be present in the data, but the effects of longer term clock drifts will be largely eliminated. This type of experiment has also been performed and is discussed elsewhere (Ref. 23).

Some theoretical work we have done has indicated that inclusion of observations on a large number of sources may allow the recovery of all of the diurnal geodetic and astrometric parameters from a set of pure differenced observations (see Appendix A). While none of the results discussed in Chapter 4 involved exclusively differenced data, differenced data were used to handle several experiments involving more than two stations, where the clocks at one or more of the stations were very badly behaved. The data on all the baselines involving a station with a badly behaved clock were differenced, and the data on the remaining baselines were left undifferenced. One advantage to this scheme is that the undifferenced data are sufficient to determine all of the source coordinates. The

differenced data are then more than sufficient to determine the coordinates of the stations with the faulty clocks.

It is possible, of course, to use more general linear combinations of observations, rather than restricting ourselves to differenced observations. If, for example, the observations which have been differenced are also summed, it is then possible to form a data set consisting of sums and differences of observation pairs. Such a data set will contain all of the information of the original data set, but with the novel property that the long term clock errors have a much greater effect on one half the data set (the sum data) than on the other half (the difference data). It should be possible to use this combined data set with the estimated standard errors for the summed data adjusted to reflect the presence of the systematic clock errors, and thereby improve our estimates of geodetic and astrometric parameters. The implementation of this technique is beyond the scope of this thesis.

There are also techniques for dealing with clock errors which involve the use of Kalman filters to develop stochastic models for clock errors. These techniques are also beyond the scope of this thesis.

2.3.3 Propagation-Medium Delay

The remaining component of the delay observable which must be dealt with is the part due to the propagation medium (e.g. the atmosphere and ionosphere). The daytime ionosphere

zenith correction at X-band is typically of the order of one nanosecond, and the nighttime zenith correction is typically an order of magnitude smaller. We have experimented with a model for the ionosphere which assumed that the ionospheric electron content followed a rectified diurnal sine wave with a maximum at local noon. The correction to the delay was then calculated with a simple ray-trace scheme. Since this model did not affect our results significantly, either in terms of the rms of the residuals or of the scatter in the baseline results, it was not used in obtaining the results discussed in this thesis, and will not be discussed further. The ionosphere must be regarded as a source of possibly systematic noise at the level of a fraction of a nanosecond. It should be remarked that it is possible to exploit the frequency-dependence of the ionospheric correction to eliminate this source of noise completely. By comparing measurements made simultaneously at two or more frequencies it should be possible to deduce the ionospheric contribution to the delay and eliminate it. While multi-frequency observations have been proposed for future experiments, the necessary multi-frequency receiver hardware was not available for any of the experiments reported here.

The neutral atmosphere has proven to be somewhat more tractable than the ionosphere. The zenith correction is typically about 7 nanoseconds and a fairly simple model has been shown to produce a noticeable improvement in the postfit residuals.

The primary reason we have had success with a simple model for the neutral atmosphere is that the neutral atmosphere is fairly stable. The main cause of both spatial and temporal variations in the neutral atmosphere is the highly variable water-vapor content of the atmosphere. But the water-vapor contribution to the atmospheric correction to the VLBI delay observable is believed to be no more than 10-15% of the total atmospheric correction, or, in other words, about the same as the ionosphere contribution in the daytime. The atmosphere model we have employed uses the VLBI data to estimate the magnitude of ρ_i, where ρ_i is the correction to the delay in the zenith direction at Station i. The theoretical value for each delay observation is corrected by $\rho_i \csc \theta_i$ at each station, where θ_i is the elevation angle for the source at Station i. (The actual model employs a small correction to the $\csc\theta_i$ term which is not important for the discussion in this chapter; the details are discussed in Chapter 3.) There are three fairly obvious weaknesses to such a model: first, the modified $\csc\theta_i$ law may not adequately model the elevation-angle dependence of the real atmosphere; second, there is no provision for azimuthal variations in the atmosphere; and third, there is no provision for time variations in the atmosphere. The third objection can be ameliorated to some degree by solving for separate zenith

thicknesses on separate days or even at shorter time intervals. The selection of the time intervals over which a given value of ρ_i will be applied is the second major variable (after the determination of the clock model) which is at the discretion of the experimenter.

2.4 PARAMETER ESTIMATION

The station locations and source coordinates are estimated from the VLBI observations by using the method of weighted least-squares, which, if the noise in the data is gaussian with zero mean, is equivalent to the method of maximum likelihood. The procedure employed is to calculate the theoretical value of the observable using the best available values of the parameters to be estimated. The weighted-least-squares or maximum likelihood estimates of the parameters are then found through an iterative procedure based on linearized equations. Since this technique is quite standard, it will not be treated further here. The observation "weight", or formal standard error, used in the weighted-least-squares analysis is based on the signal-to-noise ratio for the observation (Reference 22). The term "residual" will be used to refer to the difference between an observation and its corresponding theoretical value. The formal errors of the parameter estimates are calculated from observation formal standard errors that have been scaled so as to make the rms value of the weighted postfit residuals equal to unity.

(CRT) display for read out and a light gun which makes possible real time interaction with the computer through the CRT display. Thus it is possible to use the light gun to set up the clock and atmosphere models and select the parameters to be estimated and then have the computer solve the linearized least-squares equations, print out the parameter estimates, and graph the postfit residuals on the CRT display. The data can then be edited with the light gun, and a different clock model or other change in the parameter set can be set up and the solution can be run again, all in a matter of a few minutes. While this program cannot do anything which cannot be done in some fashion by the batch-processing program, the advantages of easy set-up and fast turn-around are enormous. It is possible with this program to explore more completely the range of possible clock models and other variations in the parameter set, and therefore to explore possibilities that otherwise would be neglected for want of time. Another advantage of real-time processing is that the CRT display of the plot of postfit residuals can be manipulated. Whereas in a batch-processed program the plotting scales must be pre-selected (according to some criterion such as maximum residual size), with real-time processing the plot can be manipulated and scales can be expanded or contracted to display all or part of the residual set to better advantage. (These plots can be photographed, and such photographs are displayed in Chapter 4.)

The Haystack processing program has some limitations which ought to be mentioned. At present, it cannot handle difference and sum data, discussed in Section 2.3.2. Also the procedures for sorting and selecting data to be processed are restrictive; for instance presently all data are required to be in strict time sequence. A more fundamental limitation on this program arises from the fact that the computer's memory is too small to accommodate easily the programs necessary to calculate the theoretical values and partial derivatives required to form the linearized least-squares equations. In order to by-pass this problem, the theoreticals and partials are calculated by the IBM computer program and stored on magnetic tape for use by the CDC program. The inability of the CDC program to calculate theoreticals restricts the program to a single iteration of the iterative solution to the least-squares equations. Fortunately a single iteration has generally been found to be sufficient to produce convergence of the parameter estimates to within an error very much smaller than the formal errors of these parameter estimates.

The analysis upon which our data processing programs are based is discussed in Chapter 3, and Chapter 4 is devoted to a discussion of the use of these programs and to the results of processing the VLBI data.

2.6 OBSERVATION SCHEDULES

Before concluding this discussion of baseline and source-coordinate estimation, it is necessary to discuss the scheduling

of observations. The observation schedule is a factor which affects the process of parameter estimation, yet the problem of optimizing a schedule for astrometric and geodetic parameter estimation has not yet been solved. A complete discussion of the process of creating an optimal schedule is beyond the scope of this thesis. There is one scheduling consideration, however, which proved to be of some importance in the analysis of the data to be discussed in Chapter 4. It is very useful to have interleaved observations on a large number of sources, in order to separate the effects of the clock errors from the effects of errors in the source coordinates. Many of our schedules did not call for such interleaved observations because the schedules were usually designed for the purpose of studying the structure of the radio sources being observed, rather than for the purpose of estimating baseline coordinates and source coordinates.

Creating a schedule can be a tedious and trying project even without the problem of having to optimize the schedule for baseline and source-coordinate estimation. At the very least, it is necessary to calculate which sources are visible at all sites at any given time, and how much time is required to switch each antenna from one source to another. In order to automate the routine calculations involved in creating a schedule, an operator-interactive computer program was written for the CDC 3300 computer at Haystack. With this program, the operator first selects the stations and sources he wishes to include in a

schedule. The computer then displays on the CRT the sources which are visible at all stations at any given time. For each source the computer also displays such pertinent information as the time required to move the antennas from one source to another, the minimum elevation angle of the source, the time elapsed since the source was observed and the total number of observations already scheduled for that source. The operator need only select with the light gun the sources he wishes to observe, and the computer will automatically increment the time by the appropriate minimum time required to move the antennas, and record the source to be observed at that time, and then display a new list of sources which are visible at all stations at the new time. This process is repeated until the schedule is complete. The program also has options which allow the operator to modify a schedule already created or to print a final schedule in a form to be used by the antenna operator at each site.

CHAPTER 3

ANALYSIS OF VLBI OBSERVABLES

3.1 INTRODUCTION

We wish to derive theoretical expressions for the dependence of the VLBI delay and delay-rate observables on parameters which are of geodetic and astrometric interest. We will then be able to use these expressions to estimate the values of these parameters from the VLBI data using conventional least-squares techniques.

3.2 DEFINITION OF COORDINATE SYSTEMS

Before continuing with a discussion of delay and delay-rate observables, we must discuss the coordinate systems which will be employed in most of the analysis which follows. There are two coordinate systems which must be considered, one which is fixed to the "rigid" Earth and one which is "nearly" inertial. We will defer discussion of the Earth-fixed coordinate system until Section 3.5.

The "nearly" inertial coordinate system we will use will be defined with its origin at the solar-system barycenter, its Z-axis will be defined as parallel to the Earth's mean pole at 1950.0 (positive north), its X-axis will be defined in the direction of the ascending node of the Earth's orbit at 1950.0 (the "first point in Aries"), and its Y-axis will be defined to complete a right-hand triad. This coordinate system will be

employed for all of the analysis in Chapter 3 unless otherwise specified. (As in Chapter 2, the unit of length will be taken to be the light-second, and the unit of time to be the second, so that $c \equiv 1$.) This coordinate system is not quite inertial, since it is subject to accelerations arising from the gravitational attraction of the nearby stars and from the orbital motion of the solar system about the center of the galaxy. The motion relative to the galactic center introduces a change in the apparent position of the radio source with a magnitude of about 10^{-6} seconds of arc per year. The effect of the gravitational attraction of the nearby stars is several orders of magnitude smaller than the effect of the galactic orbital motion. Both of these effects are small enough to be neglected in our treatment of VLBI observables.

The reason we have chosen to use a solar-system barycentric coordinate system for our analysis here is that we hope at some point to be able to combine VLBI observations with spacecraft tracking data and interplanetary radar data in order to estimate the motions of the Earth more completely than can be done with VLBI data alone. Combining various types of data in this manner is simplified if the analysis of all of the data types is done in the same coordinate system.

In Appendix B we deal with the problem of transforming time as kept by atomic clocks on the Earth to coordinate time, t, of our solar-system barycentric coordinates. We can re-write Equation (B-30) as

$$AT_i = t - 32.15 \text{ sec} - \dot{\vec{R}} \cdot \vec{r}_i + LPT \qquad (3\text{-}1)$$

where AT_i is the reading of a (perfect) atomic clock at Station i on the Earth, $\vec{R}$ is the position of the center of the Earth relative to the solar system barycenter, $\vec{r}_i$ is the position of the clock relative to the center of the Earth and LPT represents the long-period (non-diurnal) terms in Equation (3-1).* The reason for grouping the long-period terms in this fashion will become apparent later. The 32.15-sec term is introduced in order to have coordinate time agree as closely as possible with the previous definitions of ephemeris time (Reference 1, p. 15).

Equation (3-1) represents the reading of a "perfect" atomic clock located at Station i. Recognizing that "real" clocks are necessarily imperfect for a variety of unpredictable reasons, we will model the errors of each real clock by a polynomial whose coefficients we will attempt to estimate from the VLBI observations. If T_{iK} represents the reading of the clock at Station i for observation K, then we write

$$T_{iK} = (AT_i)_K + \alpha_{iK} + \beta_{iK}(t - t_{iK}) + \gamma_{iK}(t - t_{iK})^2 + \ldots \qquad (3\text{-}2)$$

---

*The superposed dot, as in "$\dot{\vec{R}}$" signifies differentiation with respect to coordinate time only. The sole exception to this convention will be in the expression for delay rate, $\dot{\tau}$, where the superposed dot signifies differentiation with respect to time as kept by an atomic clock on the Earth, as specified in Equation (3-11).

where t_{iK} is the defined coordinate-time origin for the clock polynomial. Equations (3-1) and (3-2) can be re-written to give t in the following useful form

$$t = T_{iK} + 32.15 + \dot{\vec{R}} \cdot \vec{r}_i - \text{LPT} \quad - \alpha_{iK} - \beta_{iK}(t - t_{iK}) - \ldots \tag{3-3}$$

3.3 THE DELAY OBSERVABLE

If we think of the observed radio signal as a plane wave (Figure 1) which is received at Station 1 at coordinate time t, and received at Station 2 at coordinate time $t + \Delta t$, then we can define the observed value of the delay as:

$$\tau_K(t) = T_{2K}(t + \Delta t) - T_{1K}(t) \tag{3-4}$$

Δt is simply the geometric (coordinate) time delay

$$\Delta t(t) = -\vec{B}(t) \cdot \hat{e} + \Delta\tau_A \tag{3-5}$$

where*

$$-\vec{B}(t) = [\vec{R}(t) + \vec{r}_1(t)] - [\vec{R}(t+\Delta t) + \vec{r}_2(t + \Delta t)] \tag{3-6}$$

and

$\hat{e}$ = unit vector in the direction of the radio source

$\Delta\tau_A$ = atmospheric (including ionospheric) delay

where the ionospheric correction is presumed to be appropriate for group or phase delay depending on which type of delay is to be modeled.

A simple method for using Equation (3-5) to determine Δt is to perform a regula falsi type of numerical iteration. Equivalently, one can expand the expression (Reference 14), neg-

*The errors introduced here and elsewhere by adding vectors in a Galilean sense are negligible for the purposes of this thesis.

lecting terms smaller than 10^{-15} sec in delay. We can express the site position vector at Site 2 as

$$\vec{R}(t + \Delta t) + \vec{r}_2(t + \Delta t) = \vec{R}(t) + \dot{\vec{R}}(t)\Delta t + \frac{1}{2}\ddot{\vec{R}}(t)\Delta t^2 + \vec{r}_2(t) + \dot{\vec{r}}_2(t)\Delta t + \frac{1}{2}\ddot{\vec{r}}_2(t)\Delta t^2 + \ldots \quad (3\text{-}7)$$

Then Equation (3-5) can be re-written as

$$\Delta t(t) \approx (\vec{r}_1 - \vec{r}_2)\cdot\hat{e} - (\dot{\vec{R}} + \dot{\vec{r}}_2)\cdot\hat{e}\Delta t - (\ddot{\vec{R}} + \ddot{\vec{r}}_2)\cdot\hat{e}\frac{\Delta t^2}{2} + \Delta\tau_A$$

$$\Delta t(t)\cdot\{1 + (\dot{\vec{R}} + \dot{\vec{r}}_2)\cdot\hat{e}\} \approx (\vec{r}_1 - \vec{r}_2)\cdot\hat{e} - \frac{1}{2}(\ddot{\vec{R}} + \ddot{\vec{r}}_2)\cdot\hat{e}[(\vec{r}_1 - \vec{r}_2)\cdot\hat{e}]^2 + \Delta\tau_A$$

$$\Delta t(t) \approx (\vec{r}_1 - \vec{r}_2)\cdot\hat{e} - [(\dot{\vec{R}} + \dot{\vec{r}}_2)\cdot\hat{e}][(\vec{r}_1 - \vec{r}_2)\cdot\hat{e}] \cdot [1 - (\dot{\vec{R}} + \dot{\vec{r}}_2)\cdot\hat{e}] - \frac{1}{2}[(\ddot{\vec{R}} + \ddot{\vec{r}}_2)\cdot\hat{e}][(\vec{r}_1 - \vec{r}_2)\cdot\hat{e}]^2 + \Delta\tau_A \quad (3\text{-}8)$$

where the first term on the right hand side of Equation (3-8) is of the order of 10^{-2} seconds or smaller, and the second term is smaller by a factor of the order of 10^{-4}, and the third term is smaller by a factor of the order of 10^{-11}. The part of the second term inside the third set of brackets consists of two terms, the first of which is unity and the second is smaller than unity by a factor of the order of 10^{-4}.

Now if we similarly expand the first term in Equation (3-4) as

$$\begin{aligned} T_{2K}(t+\Delta t) = {} & t + \Delta t - 32.15 \text{ sec} - \dot{\vec{R}}(t)\cdot\vec{r}_2(t) \\ & - [\ddot{\vec{R}}(t)\cdot\vec{r}_2(t) + \dot{\vec{R}}(t)\cdot\dot{\vec{r}}_2(t)]\Delta t + LPT(t) \\ & + \frac{d}{dt}[LPT]\Delta t + \alpha_{2K} + \beta_{2K}(t-t_{2K}+\Delta t) \\ & + \gamma_{2K}(t-t_{2K}+\Delta t)^2 + \ldots \end{aligned} \qquad (3\text{-}9)$$

we can then combine Equations (3-1), (3-2), and (3-9) with Equation (3-4), using Δt of Equation (3-8) to obtain

$$\tau_K(t) = \Delta t - \dot{\vec{R}}(t)\cdot[\vec{r}_2(t)-\vec{r}_1(t)] - [\ddot{\vec{R}}(t)\cdot\vec{r}_2(t) + \dot{\vec{R}}(t)\cdot\dot{\vec{r}}_2(t)]\Delta t$$
$$+ \frac{d}{dt}(LPT)\cdot\Delta t - \alpha_{1K} - \beta_{1K}(t-t_{1K}) - \gamma_{1K}(t-t_{1K})^2+\ldots$$
$$+ \alpha_{2K} + \beta_{2K}(t-t_{2K}+\Delta t) + \gamma_{2K}(t-t_{2K}+\Delta t)^2 + \ldots \qquad (3\text{-}10)$$

where the first term of the right-hand side of Equation (3-10) is of the order of 10^{-2} sec or smaller, the second term is smaller by a factor of the order of 10^{-4}, the third term is smaller than the first by a factor of the order of 10^{-10}, and of the two terms inside the brackets of the second term, the first is of the order of 10^{-13} sec^{-1}, and the second is larger by a factor of the order of 10^3. The magnitude of the clock-error terms depends, of course, on the behavior of the clocks.

It is obvious from Equation (3-10) that α_{1K} and α_{2K} cannot be determined separately from observations of τ_K alone. It might seem that the higher order terms, β_{iK}, γ_{iK} could be determined for both stations (i=1 and i=2) because of the $\beta_{2K}\Delta t$ type of term. However, for most VLBI observations $\beta_{2K} < 10^{-13}$, and $\Delta t \sim 10^{-2}$ sec, thus this term has a magnitude of less than 10^{-15} sec, which is well below the noise level in the measurement of τ_K. The contribution of the Δt term for the higher-order

coefficients is even smaller. Therefore observations of τ_K can be used to determine only the differences between the clock error coefficients at the two stations [e.g. $(\alpha_{2K} - \alpha_{1K})$, etc]. The only reason for writing two polynomials explicitly in Equation (3-10) is for convenience in handling the case where more than two stations are involved. In the procedures we employ in processing VLBI data, the values of the coefficients of the clock error polynomial at one arbitrarily selected reference are fixed at zero, and the polynomial coefficients at the other stations are understood to represent the differences between those coefficients for that station and those for the reference station.

3.4 THE DELAY-RATE OBSERVABLE

In order to discuss the delay-rate observable, $\dot{\tau}$, we must first define which of several possible time scales has been used to form the derivative of τ. The choice is somewhat arbitrary. We have defined the delay rate to be the derivative of delay with respect to time as kept by the clock at Station 1. We can write this explicitly as

$$\dot{\tau}_K(t) \equiv \frac{d\tau_K}{dT_{1K}} = \frac{d\tau_K}{dt}\,\frac{dt}{dT_{1K}} \qquad (3\text{-}11)$$

Now it is a simple matter to differentiate Equation (3-10) to obtain (Reference 14)

$$\frac{d\tau_K}{dt} = \dot{\Delta t} - \ddot{\vec{R}}\cdot(\vec{r}_2-\vec{r}_1) - \dot{\vec{R}}\cdot(\dot{\vec{r}}_2-\dot{\vec{r}}_1) - (\dddot{\vec{R}}\cdot\vec{r}_2+2\ddot{\vec{R}}\cdot\dot{\vec{r}}_2+\dot{\vec{R}}\cdot\ddot{\vec{r}}_2)\Delta t$$

$$-(\ddot{\vec{R}}\cdot\vec{r}_2+\dot{\vec{R}}\cdot\dot{\vec{r}}_2)\dot{\Delta t} + \frac{d^2}{dt^2}(LPT)\Delta t + \frac{d}{dt}(LPT)\,\dot{\Delta}t$$

$$-\beta_{1K} - 2\gamma_{1K}(t-t_{iK}) - \ldots + \beta_{2K}(1+\dot{\Delta}t) \qquad (3\text{-}12)$$

$$+2\gamma_{2K}(t-t_{2K}+\Delta t)(1+\dot{\Delta}t) + \ldots$$

where $\dot{\Delta}t$ is obtained by differentiating Equation (3-8):

$$\dot{\Delta}t = (\dot{\vec{r}}_1-\dot{\vec{r}}_2)\cdot\hat{e} - [(\dot{\vec{R}}+\dot{\vec{r}}_2)\cdot\hat{e}][(\dot{\vec{r}}_1-\dot{\vec{r}}_2)\cdot\hat{e}]$$

$$-[(\ddot{\vec{R}}+\ddot{\vec{r}}_2)\cdot\hat{e}][(\vec{r}_1-\vec{r}_2)\cdot\hat{e}]$$

$$+ [(\dot{\vec{r}}_1-\dot{\vec{r}}_2)\cdot\hat{e}]\,[(\dot{\vec{R}}+\dot{\vec{r}}_2)\cdot\hat{e}]^2$$

$$+ 2[(\vec{r}_1-\vec{r}_2)\cdot\hat{e}][(\dot{\vec{R}}+\dot{\vec{r}}_2)\cdot\hat{e}][(\ddot{\vec{R}}+\ddot{\vec{r}}_2)\cdot\hat{e}]$$

$$-\frac{1}{2}[(\dddot{\vec{R}}+\dddot{\vec{r}}_2)\cdot\hat{e}][(\vec{r}_1-\vec{r}_2)\cdot\hat{e}]^2$$

$$-[(\ddot{\vec{R}}+\ddot{\vec{r}}_2)\cdot\hat{e}][(\vec{r}_1-\vec{r}_2)\cdot\hat{e}][(\dot{\vec{r}}_1-\dot{\vec{r}}_2)\cdot\hat{e}] + \dot{\Delta\tau}_a \qquad (3\text{-}13)$$

and from Equations (3-1) and (3-2)

$$\frac{dt}{dT_{1K}} = [1 - \ddot{\vec{R}}\cdot\vec{r}_1 - \dot{\vec{R}}\cdot\dot{\vec{r}}_1 + \frac{d}{dt}(LPT) + \beta_{1K} + 2\gamma_{1K}(t-t_{1K}) + \ldots]^{-1}$$

$$\approx 1 + \ddot{\vec{R}}\cdot\vec{r}_1 + \dot{\vec{R}}\cdot\dot{\vec{r}}_1 - \frac{d}{dt}(LPT) + \ldots \qquad (3\text{-}14)$$

Then, combining Equations (3-14), (3-11), and (3-12), and keeping terms larger than 10^{-16}, we write

$$\dot{\tau}(t) \approx \frac{d\tau_K}{dt} + \frac{d\tau_K}{dt}[\ddot{\vec{R}}\cdot\vec{r}_1 + \dot{\vec{R}}\cdot\dot{\vec{r}}_1 - \frac{d}{dt}\,(\mathrm{LPT})]$$

$$\approx \frac{d\tau_K}{dt} + \dot{\Delta}t(\ddot{\vec{R}}\cdot\vec{r}_1 + \dot{\vec{R}}\cdot\dot{\vec{r}}_1) - \dot{\Delta}t\,\frac{d}{dt}(\mathrm{LPT})$$

or, writing $\frac{d\tau_K}{dt}$ explicitly, again deleting terms smaller than 10^{-16},

$$\dot{\tau}(t) = \dot{\Delta}t - [\ddot{\vec{R}}\cdot(\vec{r}_2-\vec{r}_1) + \dot{\vec{R}}\cdot(\dot{\vec{r}}_2-\dot{\vec{r}}_1)]\cdot(1+\dot{\Delta}t) - \dot{\vec{R}}\cdot\ddot{\vec{r}}_2\cdot\Delta t$$

$$- \beta_{1K} - 2\gamma_{1K}(t-t_{1K}) - \ldots$$

$$+ \beta_{2K}(1+\dot{\Delta}t) + 2\gamma_{2K}(t-t_{2K}+\Delta t)(1+\dot{\Delta}t) \qquad (3\text{-}16)$$

where the first term is of the order of 10^{-6} or less; the second term is smaller by a factor of about 10^{-4}; and the third term is smaller by a factor of about 10^{-10}. As in the case of the delay observables, only the differences between the coefficients of the clock-error polynomials (e.g., $\beta_{2K}-\beta_{1K}$) can be estimated usefully from the VLBI delay-rate observable.

3.5 CALCULATION OF THE SITE POSITIONS

In order to evaluate Equations (3-10) and (3-16), the position $\vec{R}$ of the center of the Earth and its time derivatives are calculated from a tabulation on magnetic tape of an ephemeris of the positions of all of the bodies in the in the solar system.

In order to evaluate $\vec{r}_i(t)$, we must begin by defining an Earth-fixed coordinate system in which we will express our station coordinates and baseline components. The Z-axis of our Earth-fixed coordinate system will be defined in the direction of the mean pole for 1900-05 (see Reference 10, p. 93-95). The X-axis will be defined perpendicular to the Z-axis in the direction of the Greenwich meridian. The Y-axis will be

defined to complete a left-hand triad. (The coordinate system is defined to be left-handed in order to be consistent with the spherical system involving radius, latitude and west longitude, which is also left-handed.)

The transformation from Earth-fixed coordinates to coordinates aligned with the 1950.0 system described in Section 3.2 is done as follows: If we let [u] represent the 1 x 3 matrix containing the components of $\vec{r}_i$ in Earth-fixed coordinates, and $[\vec{r}_i]$ represent the 1 x 3 matrix containing the components of $\vec{r}_i$ in 1950.0 coordinates

$$[\vec{r}_i]^T = [P][N][S][W][u]^T$$

where [P] is the precession matrix, [N] is the nutation matrix, [S] is the rotation matrix for the Earth's spin, and [W] is the rotation matrix which expresses the polar motion of the Earth. Matrix [P] has the following form (see Reference 10, p. 93-98):

$$[P] = \begin{bmatrix} \cos\xi_0\cos w\cos z - \sin\xi_0\sin z & \cos\xi_0\cos w\sin z + \sin\xi_0\cos z & \cos\xi_0\sin w \\ -\sin\xi_0\cos w\cos z - \cos\xi_0\sin z & -\sin\xi_0\cos w\sin z + \cos\xi_0\cos z & -\sin\xi_0\sin w \\ -\sin w\cos z & -\sin w\sin z & \cos w \end{bmatrix}$$

where

$90°-\xi_0$ = the right ascension of the ascending node of the mean equator of date in the 1950.0 coordinate system

$90°+z$ = the right ascension of the ascending node of the mean equator of 1950.0 in the coordinate system defined by the mean equinox and equator of date

w = the inclination of the equator of date with respect to the 1950.0 coordinate system.

The values of ξ_0, z, and w are obtained from the series:

$$\begin{aligned} \xi_0 &= 2304\overset{''}{.}948T + 0\overset{''}{.}302T^2 + 0\overset{''}{.}0179T^3 \\ z &= 2304\overset{''}{.}948T + 1\overset{''}{.}093T^2 + 0\overset{''}{.}0192T^3 \\ w &= 2004\overset{''}{.}255T - 0\overset{''}{.}426T^2 - 0\overset{''}{.}0416T^3 \end{aligned} \qquad (3\text{-}17)$$

where

T = time from 1950.0 measured in tropical centuries (36524.21988 days of 86,400 coordinate-time seconds each)

Matrix [N] has the following form:

$$[N] = \begin{pmatrix} 1 & \Delta\psi \cos\varepsilon & \Delta\psi \sin\varepsilon \\ -\Delta\psi \cos\varepsilon & 1 & \Delta\varepsilon \\ -\Delta\psi \sin\varepsilon & -\Delta\varepsilon & 1 \end{pmatrix}$$

where

$\Delta\psi$ = the nutation in longitude

$\Delta\varepsilon$ = the nutation in obliquity

ε = the true obliquity of date of the ecliptic

$\Delta\psi$ and $\Delta\varepsilon$ are calculated from the trigonometric series given in Reference 4, pp. 44-45. In order to save computer time, these series are calculated and tabulated on magnetic tape at half-day intervals, and interpolated by a fourth-difference Everett interpolation to the desired epoch (see Reference 1, p. 224). The true obliquity of the ecliptic ε is given by

$$\varepsilon = \varepsilon_0 + \Delta\varepsilon \tag{3-18}$$

where, by Reference 4, p. 98, the mean obliquity of the ecliptic is

$$\varepsilon_0 = 23°27'08\overset{''}{.}26 - 46\overset{''}{.}84T' - 0\overset{''}{.}0059T'^2 + 0\overset{''}{.}00181T'^3 \tag{3-19}$$

with T' being the time in Julian Centuries of 36525 coordinate-time days from the epoch 1900 January 0.5 (J.E.D. 2415020.0).

The spin matrix [S] has the following form

$$[S] = \begin{pmatrix} \cos\theta & -\sin\theta & 0 \\ \sin\theta & \cos\theta & 0 \\ 0 & 0 & 1 \end{pmatrix}$$

where

$$\theta = \theta_0 + \Delta\psi \cos\varepsilon \tag{3-20}$$

$$\theta_0 = \bar{\theta} + \frac{d\theta_0}{dt} \times UT1$$

$$\bar{\theta} = 6^h\ 38^m\ 45\overset{s}{.}836 + 8{,}640{,}184\overset{s}{.}542T' + 0\overset{s}{.}0929T'^2$$

$$\frac{d\theta_0}{dt} = 1.002737909265 + 0.589 \times 10^{-10}T'$$

where the last two expressions are evaluated at 0.00 UT for the day in question and UT1, the (mean solar) rotational

phase angle of the Earth is related to atomic time through the tabulated values of (UTC-UT1) published by the BIH, where UTC is a defined piecewise linear function of atomic time, A1 (see Reference 1, pp. 26-29). Alternatively, the value of (UTC-UT1) can be estimated from VLBI data. For historical reasons, however, we present in Chapter 4 (A1-UT1) rather than (UTC-UT1). It should be noted that the expressions in Equations (3-17) through (3-20) were employed by the BIH in deriving the tabulated values of (UTC-UT1) and the values for polar motion, discussed below, from photographic zenith-tube observations. Therefore these expressions must be employed in order to use the tabulated values of (UTC-UT1) and polar motion to reconstruct the angular orientation of the Earth as measured by the BIH.

The polar motion matrix has the following form:

$$[W] = \begin{pmatrix} 1 & 0 & -X \\ 0 & -1 & Y \\ +X & Y & 1 \end{pmatrix}$$

where:

X = the component of the geocentric angular position, in radians, of the pole at time t with respect to the mean pole of 1900-05 measured along the meridian toward Greenwich

Y = the corresponding angular component along the meridian 90°W of Greenwich.

X and Y are obtained from the tabulated polar-motion values published by the BIH. Alternatively we can use VLBI data to estimate these values. Both the tabulated values and the estimated values for X and Y are corrected for diurnal polar motion, as calculated by McClure (Reference 8, p. 83).

The time derivatives of $\vec{r}_i$ are calculated by taking successive cross products of the Earth's spin vector, $\vec{\Omega}$, with $\vec{r}_i$, where Ω, the magnitude of $\vec{\Omega}$, is calculated by differentiating Equation (3-20)

$$\Omega = \frac{d\theta}{dt} = \frac{d\theta_o}{dt}(UT1) + \frac{d}{dt}(\Delta\psi \cos\varepsilon)$$

$$= \frac{d\theta_o}{dt} - \frac{d\theta_o}{dt}\frac{d}{dt}(UTC-UT1) + \frac{d}{dt}(\Delta\psi \cos\varepsilon) \qquad (3-21)$$

The derivatives in the second and third terms are calculated by numerically differentiating the tabulated values for UTC-UT1 and $\Delta\psi\cos\varepsilon$. In the first term we have assumed that $\frac{dUTC}{dt} = 1$. This assumption introduces an error in site velocities of the order of 10^{-16} sec/sec. Also, $\frac{d\theta_o}{dt}$ and $\bar{\theta}$ have zero slope, except for discontinuities at the beginning of each UTC day, and so their derivatives do not appear in Equation (3-21).

3.6 ANTENNA-MOTION CORRECTIONS

Up to this point we have treated the VLBI stations as if each station were a single point fixed on a presumed rigid Earth. We must now deal with the fact that the receiving antennas are, in general, steerable paraboloids whose dimensions are on the order of thirty to sixty meters. These antennas are steered or "pointed" by rotating them about either of two mutually orthogonal axes. One of these axes is always motionless with respect to the Earth's

crust, and will be referred to as the fixed axis. The other axis rotates about the fixed axis (Figure 2). On some antennas the fixed axis is aligned with the local vertical (alt-az mount); on others it is aligned horizontally (X-Y mount); and on still others it is aligned with the Earth's spin axis (equatorial mount, as in the figure).

The analysis of the corrections needed to account for the antenna motions will be greatly simplified by the recognition that some components of the needed correction are constant, independent of the direction in which the antenna is pointing. Such components have no effect on the delay rate, and will affect the delays only by changing the apparent clock offset. If the VLBI observations are to be used to synchronize the clocks at two stations, then these constant components must be measured and removed from the clock-offset estimate. Otherwise, such constant components will not concern us.

In order to begin to analyze the effects of antenna motion on the VLBI observables, it is necessary to carefully define what point near the moving antenna will be considered as the end of the baseline, or baseline reference point, in the sense that the baseline between two antennas will be defined as the vector separation of the baseline reference points of the two antennas. The correction to the delay for the motion of the antennas has a particularly simple form if the baseline reference point is defined appropriately. Consider the moving axis, which rotates about the fixed axis. Since the axes are orthogonal, the moving axis is confined to a plane perpendicular to the fixed axis. The baseline reference point will be

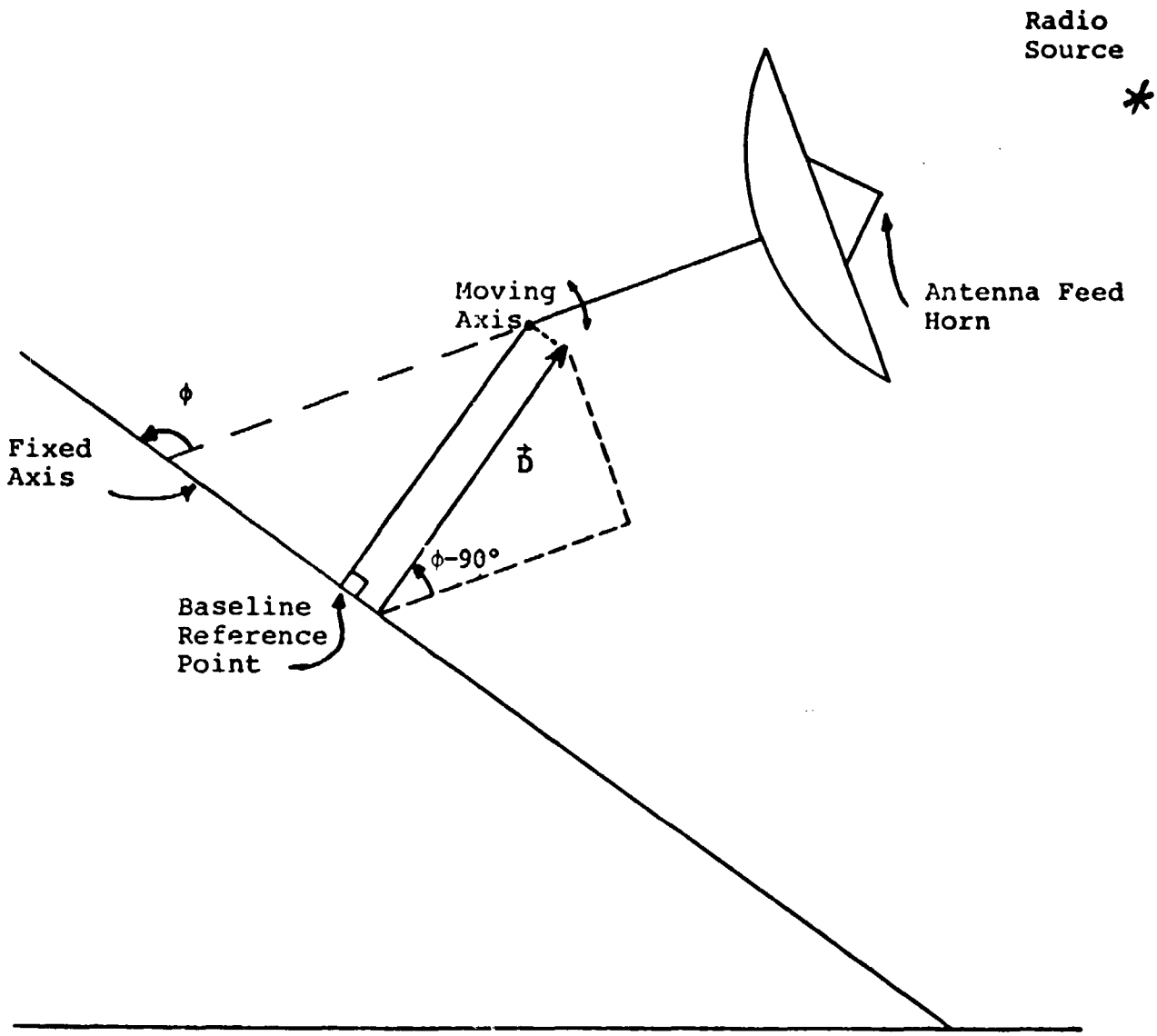

Figure 2

Geometry of Offset Antenna Axes

defined as the point where this plane intersects the fixed axis.

Now in order to calculate the contribution of the antenna motions to the geometric delay, we need to carefully define the point on the antenna where the signal will be said to be "received". This point will be taken to be the antenna feed horn since the component of the delay arising from the travel time of the signal beyond the antenna feed horn has been dealt with in Section 2.3.2 (the "cable" delay). Now in Figure 2, it can be seen that since the antenna is pointed at the source during any observation, the delay caused by the separation of the antenna feed from the moving axis will have the same constant value for all sources. Therefore we need consider only the component of the geometric delay caused by the offset, $\vec{D}$, between the axes. If the axes intersect, i.e. if $|\vec{D}| = 0$, the entire effect of the motion of the antenna will have the same constant value for all sources. If $|\vec{D}| \neq 0$, the changing correction to the delay will be simply the component of $\vec{D}$ in the direction of the radio source

$$\Delta\tau_{\text{axis offset}} = |\vec{D}|\cos(\phi-\pi/2) = |\vec{D}| \sin \phi \qquad (3\text{-}22)$$

where ϕ is the angle between the direction to the source and that of the fixed axis of the antenna (see Figure 2).

If the antenna mounting is equatorial, that is, if the fixed axis is parallel to the Earth's spin axis, the correction takes a particularly simple form, since

$$\delta = \pi/2 - \phi \qquad (3\text{-}23)$$

where δ is the declination of the source.

The correction to the delay rate for the motion of the antenna is, of course, the derivative of Equation (3-22), i.e.

$$\dot{\Delta\tau}_{\text{axis offset}} = |\vec{D}|\cos\phi\frac{d\phi}{dt} \qquad (3\text{-}24)$$

3.7 PROPAGATION-MEDIUM EFFECTS

The corrections for the propagation medium are evaluated separately for the neutral atmosphere and for the ionosphere, the latter being the only appreciable charged-particle contribution to the values of the observables. For the neutral atmosphere we utilize a modified cosecant law:

$$\Delta\tau_A = \tau_2^a - \tau_1^a \qquad (3\text{-}25)$$

where

$$\tau_i^a = \rho_i\left[\sin\theta_i + \frac{0.00143}{\tan\theta_i + 0.0445}\right]^{-1} \qquad (3\text{-}26)$$

and θ_i is the elevation angle of the source as observed from Station i. The numerical constants in Equations (3-26) represent the best-fit values of the results from ray-tracing through a standard model atmosphere; the results of the fitting process showed that Equation (3-26) agreed with the delays obtained from ray-tracing to within 1% for all elevation angles above 1° (Reference 2). The coefficient ρ_i, as can be seen from Equation (3-26), represents the zenith electrical path length (or delay) for the atmosphere over Station i. Only the water-vapor content of the neutral atmosphere presents a serious problem for the model because of its variability; its average contribution to the ≈ 7 nsec zenith electrical delay is about

10-15%.

The ionosphere is more difficult to model accurately than is the neutral atmosphere, partly because the electron density of the ionosphere changes, usually by a factor of about ten from day to night. Fortunately, for the X-band frequencies involved in these experiments, the total effect of the ionosphere on delay is never more than about one-tenth of the effect of the neutral atmosphere. Since we have not used a model for the ionosphere (see Section 2.3.3), some of the ionospheric correction will be absorbed in the neutral atmosphere correction, thereby leading to estimates for the neutral atmosphere correction which are larger (for group delay data) than the "true" neutral atmosphere correction.

3.8 EARTH TIDES

To account for the elastic properties of the earth, the position of the station at each end of a baseline is modified to include the effects of the solid-earth tides. In particular, we use the model given by Melchoir (Reference 9). The changes in the spherical coordinates of the site position are given by

$$\begin{aligned} \Delta r &= hu \\ \Delta\phi &= \frac{\ell}{r}\frac{\partial u}{\partial \phi} \\ \Delta\lambda &= \frac{\ell}{r\cos\phi}\frac{\partial u}{\partial \lambda} \end{aligned} \qquad (3\text{-}27)$$

where r, ϕ, λ denote, respectively, the geocentric radial, latitudinal, and (east) longitudinal position of the site, and where $h = 0.584$ and $\ell = 0.045$ are the relevant Love numbers.

The disturbing potential $\underline{u}$ is given by

$$u = A\{\cos^2\phi\ (a_1 \cos(2LHA + \psi_1) + a_2 \cos(2LHA-\mu+\omega+\psi_2) + a_3\cos(2LST+\psi_3) + a_4\cos[2(GST+\lambda)+\psi_4]) + \sin2\phi(a_5\cos(GST+\lambda+\psi_5)+a_6\cos(LHA-\mu+\psi_6)+a_7\cos(LST-\sigma+\psi_7)) - (1.5\sin^2\phi-0.5) \cdot [a_8+a_9\cos(\mu-\omega)+a_{10}\cos(2\mu)+a_{11}\sin(2\sigma)]\} \quad (3\text{-}28)$$

where

A	= 26.7 cm	ψ_1	= 0
a_1	= 0.908	ψ_2	= 0
a_2	= 0.174	ψ_3	= 0
a_3	= 0.423	ψ_4	= 0
a_4	= 0.115	ψ_5	= -90°
a_5	= 0.531	ψ_6	= +90°
a_6	= 0.377	ψ_7	= +90°
a_7	= 0.176		
a_8	= 0.739		
a_9	= 0.083		
a_{10}	= 0.156		
a_{11}	= 0.073		

and

μ = longitude of the moon (mean) = (4.719967 + 8399.709T) radians

σ = longitude of the sun (mean) = (4.881628 + 628.3319T) radians

ω = longitude of the lunar perigee = (5.835152 + 71.01803T) radians

T = time in centuries from 1900.0

GST = Greenwich sidereal time

LHA = lunar hour angle = GST - μ + λ

LST = solar hour angle = GST - σ + λ

This treatment of the Earth tides neglects possible inhomogeneities in the response of the earth to the tidal potential, which would make h and ℓ functions of location on the Earth. According to Melchior (Reference 9, p. 300), measurements from different parts of the Earth yield values for h that differ from the ones employed here by 0.08, and values for ℓ which differ by 0.03.

CHAPTER 4

RESULTS FROM VLBI OBSERVATIONS

4.1 INTRODUCTION

This chapter consists of a discussion of the results from a series of VLBI experiments which began in April of 1972. For convenience, these experiments have been divided into two distinct sets which I call the Phase I experiments and the Phase II experiments. The Phase I experiments were made during the period from April 1972 through May 1973, and the Phase II experiments were made during the period from July 1973 through January 1975. A brief summary of the pertinent facts about the experiments performed is given in Tables 1-3.

4.2 THE PHASE I EXPERIMENTS

Some of the Phase I experiments were undertaken for the purpose of measuring transcontinental baselines and others for the purpose of studying the structure of the radio sources (see, for example, Reference 21). Each experiment consisted of approximately twenty-four hours of observations, during which time approximately two hundred observations were made on about ten different sources (an observation consists of a single pair of Mark I tape recordings: see Reference 21. For experiments involving N stations, therefore, there are N(N-1)/2 observations that result from the pairwise combination of the N tapes that contain recorded signals from a given source at a given time). The schedules were carefully designed so that, with few exceptions, three or four sources were always

kept under observation in fairly rapid succession (<1 hour for observations on three sources). In addition, the observation schedules often provided for as wide coverage in hour angle and declination of the observed sources as was practical in order to optimize the measurement of the delay vs. time sinusoids as discussed in Chapter 2. The schedules were restricted in that no sources were observed whose declinations were higher than 40°. At the time, no sources were known at higher declinations which could be reliably used for VLBI observations. Several have since been uncovered by our group. Also, the schedules used in April and May of 1972 called for a large amount of time for observation of the source pairs 3C273-3C279 and 3C345-NRAO512, for reasons unrelated to the geodetic purposes of the experiments.

4.3 THE PHASE II EXPERIMENTS

The Phase II experiments began with observations in July 1973, and have continued to January 1975. There are two characteristics of these experiments which have made it convenient to discuss them separately from the discussion of the earlier experiments. First, these experiments have generally run for a period of four days each rather than one day each, and they have generally employed four stations (Haystack, Goldstone, NRAO and Onsala) rather than two, although there is a small number of three station experiments in both data sets. Thus, the data from each Phase II experiment com-

prised about 2,000 observations (Mark I tape pairs) rather than the about 200 observations for each of the Phase I experiments. Second, each of the Phase II experiments was scheduled primarily for the purpose of studying the structure of the radio sources (see Reference 23). The schedules for the Phase II observations have therefore tended to concentrate observations on one or two sources over periods of time extending for many hours. The lack of interleaved observations on many different sources tends to make it difficult to separate the effects of clock errors from the effects of source coordinate errors, baseline errors, and atmospheric effects. Although this problem might not have been serious had the clocks at all of the stations been well behaved, the fact is that the clocks at two of the stations, NRAO and Goldstone, were demonstrably very badly behaved during most of these experiments. In spite of these problems these data proved of some use for geodetic and astrometric measurements.

4.4 DATA-PROCESSING PROCEDURES

Before discussing the specifics of the results of the analysis of these data, it will perhaps be useful to discuss the general procedures employed in processing each data set.

The first step in processing the data involves the use of two computer programs, VLBI1 and VLBI2. These programs are used to estimate the "best" values (in the maximum likelihood sense)

of delay and delay rate for each pair of tape recordings, one tape from each of two stations, containing the radio signals received from a given source. The development and use of these programs is described elsewhere (References 5 and 21).

4.4.1 Editing the Data

The next step in processing any of these data sets involves the elimination of the group delay ambiguity (see Reference 21). In order to detect these ambiguities, VLBI3 is used to calculate theoretical values for each observation and then to form the residuals or differences between the observed values and their corresponding theoretical values. These "theoreticals" are based on accurate a priori values for the baseline coordinates, the source coordinates and the neutral atmosphere, as well as on preliminary estimates for the coefficients of the offset and rate terms in the clock error polynomial based on the unedited VLBI data. The delay residuals from such a computer run are shown in Figure 3, and the rate residuals in Figure 4*. Most of the observations in Figure 3 cluster along straight lines, which lines are separated by a group delay ambiguity spacing, which in this case is 1/3 μsec. The process of eliminating these ambiguities involves nothing more than adding or subtracting N times the ambiguity spacing for each point, so as to make all of the

---

*If the reader is not already familiar with these plots, the explanation in Appendix C will help in understanding the codes employed.

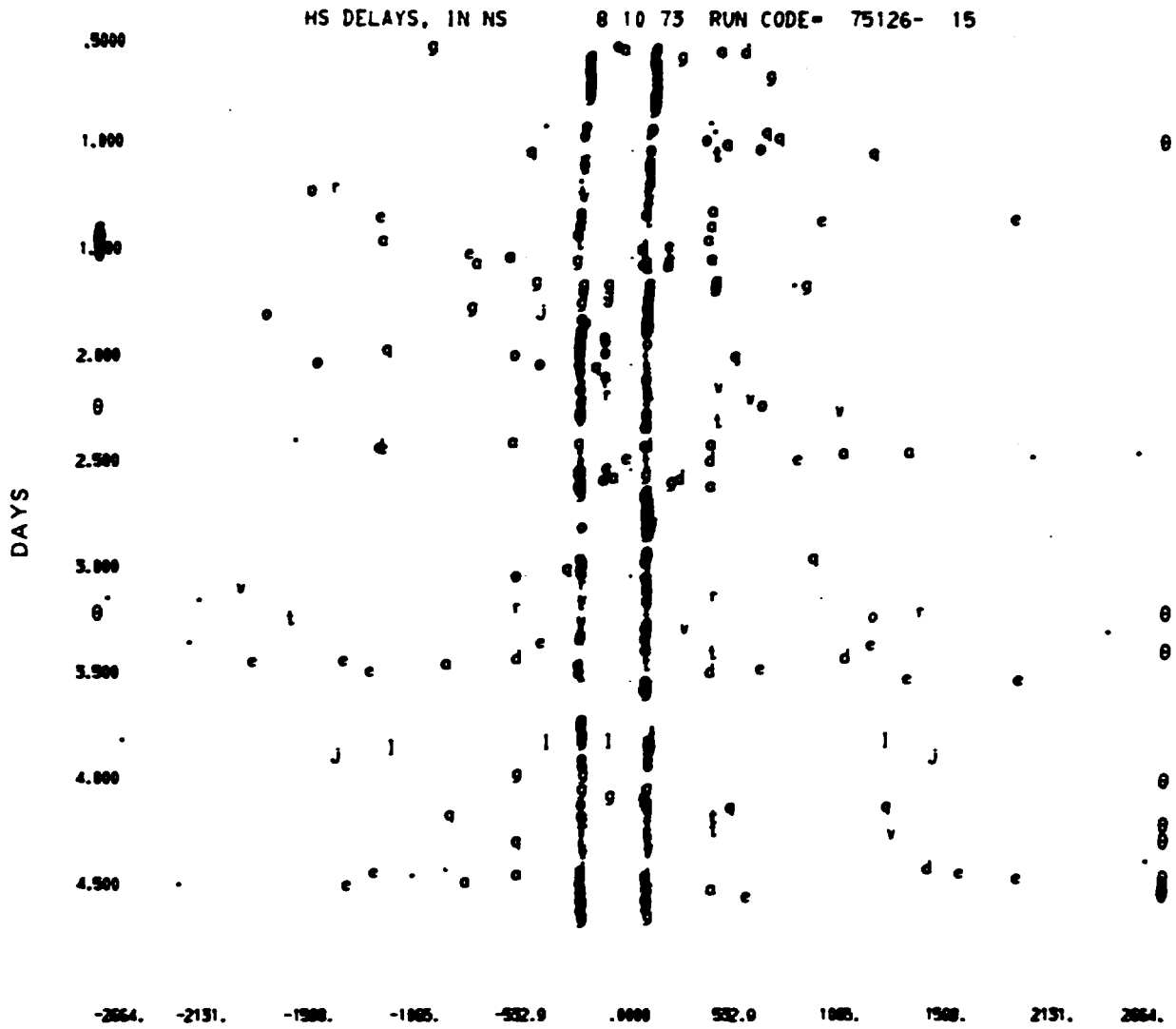

Figure 3. Residuals from Unedited Delay Data

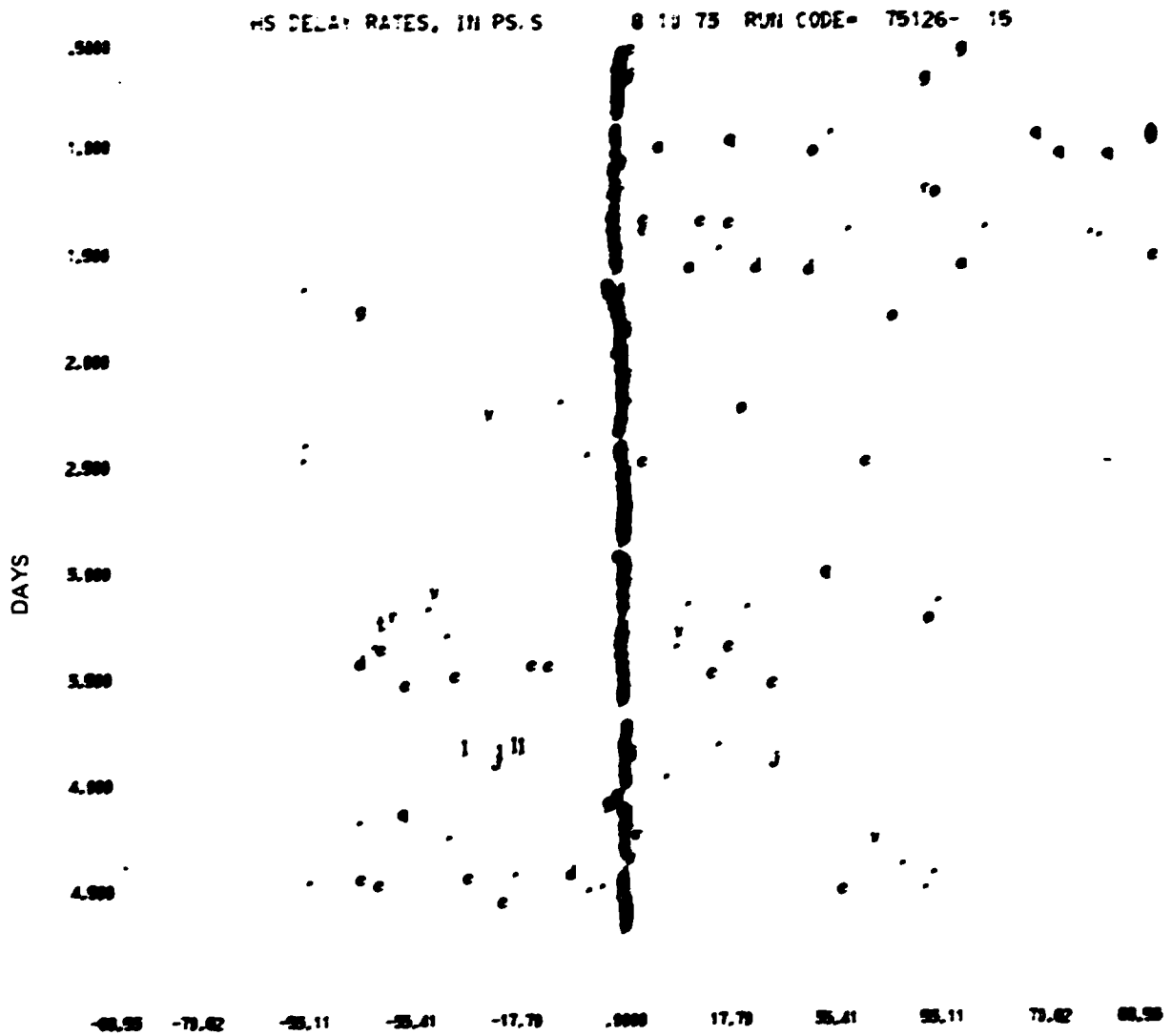

Figure 4. Residuals from Unedited Delay-Rate Data

parallel lines in Figure 3 coincident. It makes little difference which line is chosen (i.e. which line is not moved at all) since this choice will affect only the value of the clock offset. There are only two cases where the selection of the total ambiguity correction is important. First, if more than two stations are involved, the ambiguities must be selected so as to preserve closure of the delays around any triangle*. Second, if the VLBI observations are to be used to synchronize the clocks at the two stations, the ambiguity spacing must be large compared to the a priori errors in the more conventional methods for synchronizing clocks (e.g. broadcast time signals or portable clocks). These errors are typically a fraction of a microsecond. A second technique for selecting the correct ambiguity could involve the use of an instantaneous bandwidth wide enough to resolve the group-delay ambiguity (Reference 21, p. 108-110). The required instantaneous bandwidth would be only slightly greater than that obtainable with the present recorder systems. A third technique could involve suitably changing the separations of the sampled frequency bands (Reference 21).

It is obvious from Figure 3 that there are some points which do not cluster along lines separated by the group-delay ambiguity spacing. These observations must be edited out.

*It should be obvious from the definition of delay [Equation (3-4)] that, for Stations 1, 2, and 3:

$$\tau_{12}(t_1) - \tau_{13}(t_1) + \tau_{23}(t_2) = 0 \ .$$

Commonly such "bad" points can be more easily identified in the delay-rate residual plot, where there is no question of ambiguities (Figure 4).

It may well be asked at this point, what causes so many "bad" observations, and what criteria are used to eliminate them? The answers to the first question are myriad. Bad data points can be caused by any failure in the receiver-recorder hardware at either site, including such things as bad magnetic tapes. The only criteria used to eliminate these "bad" observations are the magnitude of the residual, and/or its failure to lie "close" to a "smooth" curve passing through other residuals for the same source. In general, I have tried to be judicious in eliminating all suspicious or marginal observations. The data sets we have here are so thoroughly over-determined that the effect of not including an observation which is, in fact, valid will in general be negligible, whereas the effect of including a "bad" observation could be significant. Although it is possible in principle to investigate all of the myriads of combinations of data sets formed by including some data points and excluding others, the astronomical number of such possibilities boggles the mind. I have therefore sought to eliminate as far as possible the "bad" and "marginal" observations, and deal only with a single sub-set of each data set which seems to contain thoroughly reliable data. In general, about 20 to 25% of the observations have been eliminated. Of these observations, about 10% were eliminated because the radio sources were too

weak to produce reliable fringes.

4.4.2 Determining Clock Behavior

We seek next to deduce the behavior of the station clocks. As mentioned in Chapter 2, if the clocks are not well behaved, the determination of the clock behavior can be the most difficult problem in the entire process of reducing VLBI observations. The best clues to the behavior of the real clocks come from the residuals from the type of computer run we have just discussed. To preserve these clues, it is desirable to fix all of the non-clock parameters because these parameters have non-zero correlations with the clock parameters. Therefore if all the parameters were adjusted, the mindless least-squares estimator would attempt to reduce the effects of the clock on the sum of squares of the residuals by adjusting the non-clock parameters. This could destroy, or at least confuse, the evidence of the clock behavior contained in the residuals. For the purpose of illustrating this procedure I have included in the figures some residual graphs which show some typical effects of clock problems. Figure 5 shows the effects of a discontinuity in the clock rate at Onsala. (The determination of which one of the two station clocks is causing the problem seen in any residual set can be difficult. In this case the problem was solved by an examination of the station log books, which contained a note indicating that the Onsala hydrogen maser clock was retuned at the time indicated by the break in the residual trend

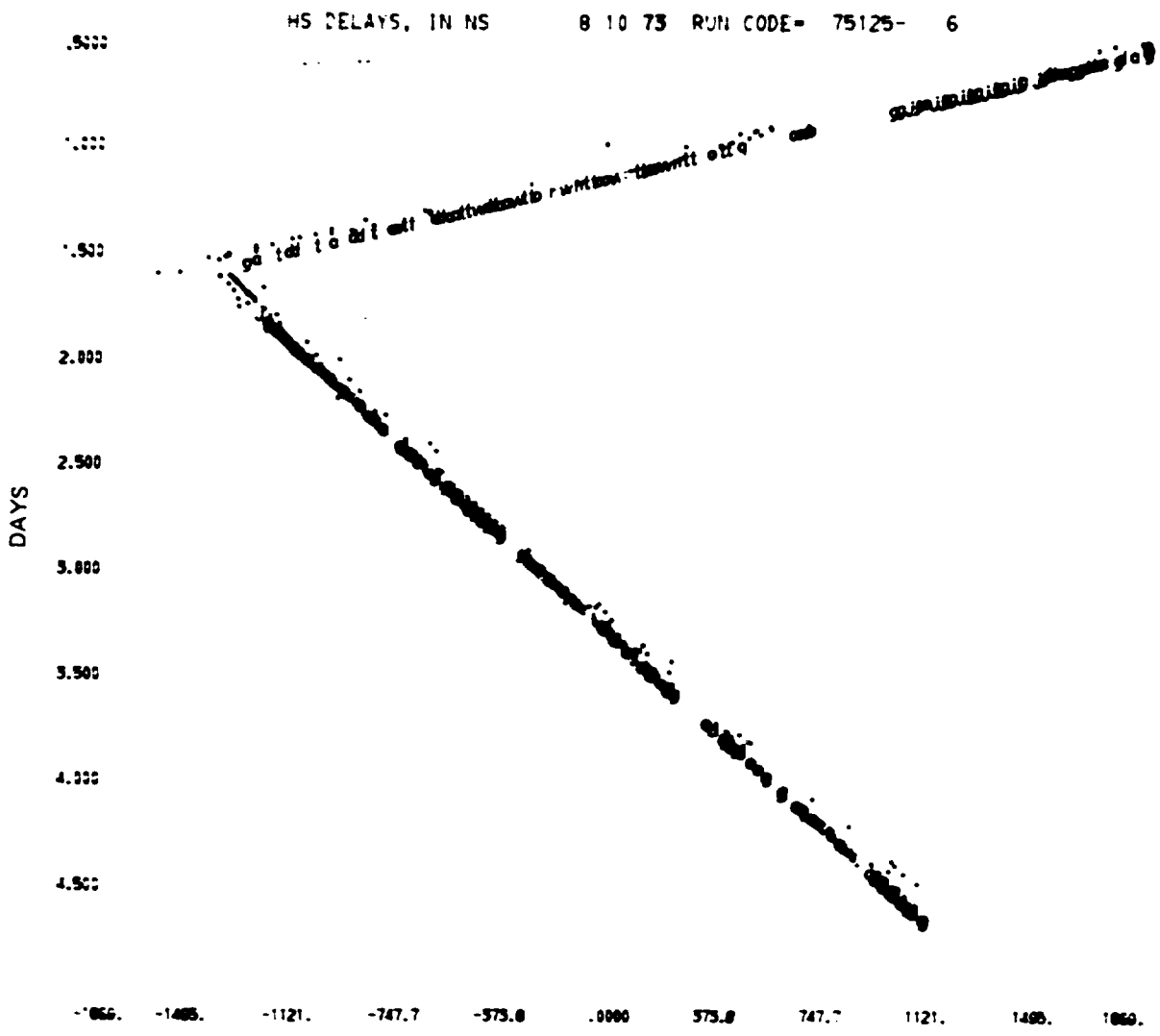

Figure 5. Delay Residuals Showing the Effect of a Discontinuity in the Clock Rate at Onsala

in Figure 5. In the multi-station case it is often possible to determine which station clock is causing a particular trend in the residuals by noting which station is common to the baselines whose residuals exhibit that trend.) Figure 6 shows the effect of estimating the coefficients for a separate first-order clock-error polynomial at Onsala for each of the straight lines in Figure 5. There is no discernible evidence of any remaining clock problems. Figure 7 shows the effect of high-order derivatives in the clock error at NRAO. This effect would be disastrous for even meter-level geodesy were there no way to correct for the effect -- its magnitude is nearly 500 ns, and one meter is only 3 ns of light-travel-time. Figure 8 shows the same data, but this time the coefficient of the second-order term in the clock-error polynomial has been estimated as well. The parabola shown in Figure 7 is gone, but the remaining drifts are still about 40 ns in amplitude. How well these problems can be dealt with will be discussed later on in this chapter.

4.4.3 Testing for Consistency

With the clock problems deciphered as well as possible, the next step is to solve for all of the baseline, source-coordinate, atmosphere and clock parameters. After these solutions have been obtained for all of the data sets available, the

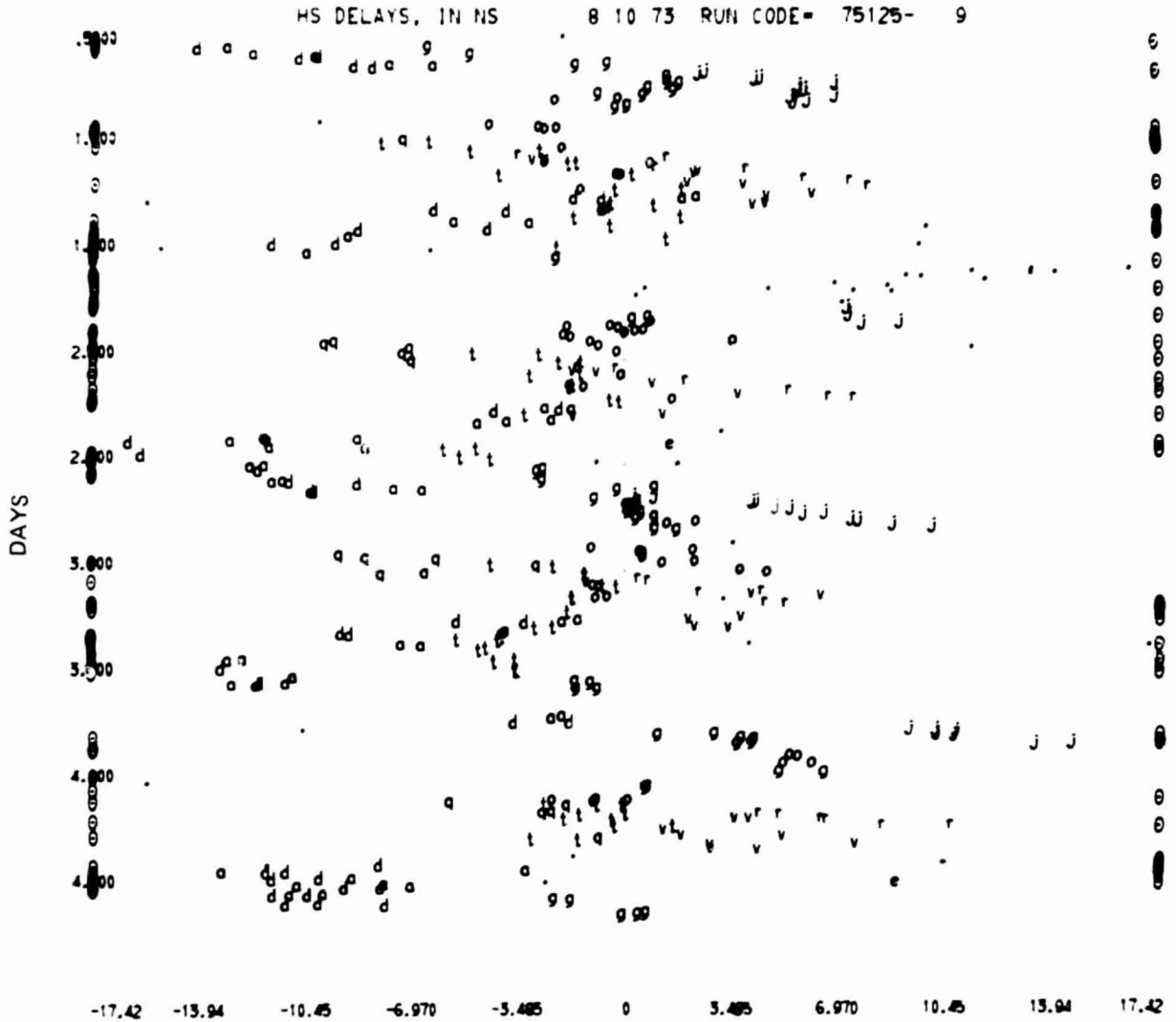

Figure 6. Delay Residuals from the Same Data as Figure 5, with Separate First Order Clock Polynomials Before and After the Rate Discontinuity at $\tau \simeq 1.5$ days.

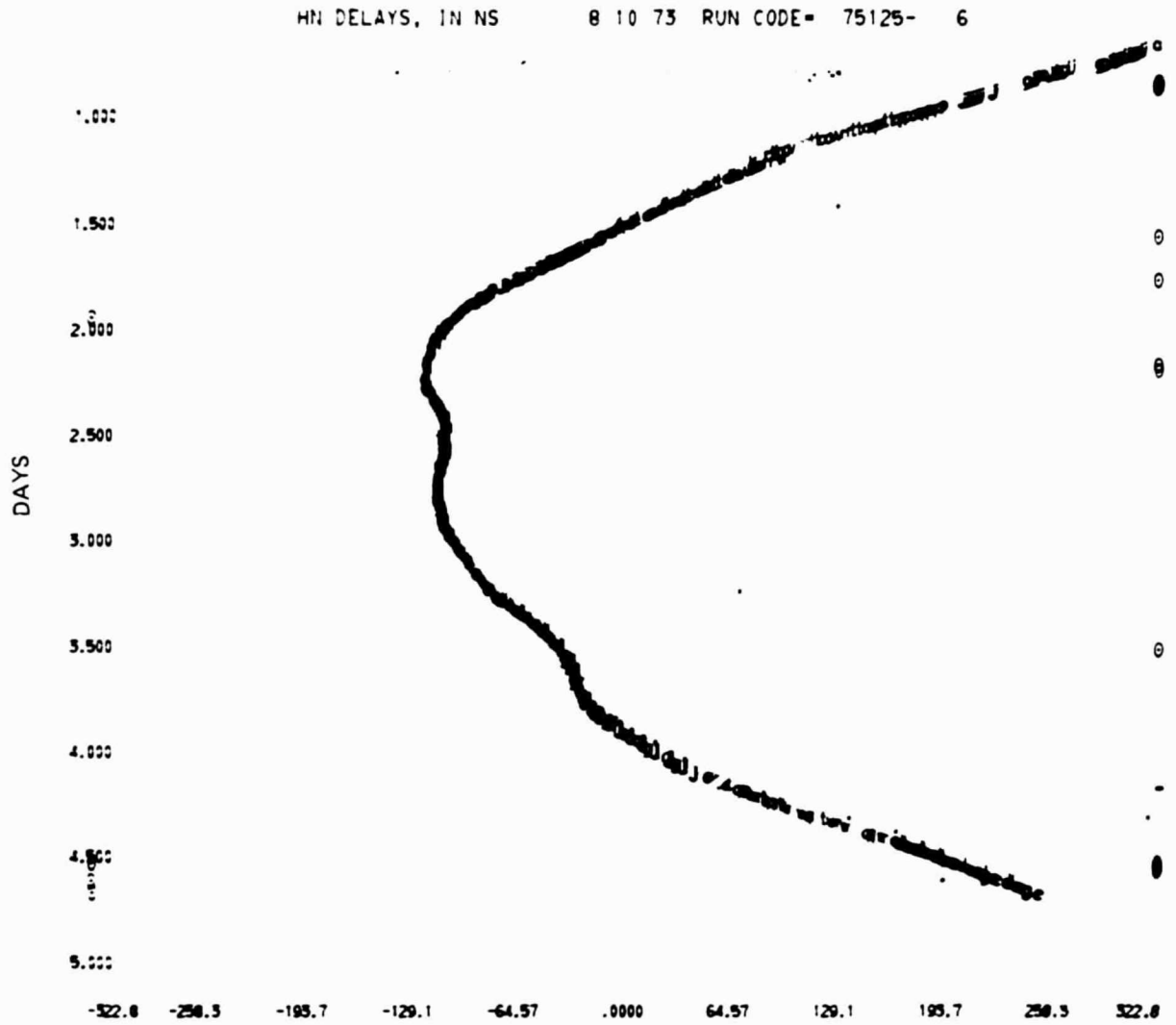

Figure 7. Delay Residuals Showing the Effects of Significant High Order Derivatives in the Clock Error at NRAO

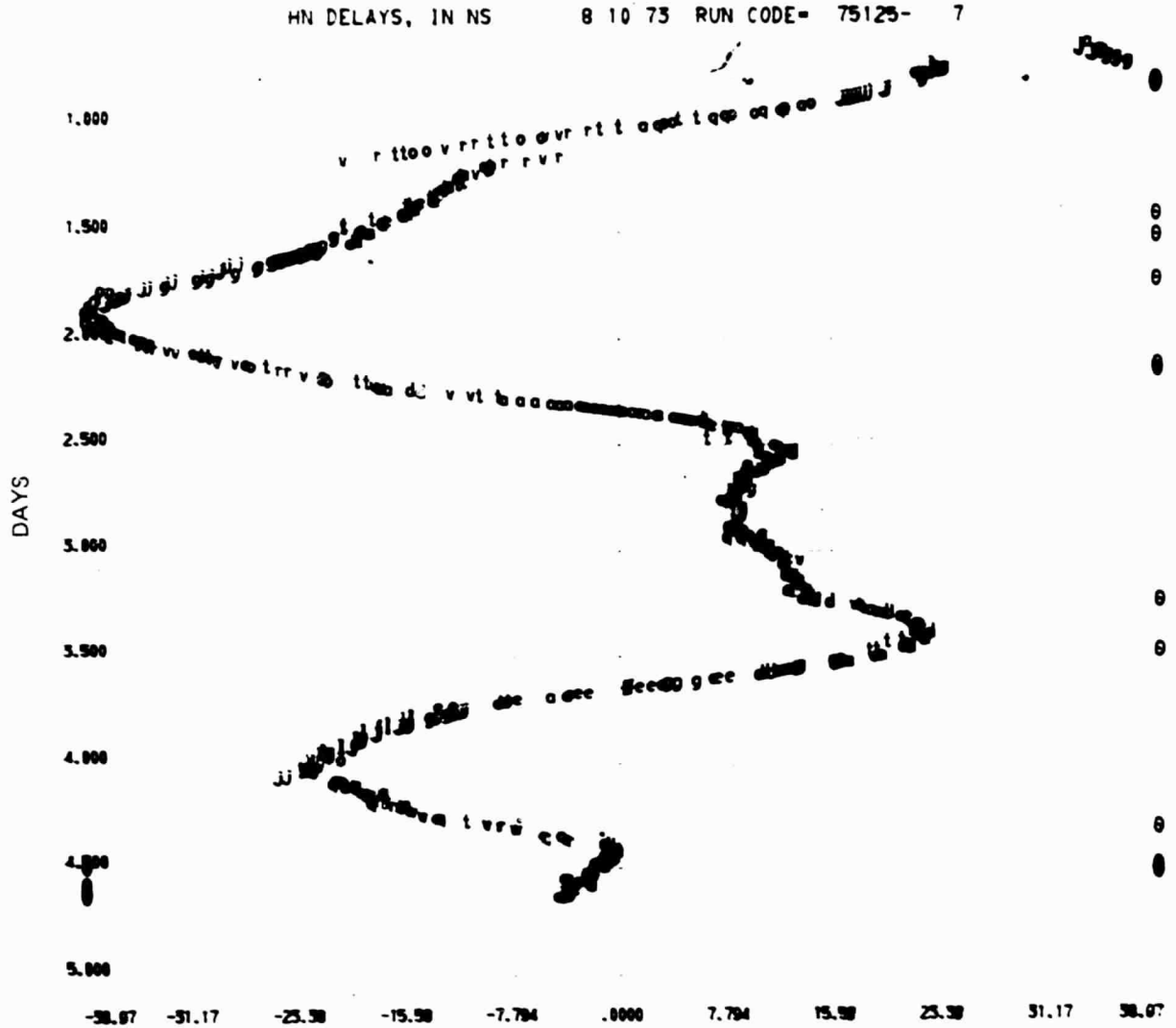

Figure 8. Delay Residuals from the Same Data as Figure 7, with the Coefficient of the Second Order Term in the Clock Error Polynomial Adjusted

final step is to check the consistency of the various parameter solutions. It should be recognized, however, that consistency of results is a necessary condition but not a sufficient condition for confidence in those results. Convergence toward an incorrect result is a well known phenomenon in the history of science and it usually results from the fact that a series of investigations has been prematurely terminated when those investigations seemed to produce satisfactory results*. Nevertheless, the importance of consistency cannot be overstated, for the idea of repeatability of results is deeply ingrained into the very concept of measurement, any kind of measurement. One expects that use of the concepts of consistency and repeatability, combined with careful checking and a healthy attitude of skepticism will produce reliable results.

4.4.4 Processing Problems with the Phase I Data

All of the Phase I results which will be discussed in Section 4.5, with two exceptions, were obtained from solutions in which the clock errors were modeled by estimating the coefficients of the first and second terms of the clock-error polynomial at each station except Haystack. (As discussed in Chapter 3, the coefficients of the clock-error polynomials at Haystack were fixed at zero, and the polynomials at each of the other stations were interpreted as the differences between

---

*This phenomenon is sometimes referred to as the "sheep effect".

the clock errors at that station and the clock errors at Haystack.) The two exceptions are the February 4, 1973 data (Run 75125-19)* which required the estimation of the coefficient of the second-order term in the clock error polynomial, and the June 27-28, 1972 data (Run 75125-16)*, which seemed to have some inconsistency between the delay and the delay-rate data of the type described in Chapter 2. The solution reported in Section 4.5 is a delay-only solution with a clock break at 1:04 (UTC) on the 28th of June 1972. The residuals are shown in Figures 9 (delay) and 10 (delay rate). The delay residuals have no particular bias, whereas the delay-rate residuals are strongly biased and have a discontinuity at the point where the clock break occurs (between 1.0 and 1.125 on the vertical scale). It is arguable that these data should simply have been eliminated from further discussion, but I have included them, if for no other reason than to serve as an example of the type of problem that can plague these data. The residuals on the remaining Phase I data sets exhibit no problems comparable to the June 27 data, but neither are they completely trouble-free. Figure 11, for example, shows the delay residuals from the August 29-30, 1972 data set. The residuals for 3C 120 (e) have been connected by a line so that they may be more

---

*See Appendix C for an explanation of the run code numbers.

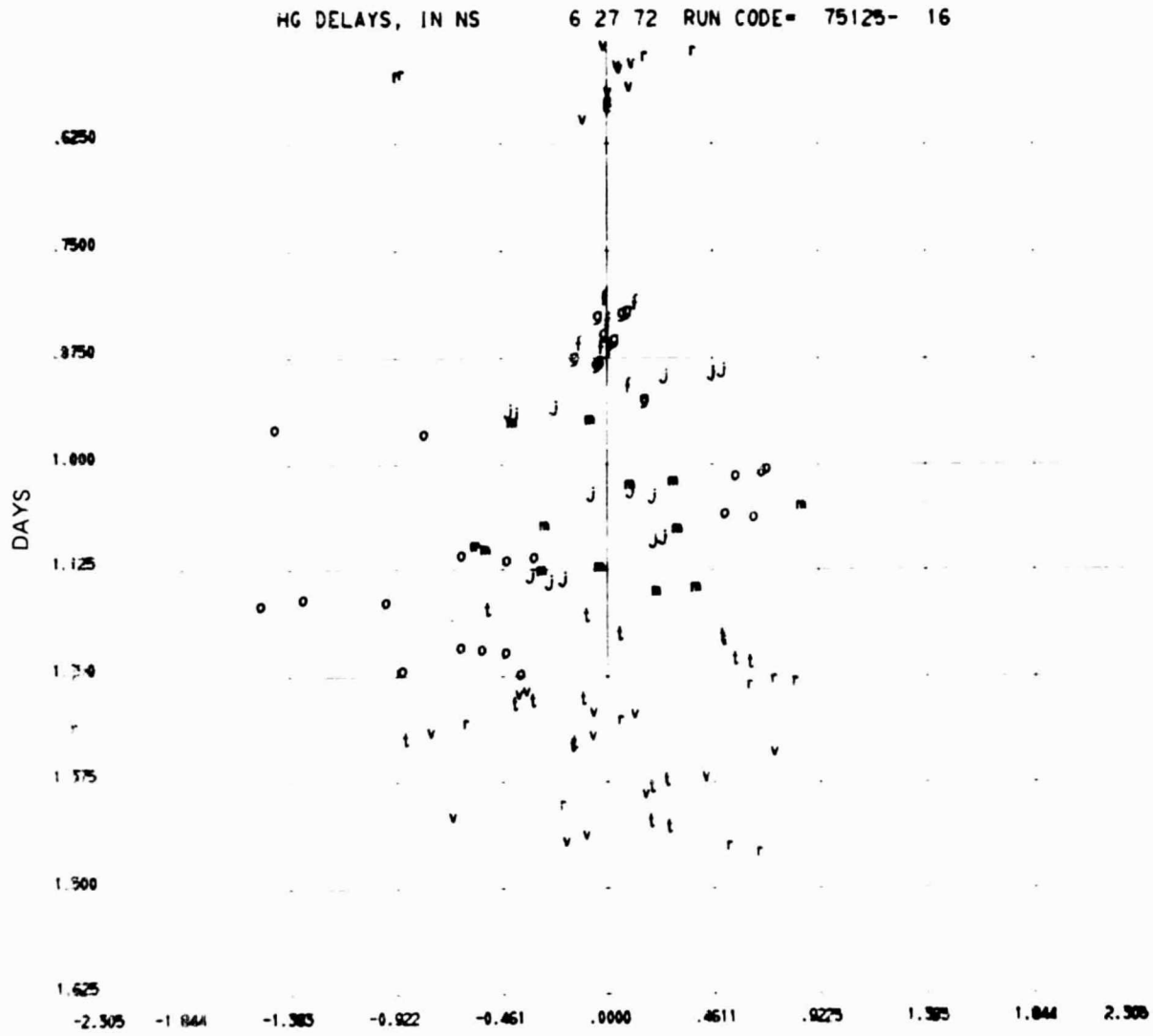

Figure 9. Delay Residuals from June 27-28, 1972

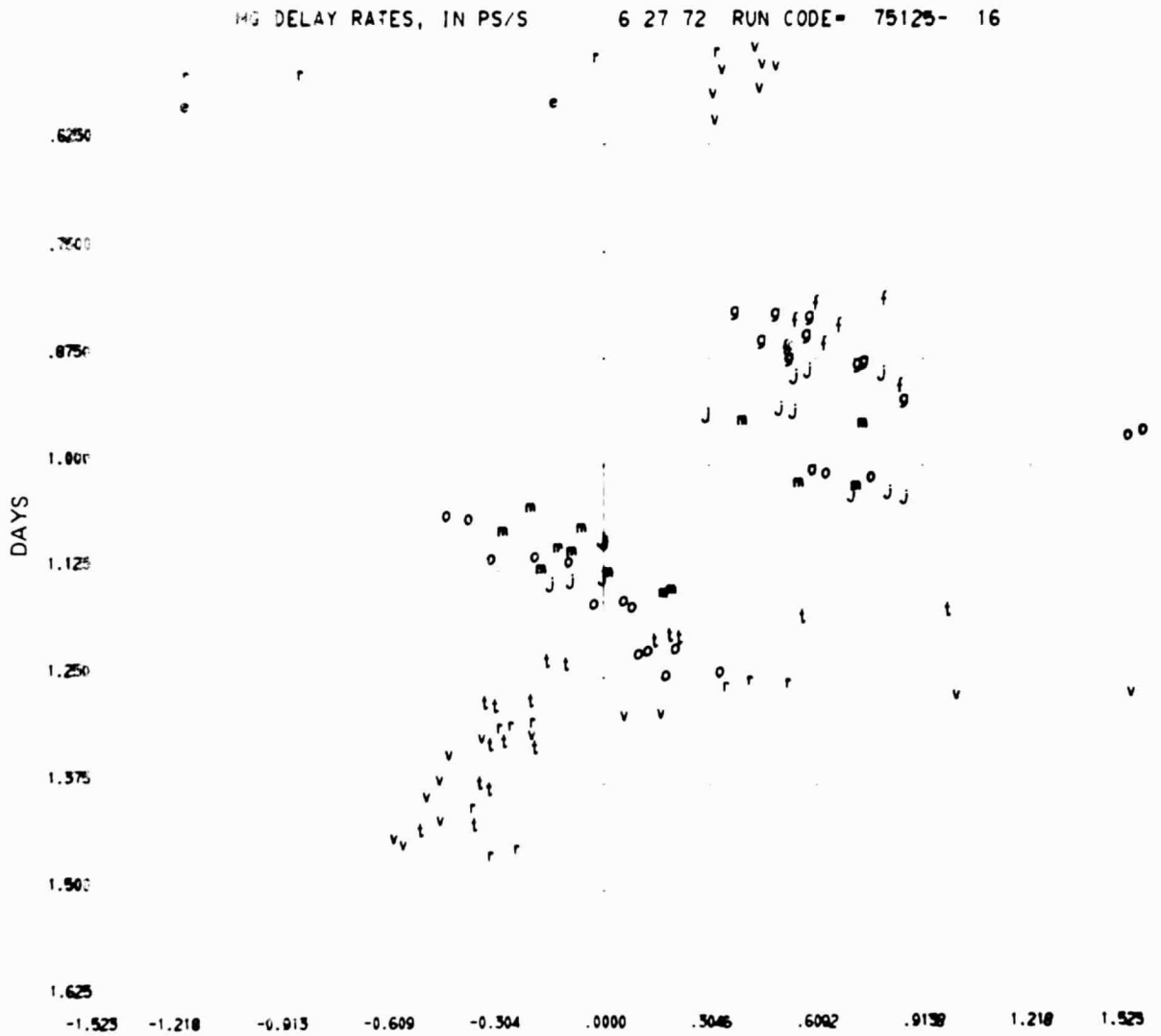

Figure 10. Delay Rate Residuals from June 27-28, 1972

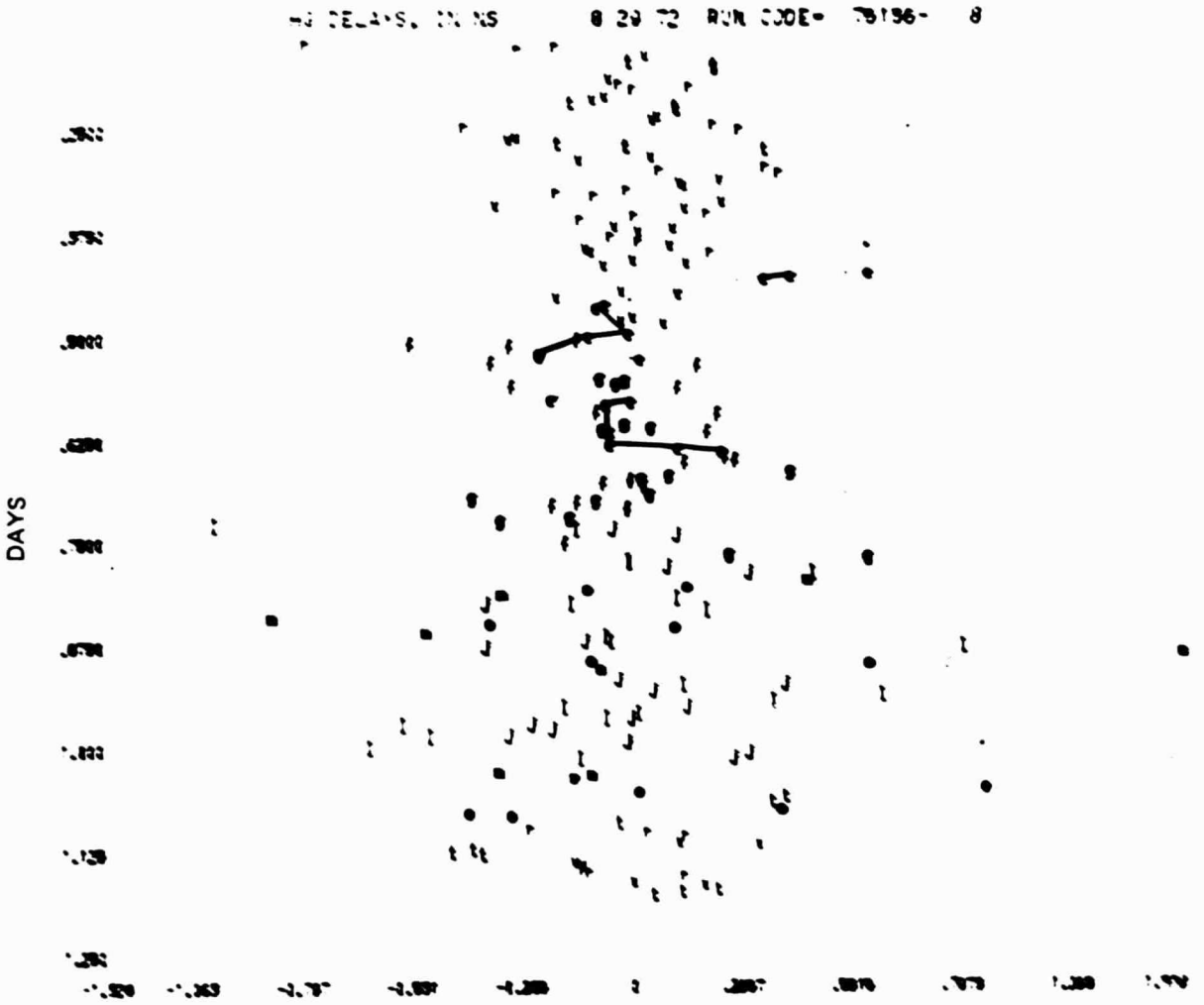

Figure 11. Delay Residuals from August 29-30, 1972

easily seen. It is obvious that these residuals are systematic, yet all attempts to formulate a reasonable explanation for this behavior have failed. System problems can be largely, but not totally, ruled out because the problem does not seem to affect any other source even though observations on several sources are interleaved in this time period. (Source-dependent system problems are not completely impossible; they are only extraordinarily unlikely.) Source structure would have to exist on a scale of about 10^{-2} arc-second to cause an effect of this magnitude. The trouble with a source structure explanation is that the fringe amplitude data for this day give a strong indication that the unresolved component of the source is point-like (Reference 16). The remaining obvious possibility is that this residual curve represents some sort of atmospheric effect. The trouble with an atmospheric effect explanation is that none of the other sources, some of which are at comparable elevation angles, show any similar effects. While it is not possible to rule out pathological situations such as small clouds which just happen to cover this source and follow it through the day, such explanations have to be regarded as extremely unlikely. We are left with reasons for disbelieving all of the likely explanations for this problem. It is possible, and unfortunately even probable, that the delay and delay-rate data simply do not contain the information required to unambiguously resolve this problem.

Not all of the peculiar residual effects which are seen

defy explanation. Figure 12 shows Haystack-Goldstone delay residuals for May 9-10, 1972. The residuals for 3C345 (o) have been connected by lines. It can be seen that the scatter in these observations starts at about ±3 ns, and then drops steadily until the scatter is a small fraction of a nanosecond. The reason for this peculiar behavior is that the structure of the source can cause large changes in the correlated flux as the projection of the baseline changes (see Reference 23), and, hence, in the signal-to-noise ratio for the delay observation. For this particular set of observations the correlated flux was near zero at the start of the observations, and increased rapidly throughout the observation period. The decrease in the scatter of the residuals is nearly proportional to the increase in the signal-to-noise ratio.

4.4.5 Processing Problems with the Phase II Data

As was mentioned earlier, the processing of the Phase II data was a good deal less straightforward than the processing of the Phase I data. The main problem with the Phase II data lay in the fact that the clocks at NRAO and Goldstone were very badly behaved. A typical effect of the clock error at NRAO can be seen in Figures 7-8. Figure 7, as described earlier, results from a solution in which only the coefficients of the offset and rate terms of the clock-error polynomial were estimated. Figure 8 shows the same data but with the coefficient of the second-order term in the clock-error polynomial also

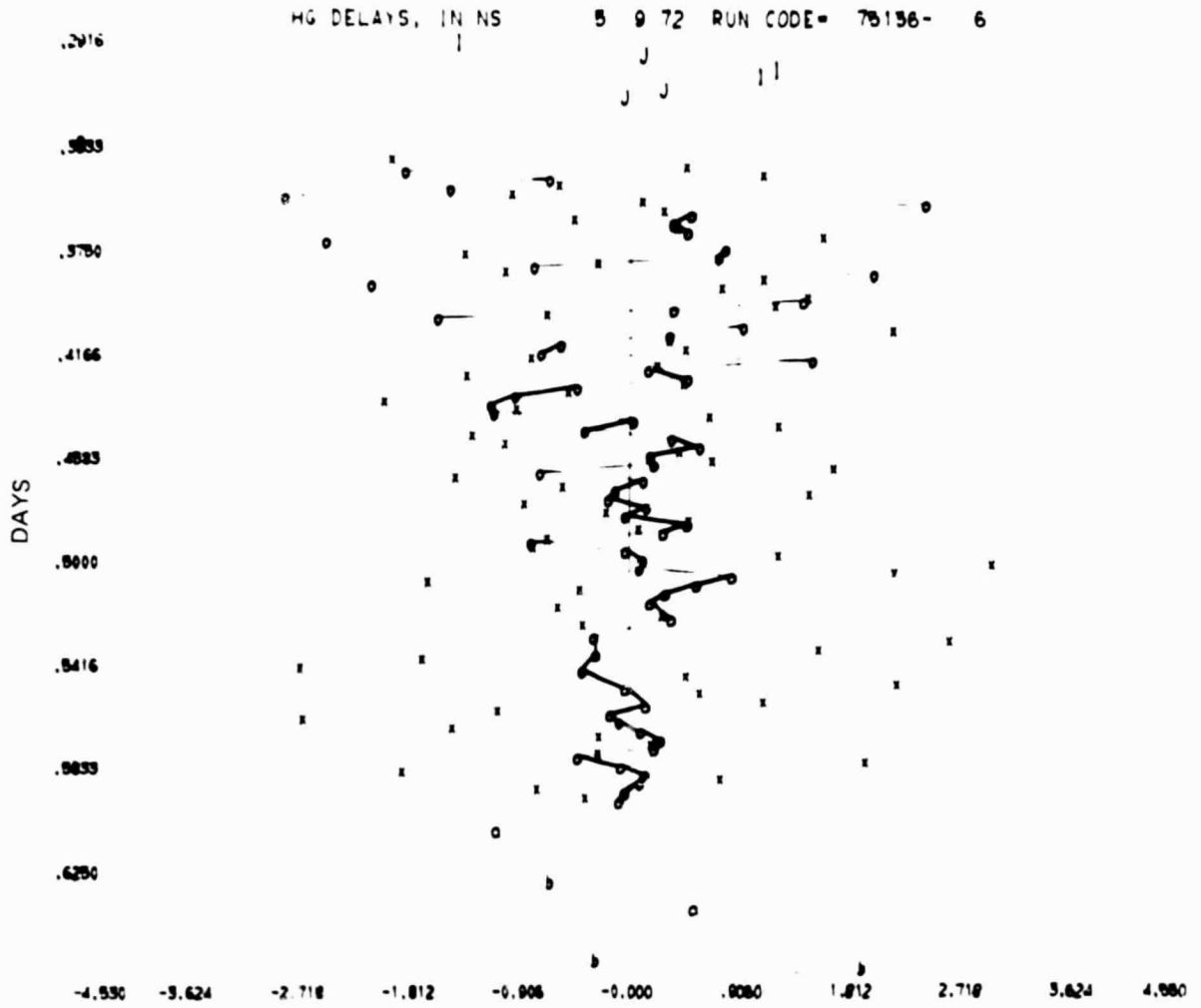

Figure 12. Delay Residuals from May 9-10, 1972, Showing the Effects of a Rapid Increase in the Signal-to-Noise Ratio for 3C 345 (0)

estimated. Figure 13 shows the top part of Figure 8 with the vertical scale expanded. In Figure 13 it can be seen that in addition to the variation in the clock rate there were two discontinuities in the clock offset, each with a magnitude of about 10 ns. Not only were there discontinuities in the clock offset, but a careful inspection of the lines of residuals will show that the two separate lines overlap in the region between t = 1.083 and t = 1.166. The only reasonable explanation for this behavior is that the clock offset must have "jumped" back and forth between two values separated by about 10 ns (Reference 12).

There are two ways of handling this type of pathological clock behavior with the present data-processing program (VLBI3). The first way is to try to fit the curves in Figure 8 with polynomials, and the second is to form differenced observations, or differenced and summed observations, as discussed in Chapter 2.

Figures 14-20 show some of the stages of the process of determining the "best" set of polynomials to use to fit the clock errors of a given set of data. Figure 14 shows the Haystack-NRAO delay residuals from the observations of October 1973, from a solution in which the coefficients of the first three terms of the clock-error polynomial were estimated and all the baseline coordinates, source coordinates and atmosphere parameters were fixed at a priori values. There are two fairly clear discontinuities, one each near t = 3.25 and t = 3.75 on

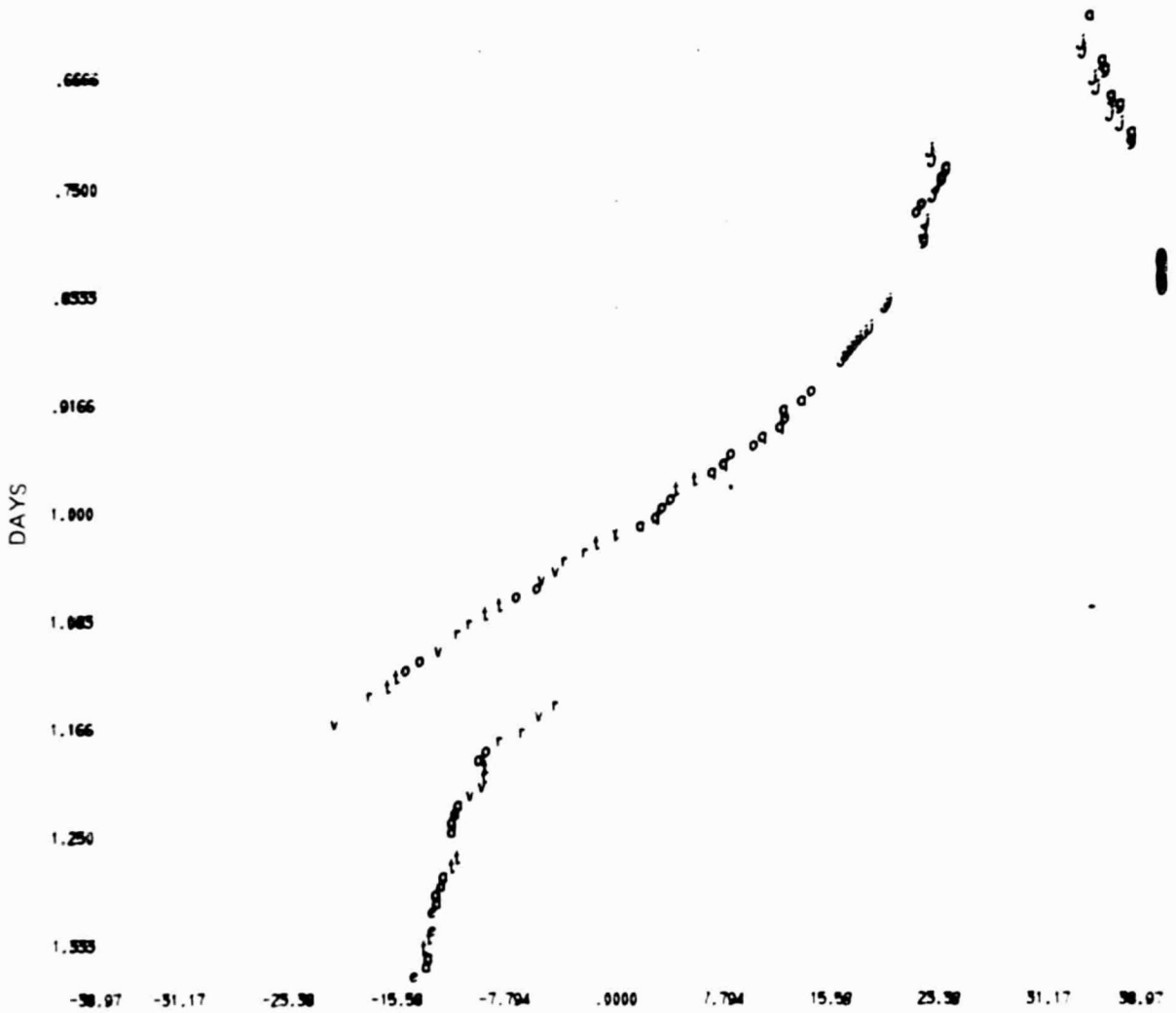

Figure 13. Detail of the Top Part of Figure 8, with the Vertical Scale Expanded

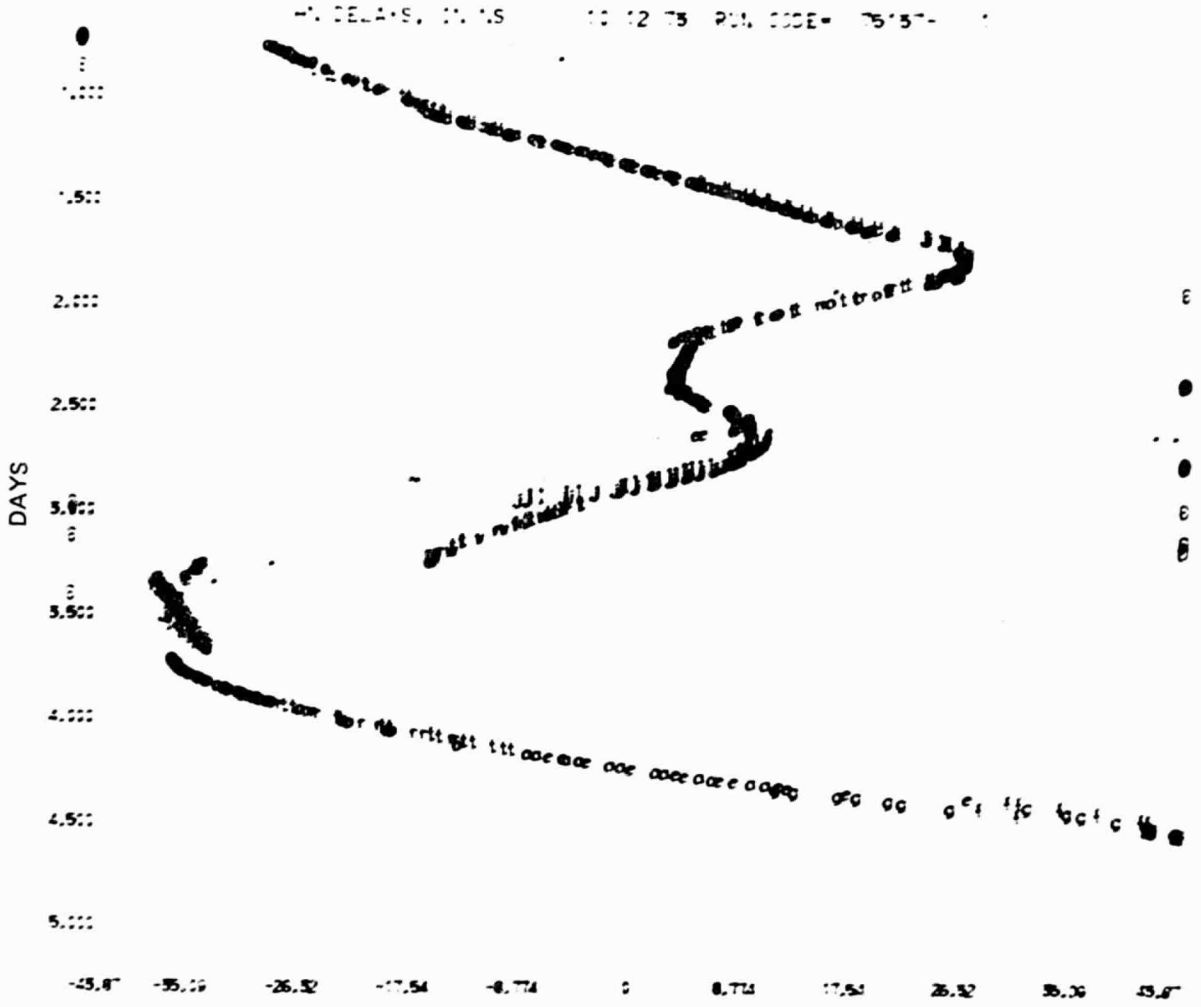

Figure 14. Delay Residuals Showing the Effects of Significant High Order Derivatives in the Clock Error at NRAO

the vertical scale. Since there are three distinct extrema in the first section of the curve, it looks as though a fifth-order clock-error polynomial is called for in this section. The second section of the curve is so short that a first-order polynomial (straight-line) will probably be adequate. The last section of the curve shows some curvature and will require at least a second-order polynomial. Figure 15 shows the residuals after fitting these polynomials to the data. The magnitude of the variation is reduced from 40 ns to about 10 ns, but it is obvious that some higher frequency noise is present. For the next stage, I tried fitting coefficients of a third-order clock-error polynomial between each extremum of the first section of the curve in Figure 15. The last section of the curve presents some special problems, however. It is shown with an expanded vertical scale in Figure 16. It is obvious that there is a discontinuity of some sort near t = 4.375 on the vertical scale, but where exactly is the break? The curves overlap, just as they did in Figure 13. The simplest way to deal with this problem is to eliminate all of the points in the bottom right-hand part of the curve. The remaining points show enough curvature to probably require at least a second-order polynomial. The residuals from this solution are shown in Figure 17. The residuals are now at a level of about 3 ns and are still quite systematic; however, at this level it is very difficult to sort out clock effects from the effects of errors in the a priori baseline and source-coordinate parameters. These errors

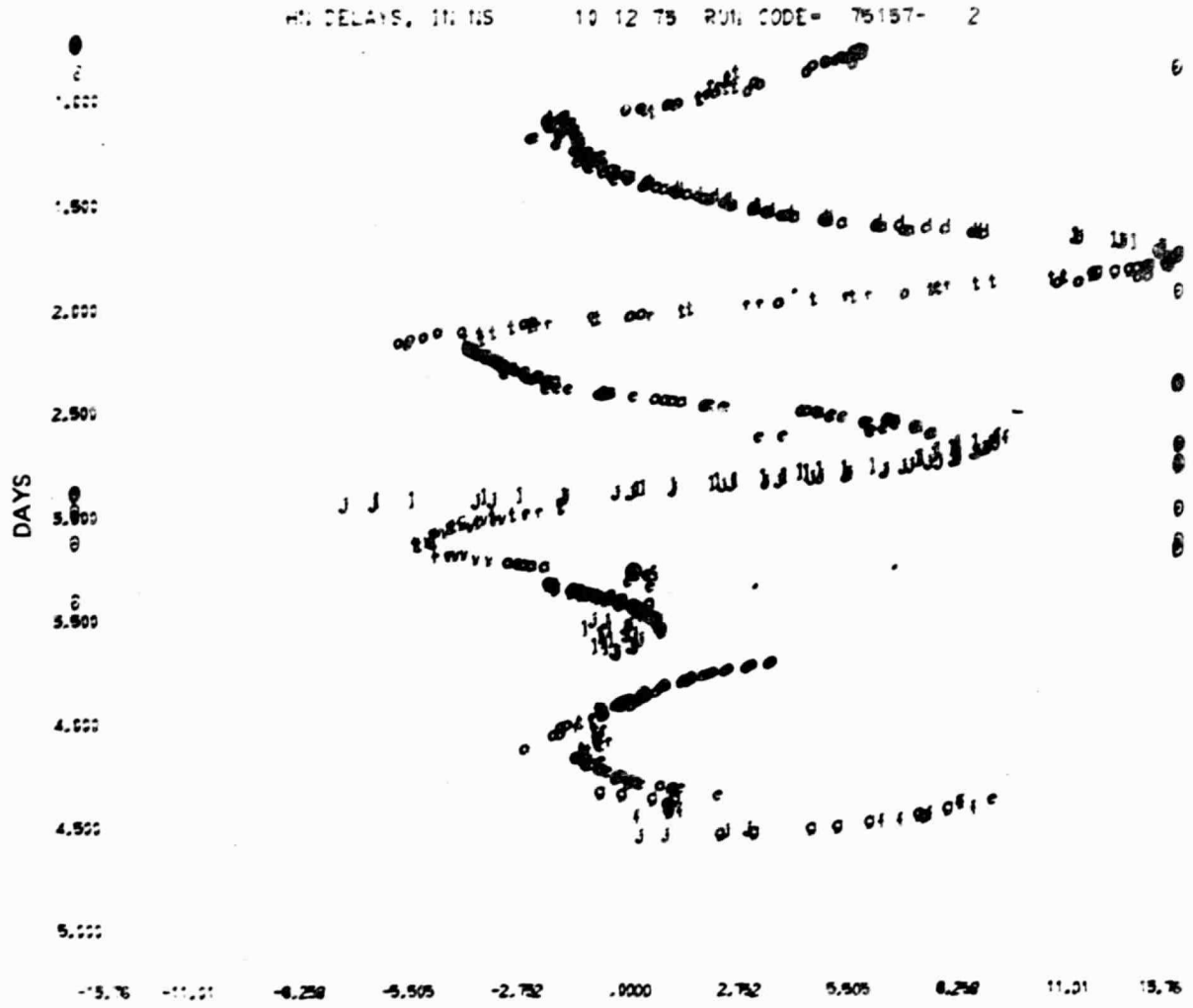

Figure 15. Same Data as Figure 14, with a Clock Error Model as Described in Section 4.4.5

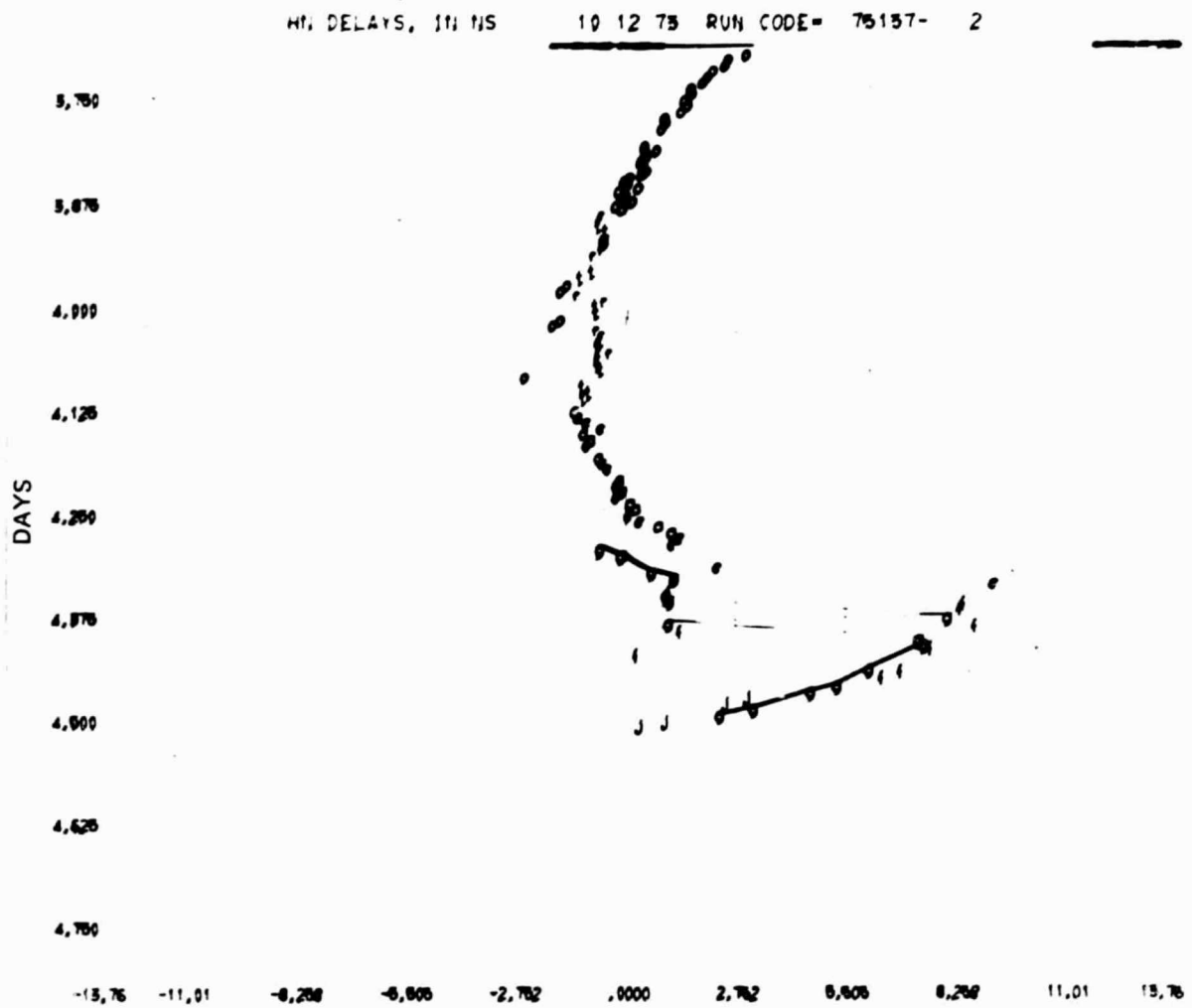

Figure 16. Detail of the Bottom Part of Figure 15, with the Vertical Scale Expanded

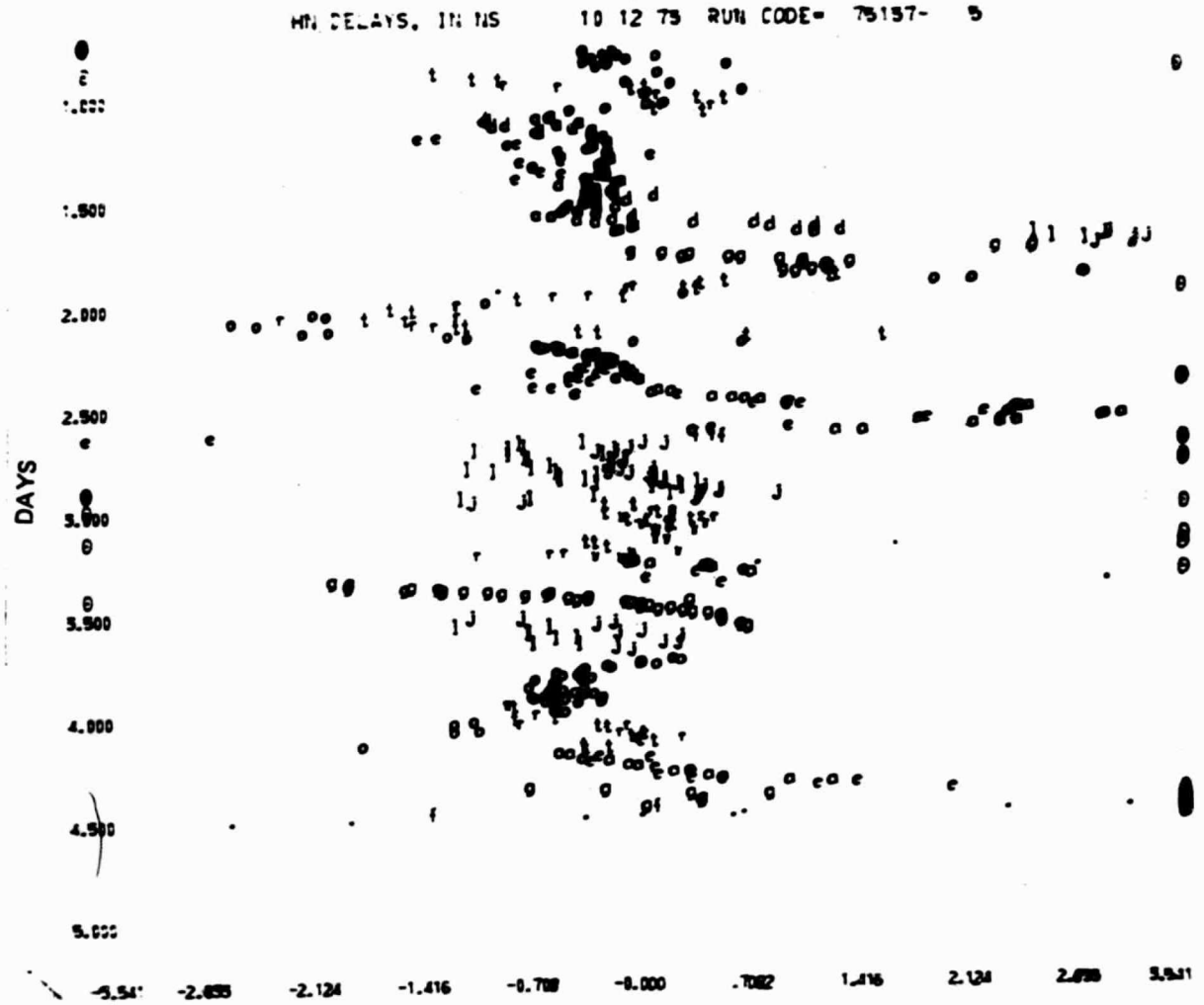

Figure 17. Same Data as Figure 14, with a Clock Error Model as Described in Section 4.4.5

represent the limiting factor in our ability to determine clock effects by this method.

In Figures 18-20 we see the residuals from a similar set of computer runs set up to determine a useful parameterization of the clock errors for data obtained in October, 1973, from the Haystack-Goldstone baseline. In Figure 18 are shown the residuals from a solution in which only the coefficients of the offset and rate terms in the clock-error polynomial have been estimated. Since there were two extrema on the residual p[illegible], the coefficients of a fourth-order polynomial were estimated, and the resulting graph of residuals is shown in Figure 19. The amplitude of the extrema decreased by less than a factor of two. Next I tried to estimate the coefficients of a separate second-order polynomial in each interval between the cusps (at t≈ 2.5, t ≈ 2.75 and t ≈ 2.85 on the vertical scale) which appear in Figure 19. The resulting residuals are shown in Figure 20. Once again, I approached the point where clock errors are hard to separate from a priori coordinate errors.

There are many reasons why the above procedure is unsatisfactory, not the least of which is that it is very tedious and requires large amounts of computer time. More fundamentally this technique is too dependent upon the all-too-fallible judgment of the operator. The number of possible parameterizations of the clock is too large, and the criteria for selecting one over another are too vague. This technique works reasonably well

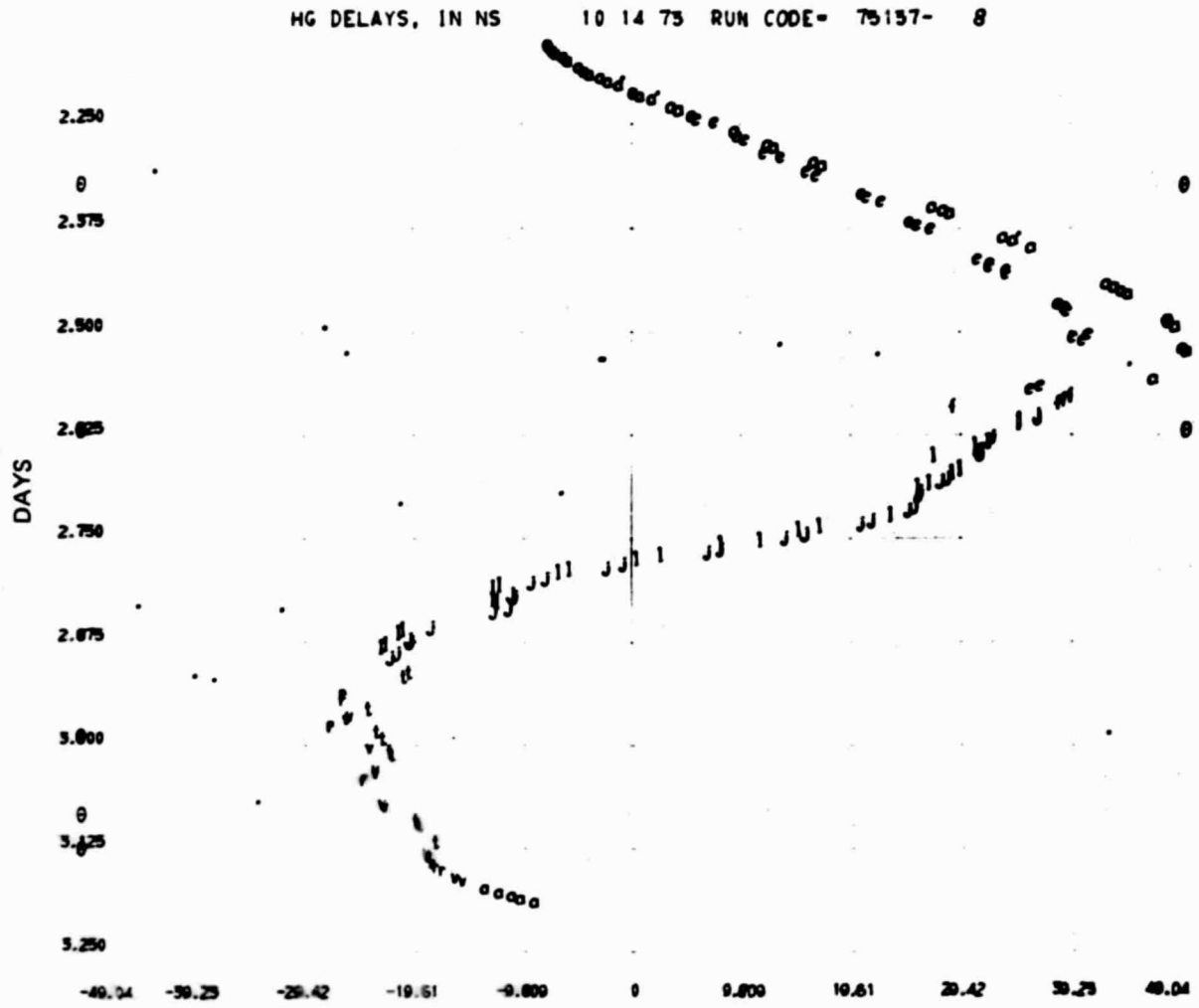

Figure 18. Delay Residuals Showing the Effects of Significant High Order Derivatives in the Clock Error at Goldstone

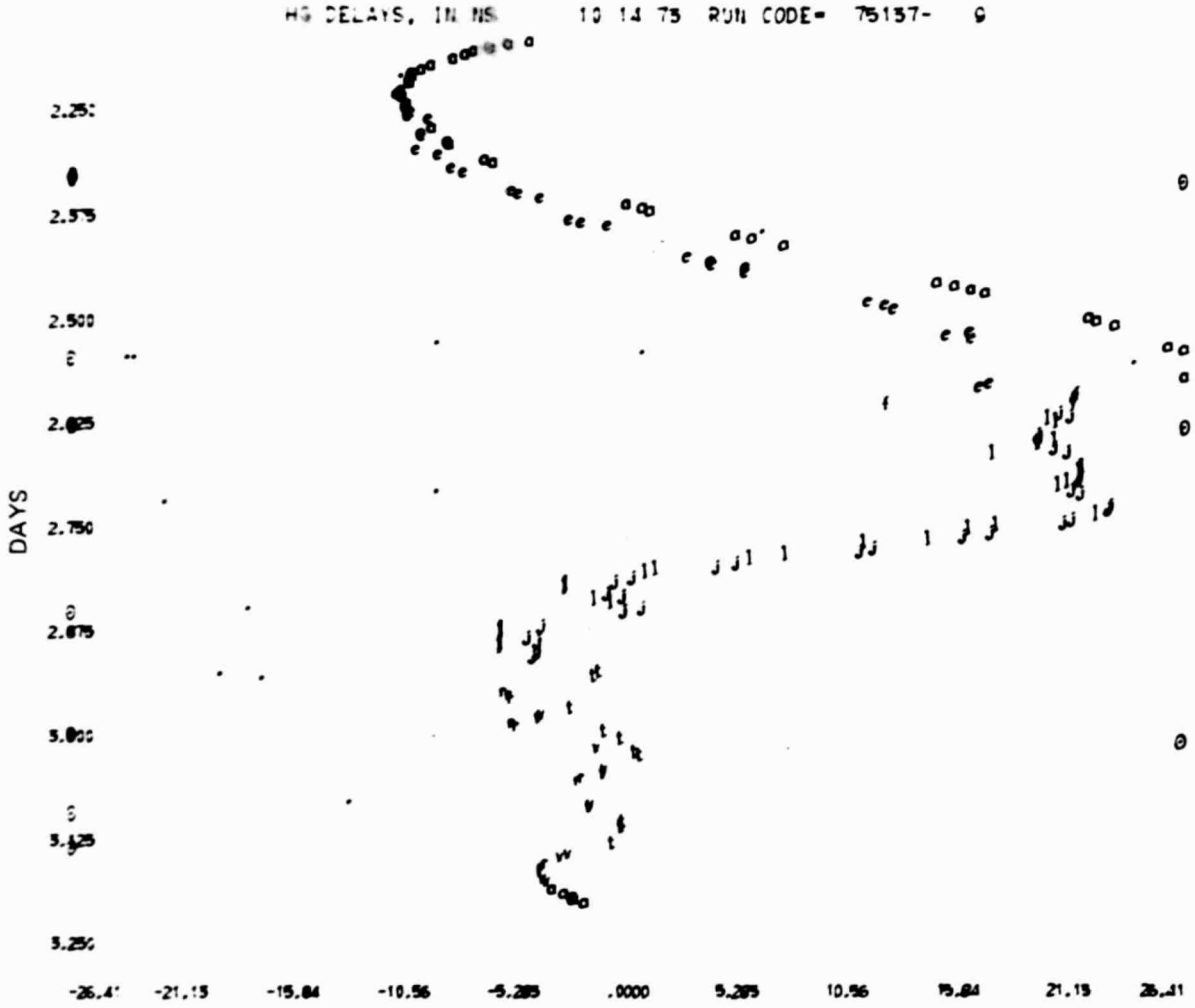

Figure 19. Same Data as Figure 18, with a Clock Error Model as Described in Section 4.4.5

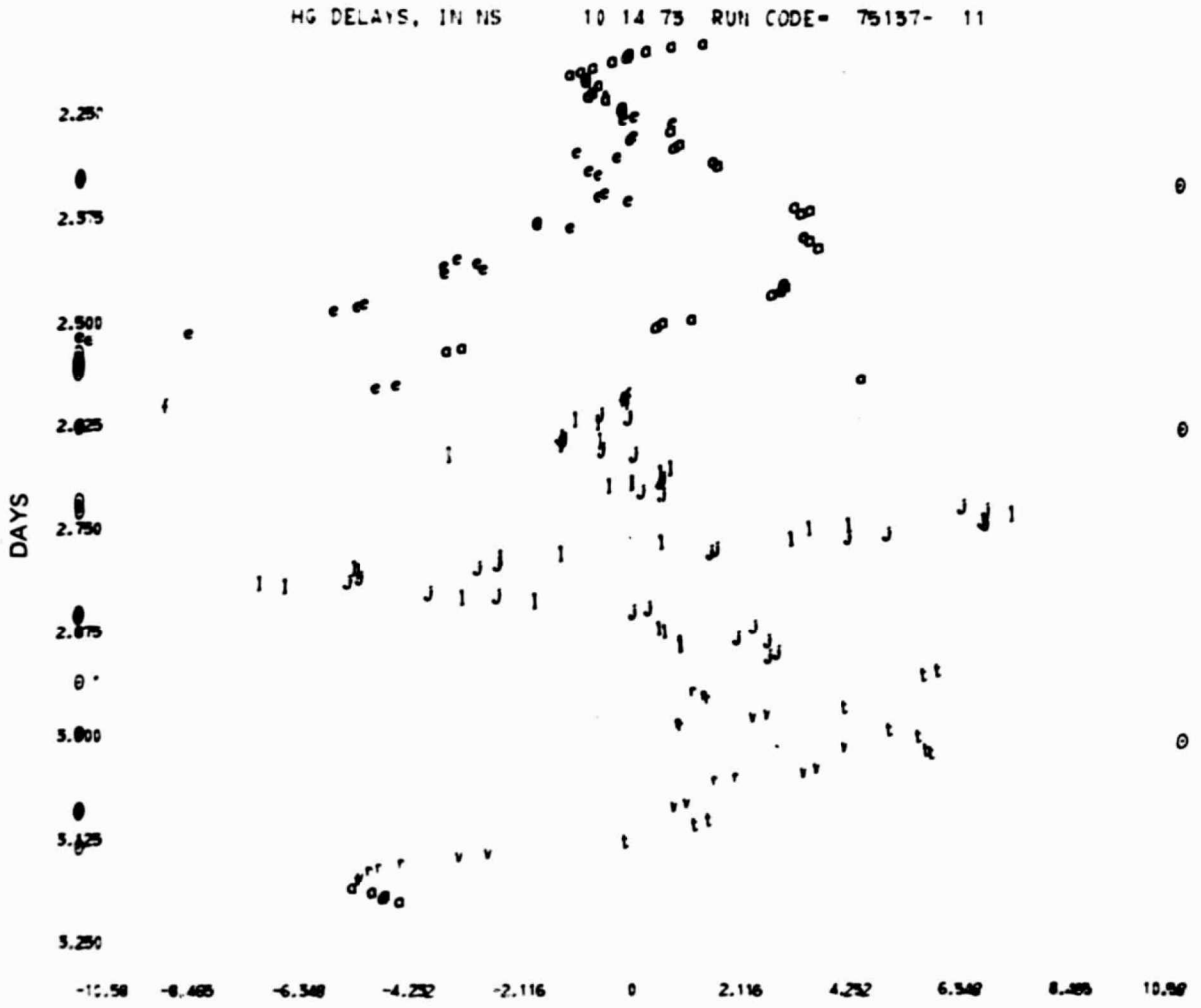

Figure 20. Same Data as Figure 18, with a Clock Error Model as Described in Section 4.4.5

when the clocks are well behaved, that is, when there is at most a small number of very distinct problems such as the clock-rate discontinuity shown in Figure 5. However, for badly behaved clocks the inadequacies of this technique led to the use of a scheme involving differenced observations as discussed in Chapter 2.

With differenced observables, the sensitivity of the data to clock errors drops dramatically. As noted in Chapter 2, if the observations to be differenced are exactly simultaneous, the clock errors disappear completely from the differenced observations. If the observations are not exactly simultaneous then the degree to which the clock errors are eliminated depends on the spectrum of the fluctuations in the clocks. That is to say, if the periods of the main Fourier contributions to the power in the fluctuations are short compared to the intervals over which differences are formed then there will be little advantage in using differenced data. If, however, the periods of these fluctuations are long compared to the differencing intervals, then the fluctuations will be largely eliminated by forming differenced observations, or other suitable linear combinations.

With differenced observations the problem of selecting the pairs of observations to be differenced replaces the problem of selecting among clock-polynomial possibilities. There is an astronomically large number ($\sim 2 \times 10^5$) of ways to combine the 600-odd observations in Figure 8 by pairs. The general con-

straints that we wish to observe in forming pairs for differencing are that the observations be closely spaced in time, and that they not be observations on the same source. (Forming differences of closely spaced observations of the same source loses almost all the geodetic and astrometric information contained in the observations.) To determine a reasonable criterion for the maximum spacing in time to be used for the differenced observations, it was noted that the clock-rate coefficients were typically around 2×10^{-12} sec/sec, so that a spacing of 30 minutes would give a maximum clock error for each differenced observation of less than five nanoseconds. Couple this result with the fact that the clock-rate offset can still be estimated with the differenced data (albeit with greatly reduced sensitivity) and it should be clear that differencing the data can reduce the effect of the clock error to the level of nanoseconds. (Differences which span clock discontinuities such as are seen in Figure 13 must be weeded out, of course. Fortunately, there are only a very small number of such cases.) Since there were about ten thousand observations to be differenced in the entire Phase II data set, it was not practical to select the difference pairs by hand, and a computer program was therefore written to select such pairs according to the following algorithm: The observations were scanned sequentially in time. If each of the first pair of observations was on the same source, the first observation was deleted, and the next two observations were con-

sidered as a pair. This process was repeated until a consecutive pair of observations was found on two different sources. The time interval between the observations was then checked. If it was found to be greater than 30 minutes, then the first observation was again deleted, and the process of searching for a consecutive pair of observations with different sources was resumed. If the time interval was found to be less than 30 minutes, then a differenced observation was formed from this pair of undifferenced observations, and the process of searching for a pair of observations on different sources was resumed with the observations following this pair. This scheme is not optimal; its virtue is simplicity. In particular if the observations are grouped, for example, by triplets on a given source this scheme may result in deleting more observations than is strictly necessary. That is, by deviating a small amount from a strict time sequence it may be possible to construct many more pairs within the 30-minutes time constraint if there are a number of clusters of observations on the same source within this limit. However, the general problem of constructing an optimal scheme for selecting differenced pairs has not been tackled.

The results quoted in Section 4.5 for the Phase II data up through July 1974, are all from solutions in which the data from every baseline involving NRAO or Goldstone were differenced according to the above scheme, except for the August 1973 data, in which the Goldstone clock was determined to have been well

enough behaved that only the data involving NRAO were differenced.

4.5 DISCUSSION OF THE RESULTS

4.5.1 Introduction

To obtain the results discussed in this section, the formal errors for the individual observations were first calculated from the signal-to-noise ratio as discussed in Reference 22. In order to test how closely the formal errors corresponded to the real scatter in the postfit residuals, the delay and delay-rate postfit residuals were calculated from a solution in which only the delay data were used to estimate the baseline, source-coordinate, atmosphere, and clock-error parameters. The rms value of the weighted residuals was then calculated:

$$W = \sqrt{\sum_i \frac{r_i^2}{w_i^2}/N}$$

where r_i is the residual for the i^{th} observation, w_i is the corresponding formal error, and N is the total number of observations. If the formal errors accurately reflect the scatter in the residuals, then W should be close to unity. The values of W for the delay residuals were nearly all in the range of 2.5 to 3.5, and the values of W for delay-rate observations were found to range from about 60 to about 130. The reason that the delay-rate formal-error calculations are so at variance with the observed scatter in the delay-

rate residuals is that the formal error calculations do not consider instrumental instabilities. In particular, the formal errors based on the signal-to-noise ratios have values on the order of 10^{-15} sec/sec, whereas the frequency standards used in the experiments were usually stable to no better than 10^{-13} sec/sec (Reference 12).

In order to ensure that the relative weighting of the delay and delay-rate data is appropriate for the residual scatter actually seen in each type of data, the formal errors for each observation were multiplied by the appropriate value of W calculated as discussed above. The resulting values for the formal errors were found to produce values for W from combined delay and delay-rate solutions which were close to unity. Since the clock errors appear to dominate the delay-rate errors, the formal errors for the delay rate should have been nearly uniform, rather than being based on the signal-to-noise values for those observations. However, a qualitative analysis indicates that the necessary changes in the delay-rate weighting function would not have a significant effect on the final estimates of the parameters.

4.5.2 Baseline Results

The baseline results displayed in Table 4* give the baseline length and the X, Y, Z components in the Earth-fixed coordinate system described in Chapter 3.** The reasons for displaying the length in addition to the three cartesian components are two-fold: first, the baseline length is intrinsically interesting since it is possible to construct the vector separations of a net of three or more stations solely from measurements of the lengths of the baselines between these stations; second, because length is invariant under rotation, it is unaffected by errors in the tabulated values for polar motion and UT1.

It can be seen from Table 4 that the baseline length solutions for each baseline from the different sets of observations have an rms scatter about the weighted mean of less than one meter. The scatter in length ranges from 79 cm for Haystack-Alaska to a mere 7 cm for Haystack-NRAO. The scatter in the baseline cartesian components is considerably larger, ranging up to 324 cm for the Z component of the Haystack-Alaska baseline. The reasons for the larger scatter on the components are two-fold: first, the components are affected by errors in the tabulated polar motion and

---

*See Appendix C for a discussion of the entries in Table 4.

**The metric-system lengths given in Table 4 and elsewhere in this thesis were based on the speed of light being 2.997925×10^5 km/sec.

UT1 values; second, the baseline error ellipsoids* tend to be "pancake" shaped, with the smallest axis roughly parallel to the baseline -- this is evidenced by the fact that the formal errors of some of the baseline components are larger than the formal errors of the baseline lengths.

It will be noticed that the deviation from the mean in some cases is very much larger than the quoted formal error (cf. the Haystack-Goldstone length from Run Number 75125-11 in Table 4). Are these results to be interpreted as wildly improbable statistical scatter? No, because the formal errors are based on an assumption that the noise in the data is gaussianly distributed with zero mean. In actual fact there are almost always systematic effects clearly visible in the postfit residuals. (These systematic effects are probably caused largely by clock variations and other instrumental variations and in part by the atmosphere and ionosphere.) When the deviation from the mean is very much larger than the formal standard error it is quite likely that the systematic errors predominate over the statistical errors. For this reason the scatter of the various results is likely to be a better measure of the true errors (systematic errors plus statistical errors) in the corresponding parameter estimates than are the formal errors themselves. It seems fair to say that, on the basis of the scatter of the various data

*For a discussion of error ellipsoids, see Reference 15, pp. 51-53.

sets, we have determined the length of all of our baselines with an uncertainty of less than one meter, and we have determined the equatorial components of each baseline with an uncertainty of about one meter, and the polar component with an uncertainty of several meters.

At this point, a word needs to be said about the relationship between these results and the results reported in References 13 and 18, which results were based on some of these same data. The primary difference between these results and those reported earlier was brought about by a change in the weighting function used in processing these data. In the earlier analysis the values for the standard errors in the observations were based on the signal strength and on the elevation angles, since it was assumed that the atmosphere would degrade the quality of the low-elevation data. However, no evidence could be found to support the idea that the low-elevation-angle observations were of significantly poorer quality than the high-elevation-angle observations. Indeed, a graph of residual magnitude vs. the root-sum-square value of the atmosphere corrections for the two sites shows no discernible dependence of residual size on atmosphere correction. The graphs for delay and delay rate are shown in Figure 21. The horizontal scale on these graphs represents the root-sum-square value of the atmosphere correction at each site, with the zenith electrical path length (ρ_i) of the atmosphere normalized to unity. (To convert the horizontal scale to an approximate value for atmospheric correction in seconds of time for delay

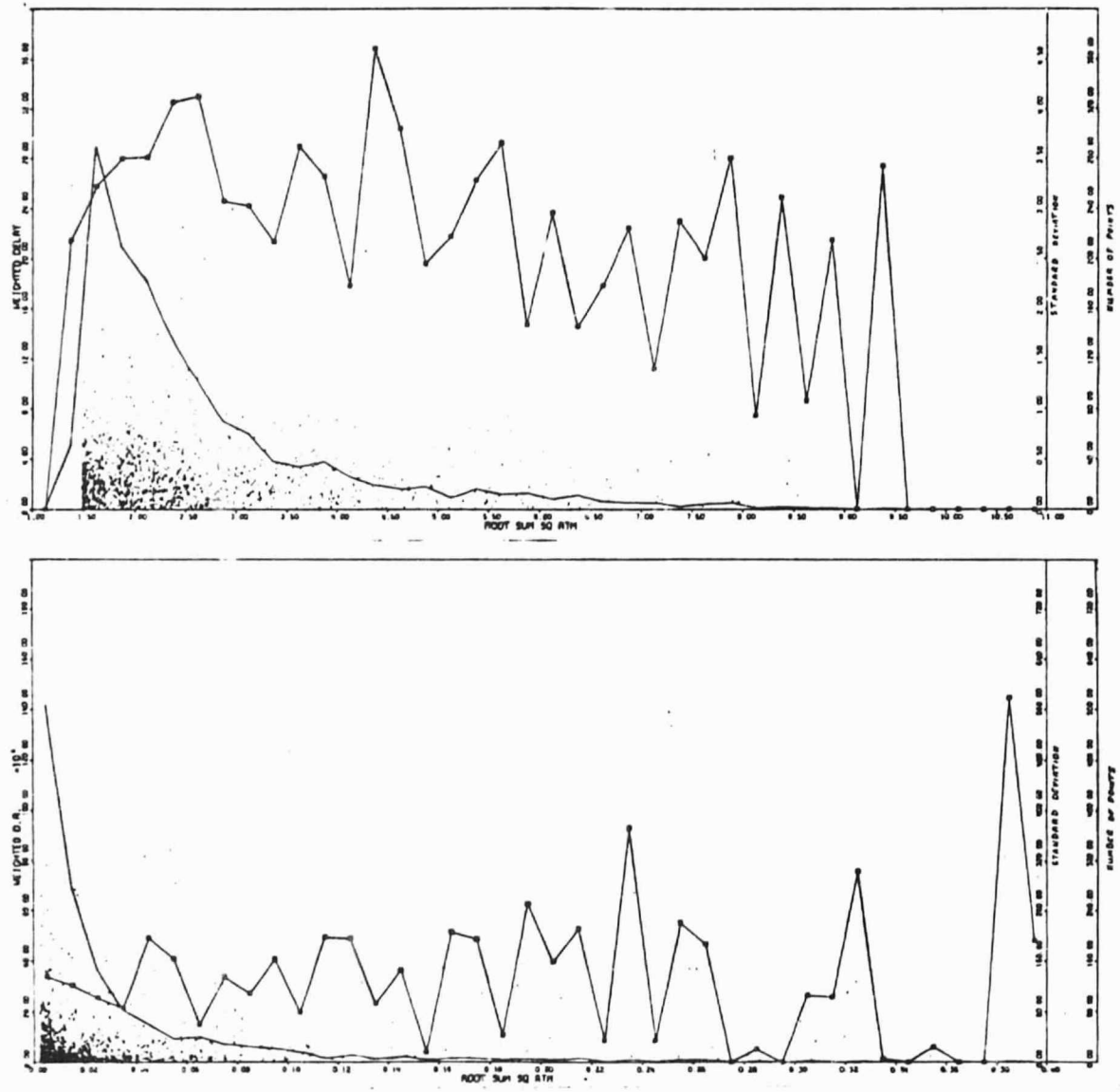

Figure 21. Magnitude of Delay and Delay Rate Residuals as a Function of Atmospheric Correction (see Section 4.5.2).

and seconds per second for delay rate, simply multiply each scale by 7×10^{-9} sec.) In order to eliminate the effects of variation in the signal-to-noise ratio between observations of different sources, each residual has been normalized to a dimensionless quantity by dividing the residual by its formal standard error based on the signal-to-noise ratio for that particular observation (Reference 22). In order to facilitate interpretation of these graphs, each graph has been divided into vertical segments with two segments between each fiducial mark on the horizontal scale. For each segment the total number of points within the segment has been graphed (plain curve) as well as the standard deviations of those points (curve marked with boxes as: -□-□-□). It can be seen that this latter curve shows no pronounced trend toward either larger or smaller residual standard deviation as the atmosphere correction increases. This graph should not be interpreted to mean that the atmosphere does not degrade the data, but rather that the residuals may be dominated by non-atmospheric effects. Therefore, the results quoted in this thesis have been based on relative standard errors for the observations derived from the signal-to-noise ratios only. This difference caused only small changes in the final estimated parameter values, but sometimes caused large changes in the formal errors for these parameter estimates. The other differences between these results and the results published earlier are all due to small corrections in the theoretical models used in VLBI3. These corrections are fivefold. (The maximum magnitudes of these effects are given in parentheses.) First, the BIH UT1 values have been used instead of the U.S. Naval Observatory UT1 values (~10 msec). Second, the effects of diurnal polar motion

have been added (~50 cm). (The diurnal polar motion and the change in UT1 values will not affect the estimation of baseline lengths, since both effects represent rotations of coordinates.) Third, the Earth-tide model has been improved (~3 cm). Fourth, the effects of antenna motion on delay rates have been added (~1.7 ps/sec; this affects only the Alaska data); and fifth, the effects of the time derivative of (A1-UT1) have been included in the delay rates (0.04 ps/sec). These effects are described in Chapter 3.

4.5.3 Source-Coordinate Results

The source-coordinate solutions are listed in Table 5. The reference for right ascension is the right ascension of 3C 273B, which has been fixed at $12^h\ 26^m\ 33^s.236$ (Reference 13). The coordinates shown in Table 5 are appropriate for solar-system barycentric coordinates — that is, the effects of elliptic aberration are not present. The scatter in right ascension for those sources for which there was a reasonable number of observations ranges from 0".02 to 0".09 (note that the table entries are in time-seconds rather than arc-seconds) while the scatter in declinations ranges from 0".02 to 0".23. The largest scatter in the declinations occurs for sources whose declinations are in the range of +5° to -5° (3C120, 3C273, 2134-00). This increase in scatter for the low declination sources is to be expected, since the sensitivity of delay and delay-rate observations to the declination of the sources decreases as the declinations go to zero. (The reason for this decrease in sensitivity to the source declination is that the derivative of delay rate with respect to source declinations goes to zero as the declination goes to zero. The reason for the decrease in sensitivity for delays is slightly more compli-

cated. If we resolve the delay into a sinusoidal component and a constant component [as in Equation (2-3)], then the derivative of the sinusoidal component with respect to declination goes to zero as the declination goes to zero. The only sensitivity to declination at zero declination from either delay or delay-rate observations thus comes from the constant component of delay.) Our previously published results on source coordinates (Reference 13) were based on some of these same data. The results in Table 5 agree with those earlier results for each coordinate to within less than 1.5 times the standard errors quoted in the reference. It seems fair to say that, except for the declinations of the low-declination sources, we have determined the positions of these sources with a standard error of less than a tenth of an arc-second in all cases.

4.5.4 Baseline-Closure Tests

It is all very well to repeat a measurement N times and then claim that the scatter in the results is related to the real uncertainties in the measurement procedure, but actually this scatter only places a lower bound on the uncertainty. If there are systematic errors which repeat from run to run, the effects of these errors will not show up in the scatter of the results. It is therefore desirable to have additional tests of the consistency of the data which are not based on mere repetition. One important test involves separating the multi-station experiment data by baseline and solving for each baseline separately, and then checking to see how well the resulting baseline solutions form closed triangles. The results from this type of test are given in Table 6. The stations involved in each triangle are indicated by the same station codes as are used in Table 4.

The column labeled "Data" indicates which experiments the data for each baseline came from, according to the following code:

1 = May-June, 1972

2 = August, 1973

3 = October, 1973

4 = January, 1974

5 = March, 1974

6 = April-May, 1974

7 = July, 1974

8 = January, 1975

It will be seen that in Table 6 all the data from baselines in a given triangle were taken from the same experiment.

All of the X and Y component closure errors for the H-N-S triangle are less than one meter, and the Z component, which is more poorly determined, closes to within two meters or better. On the H-N-G triangle the X components all close to within 30 cm or less, while the Y and Z components, which are less well determined (cf. Table 4) close to within 2.5 meters or less. The remaining triangles are too degraded by the poor coverage of data on the G-S baseline to match these results, but nevertheless their closure results are in fair agreement with their much larger formal errors.

It has been argued that in a three-station experiment the delays on the third baseline are not independent of the delays on the remaining two baselines, and that therefore the closure

test as just examined does not really test the validity of the VLBI measurements. To sidestep this problem the baseline results used to compile Table 6 were re-combined into triangles with the requirement that no more than two of the baselines could be obtained from data from a single experiment. A small fraction of the hundreds of such possible combinations is shown in Table 7. The problem with examining closure in this manner is that the results have been degraded by possible errors at the meter level in the tabulated polar-motion and UT1 information used in the solutions. Therefore these results cannot be expected to close to much better than one meter or so. Nevertheless the results of this closure test place bounds on the total errors in the baseline parameter estimations, for on the triangles which have a reasonable amount of data for all baselines (H-N-S and H-N-G) practically all of the closure errors are less than two meters. These results at the very least fail to contradict our claim to meter level or better accuracy in the baseline determinations.

4.5.5 Antenna-Axis-Offset Solutions

Another interesting test of the consistency of the VLBI measurements concerns the magnitude of the antenna-axis offsets discussed in Chapter 3. The axis offset is one of the few parameters which affects the VLBI observables and can be measured accurately by conventional techniques to the centimeter level or better. If we therefore use the VLBI data to estimate this axis offset, and compare the results to the known values we can

perhaps set some bounds to the expected errors in the baseline solution values. This test is not perfect, as the sensitivity of the measurements to the axis offset will not, in general, be the same as the sensitivity to the baseline components. Nevertheless, this test provides an interesting check on the entire VLBI procedure. The results from this type of test are shown in Table 8 where the data-set codes are the same as in Tables 6 and 7. The measured values for the various antenna axis offsets are as follows*:

Alaska	7.2898 m
NRAO 140'	14.9273
Onsala	2.15

The Alaska and NRAO results seem to confirm our statements regarding meter-level accuracy of the solutions. A question which requires an answer, of course, is why there is so little sensitivity to the Sweden axis offset, especially as compared to the NRAO sensitivity, since both telescopes are equatorially mounted. A possible reason for the difference is that the

---

*The value of the Alaska antenna-axis offset was obtained from a personal communication from Mr. Sal Rocci of Rohr Industries, Soladyne Division, San Diego, California. The value of the NRAO antenna-axis offset was obtained from NRAO Drawing #36D00022, March 28, 1973. The value of the Onsala antenna-axis offset was obtained from Reference 12.

Sweden baselines are necessarily poorer in declination coverage because of the high latitude of the Sweden station, and poorer in hour-angle coverage because of the longitude of the Sweden station.

4.5.6 Polar Motion and UT1

It has been recognized since the late 19th century that the Earth's rigid crust is not fixed relative to its pole of rotation, nor is the Earth's rate of rotation constant. The I L S and the B I H have monitored the location of the pole of rotation since the early part of the 20th century and they publish at 5-day intervals the Cartesian coordinates of the pole relative to a defined mean pole. In addition, by the middle of the 20th century, clocks had been developed which had sufficient stability to allow determination of the irregularities in the Earth's rate of rotation. Thus, in 1956, the B I H began measuring and publishing the difference between time as kept by the spinning Earth (UT1) and time as kept by their atomic clocks (A1 or UTC) (Reference 1).

We have used both the Phase I and the Phase II data sets to estimate both the coordinates of the pole with respect to an Earth-fixed coordinate system and the differences between A1 and UT1. The differences between our estimates and the B I H estimates are tabulated in Table 9. For those experiments in the Phase I data set that involved only a single baseline, only one component of the pole position was esti-

mated, along with the A1-UT1 offset, since there are only two degrees of rotational freedom for each baseline. In any event, the component of the pole position and the (A1-UT1) offset cannot be estimated simultaneously with the estimation of the orientation of the baseline. To do so would be to attempt to determine the orientation of the baseline in addition to its 3 vector components. To surmount this problem, the coordinates of the pole and the (A1-UT1) offset were fixed at the B I H values for part of the data in both the Phase I and the Phase II data sets. The selection of the data set to be fixed was, by nature, somewhat arbitrary, and it should be noted that any errors in the B I H polar motion and (A1-UT1) values for the days selected will bias all of the polar motion and UT1 estimates. In the Phase I data set, the X component of the polar motion and the A1-UT1 offset were fixed for the August, 1972 data, in order to be consistent with our previously published results (Reference 18). In addition, the Haystack-Goldstone data set from January, 1975, because of its similarity to most of the Phase I data sets (one baseline, one day of observations, and well-behaved clocks at both stations) was processed with the Phase I data. Three of the Phase I experiments involved three stations, and therefore the second (Y) component of the polar motion could be estimated for any two of these experiments if it were fixed for the third. The Y component of the polar motion was therefore fixed for the June 6-

7, 1972 data. In the Phase II data set (exclusive of the January, 1975 data) both components of the polar motion and the (A1-UT1) offset were fixed for the January, 1974 data. All of the Phase I and the Phase II data should have been included in a single computer run to estimate all of these polar-motion and UT1 parameters simultaneously. Unfortunately neither of our data processing programs is able to handle the number of parameters required for such a solution. We have therefore processed the Phase I data in two separate solutions, as described below, and the Phase II data in five separate solutions. It would be possible, of course, to reduce our observations to "normal points", that is, to condense each data set down to its relevant essentials and thereby streamline the computer analysis of the entire data set. The computer programs required to create such normal points have not yet been written.

The polar-motion and (A1-UT1) values for the first 8 experiments given in Table 9 are not identical with the values published in Reference 18. One of them, the X component of polar motion for March, 1973, is different from the published value by more than twice its formal error. There are several differences between the way in which the data were handled for the results reported in this thesis and the way in which they were handled for results reported in Reference 18, in addition to the differences noted in Section 4.4.4. First, all of the Phase I data (except the January, 1975 data which had not yet been obtained) were included in a single solution for the results

reported in Reference 16. For the results reported in this thesis, the data before August 1972 were included in one solution, and the Phase I data after August 1972, together with the Haystack-Goldstone data from January 1975, were included in a second solution. Second, because of the problems noted in Section 4.4.4, the data from June 27-28, 1972, were not included. All of these changes affect the way in which the systematic errors present in these data affect the solutions. The fact that three of the results changed by about twice their formal errors suggests that the "real" uncertainties in many of these results might be at least of the order of twice the formal errors (see, also, p. 112). The mean and standard deviation of the differences between our polar motion and UT1 estimates and the corresponding BIH measurements is given in Table 10. The corresponding values from Reference 18 are also given.

The postfit residuals from the solutions discussed in this section have a somewhat different character than the residuals from the solutions discussed in Sections 4.5.2 and 4.5.3. A "typical" set of residuals from a polar-motion and (A1-UT1) solution is shown in Figure 22. The residuals shown are the August 29-30, 1972 delay residuals from the second Phase I solution discussed above. The residuals are much more systematic than the residuals from solutions which include only the August 29-30, 1972 data (cf. Figure 11). These systematic trends are apparently caused by variations in the instrumental delay since the trends seem to be common to all of the data even though the data include interleaved observations on many different sources. These trends are apparently being masked in the single-day solutions by adjustments of the baseline.

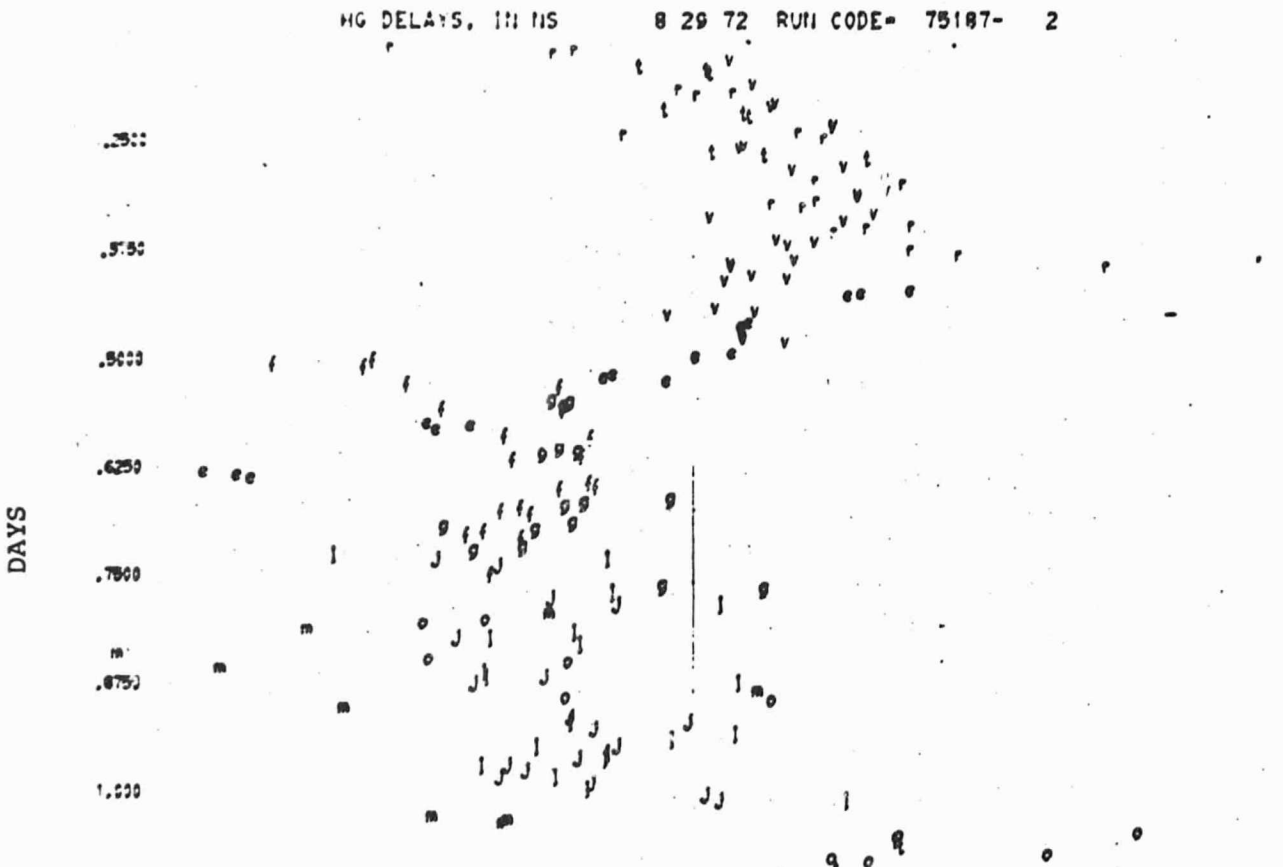

Figure 22. Delay Residuals from a Polar Motion and UT1 Solution

coordinate and source-coordinate parameters. Figure 23 shows residuals from a solution involving the same data set as employed in Figure 22 but with the coefficients of a third-order clock polynomial being estimated for each day's data. The systematic trends shown in Figure 22 are greatly reduced. Two of the eight polar motion and (A1-UT1) values estimated in the solution using third-order clock polynomials differed from the results shown in Table 9 by nearly five times the formal errors for those parameters. More work is needed to investigate fully the effects of systematic errors on the polar-motion and A1-UT1 results.

4.5.7 The Precession Constant

The action of the gravity fields of the Sun and Moon on the Earth's equatorial bulge produces a motion of the Earth's spin axis which is referred to as the luni-solar precession (Reference 22, pp. 181-184). In ecliptic coordinates the motion of the spin axis can be described by two parameters. In effect, the first parameter is the "mean" angle between the spin axis and the ecliptic pole, and is referred to as the mean obliquity. (See Reference 24 for precise definitions.) The second parameter, in effect the rate at which the spin axis rotates about the ecliptic pole, is referred to as the precession constant. In Reference 1, the values for these constants at the 1950.0 epoch are given as:

Mean Obliquity = 23° 26' 44".84

Precession Constant ≡ P = 5026".75/century

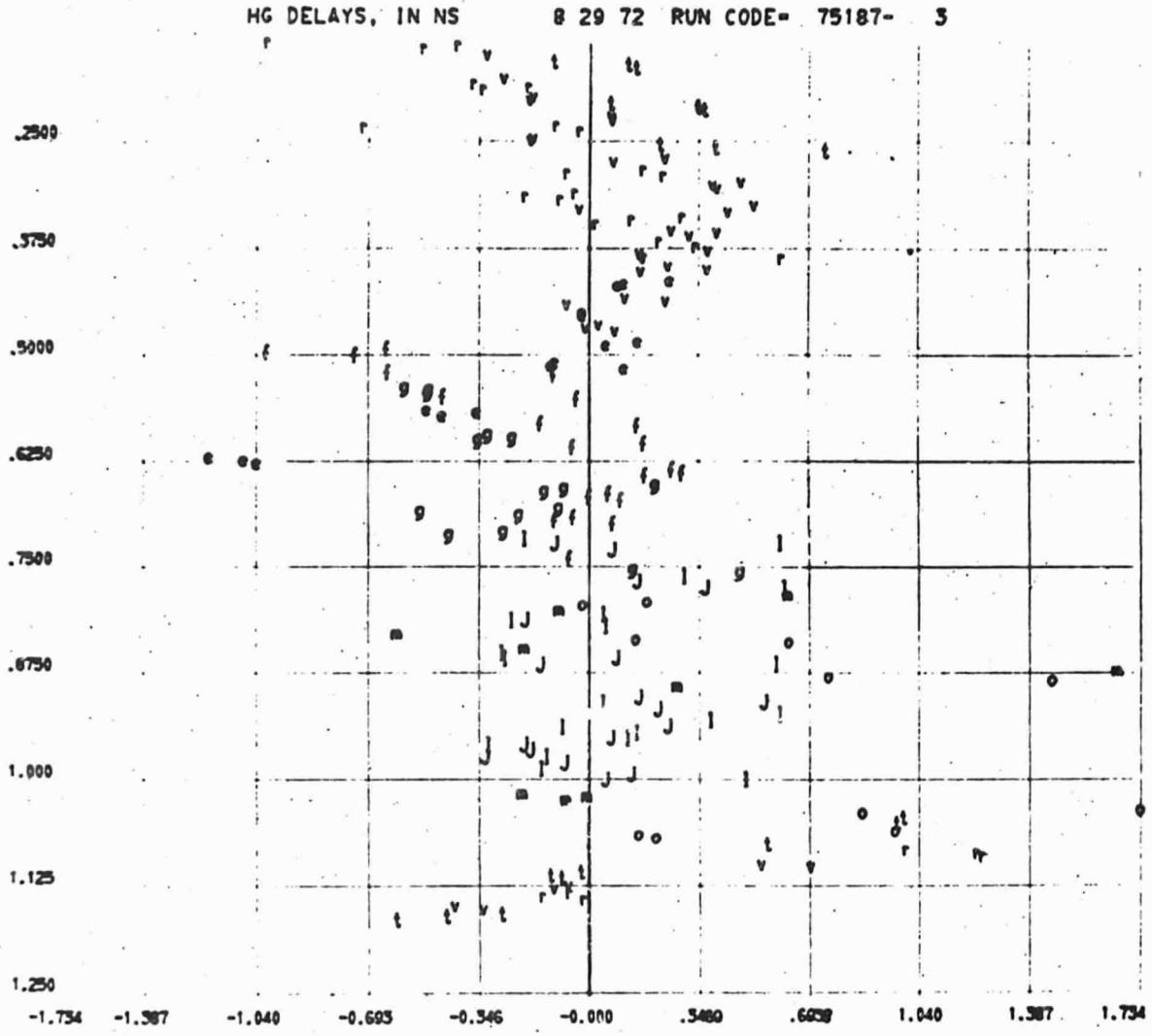

Figure 23. Same Data as Figure 22, with a Clock Error Model as Described in Section 4.5.6

In other words, the spin axis completes one revolution about the ecliptic pole in ~26,000 years. Since VLBI observations have virtually no sensitivity to the location of the ecliptic plane, we do not expect to measure the mean obliquity from VLBI data alone. However, we can measure that portion of precession which results from the motion of the Earth's pole in space.

As mentioned in Section 4.5.6, it is not possible with our present processing programs to combine all of our data into a single solution. We have therefore selected a subset of our data to use in solving for the precession constant. We selected these data according to two criteria: first, the data should be reasonably free of clock problems; second, the data should span a reasonably long time interval. We therefore selected the Haystack-Goldstone data from August 1972, November 1972, February 1973, March 1973, and January 1975, for a single solution to estimate the precession constant, P. [The baseline coordinates, source coordinates, clock-error coefficients, and polar-motion and (A1-UT1) parameters were also estimated.] The result from this solution was:

P = 5036±1 arc-sec/century

To see whether the addition of a third site would improve our sensitivity to the precession constant, we used the Haystack-NRAO-Goldstone data from August 1973 and January 1975 to estimate P with the following result:

P = 5029±2 arc-sec/century

The difference between this value and the classical value (~2 arc sec/century) represents an angular error of only 0".03 over the 1.5 years spanned by the data. For the first solution discussed

the angular error is about 0".2 over the 2.5 years spanned by those data. These equivalent differences in angle are comparable in magnitude to the scatter in the source-coordinate results reported in Section 4.5.3. More accurate VLBI data or a longer time span of data or both will be required to add significantly to our knowledge of the precession constant.

4.5.7 The Love Numbers

The model for the motion of the Earth's crust in response to the tidal generating potential of the Sun and the Moon is described in Equations (3-27) and (3-28). Since the positions of the Sun and Moon are quite well determined, we can calculate the disturbing potential, u, to much higher accuracy than is required for Earth tide calculations. What is less well determined is the response of the Earth to this potential, as expressed by the Love numbers ℓ and h. We would, therefore, like to estimate these numbers from the VLBI observations.

Now the magnitude of the vertical displacement of the Earth's crust [see Equation (3-27)] is about 30 cm, whereas the lateral displacements are about an order of magnitude smaller. Since 30 cm is about the size of the scatter in most of our baseline results it is clear that we will have little chance of obtaining a useful estimate of the lateral tidal displacements. However, we did anticipate obtaining a useful estimate of h. We obtained the following estimates from different sets of data:

$h = .54 \pm .02$

$h = .52 \pm .02$

$h = .66 \pm .03$

where the first value is from a data set containing the same data as described in the first solution in Section 4.5.7, the second value is from a data set containing all of the Haystack, Goldstone, and Alaska data from April 1972 through August 1972, and the third value is from a data set containing Haystack, NRAO, and Goldstone data from August 1973 and January 1975. In all solutions, the baseline coordinates, source coordinates, clock-error coefficients, and polar-motion and (A1-UT1) parameters were also estimated. The total discrepancy between the first and third values listed above represents a change in station displacement of about 6 cm. It seems clear that with markedly improved VLBI data (the prospects for which will be described in Chapter 5) VLBI will become a sensitive test for measuring Earth tide effects. In fact, it can be shown that by exploiting the fact that the phase of the tidal perturbation is often well known, it should be possible to estimate a separate value for h at each station, and thereby determine the inhomogeneities of the Earth's response to the tidal potential. The programming required to implement this possibility has not yet been undertaken.

CHAPTER 5

CONCLUSIONS AND PROGNOSIS FOR FURTHER PROGRESS

In Chapter 4 we saw that VLBI observations have been used to estimate baseline lengths with uncertainties of less than one meter, and to estimate source coordinates with uncertainties less than a tenth of an arc-second. In addition, these data were used to estimate polar motion, A1-UT1, the precession constant, and the Love number, h. Still, there is a great deal more work that needs to be done with these same data. Much of this work involves improved methods of dealing with very badly behaved system clocks, including such things as optimizing schemes for forming differenced observations and for forming more general linear combinations of observations. In addition, one would want to experiment with the use of Kalman filters and stochastic models for clock errors. Other things which could be done to improve our treatment of these data include improvements in our data processing programs which would allow, for instance, more parameters to be estimated simultaneously. (The present programs are restricted to a maximum of about 120 parameters.)

We also anticipate improvements in the equipment used to make VLBI observations, improvements which should eliminate many of the problems discussed in Chapter 4. The most obvious problem is the one caused by badly behaved system clocks. Since we have seen that hydrogen maser clocks can be made to operate close to their purported stability limit of one part in 10^{14} (cf.

Figure 11), the obvious solution to the clock stability problem is to insure that only such clocks are used as meet these specifications. Another method of improving clock behavior would involve the use of two or more clocks at each station. Each clock could be used to monitor the performance of the other clock(s). This method is likely to prove to be prohibitively expensive, unfortunately. As discussed in Chapter 2, clock problems can also be eliminated by using suitable linear combinations of observations.

In the future it should be possible to eliminate the ionospheric effect on the VLBI observations by using receivers capable of making observations simultaneously at two frequencies, say, at S-band and at X-band. The neutral atmosphere, being non-dispersive, presents a more difficult problem. One method of dealing with the neutral atmosphere depends on resolving the atmospheric effect into two components, one due to the water-vapor content of the atmosphere (the "wet" component), and the other due to the rest of the atmosphere (the "dry" component). The advantage of this scheme is that the dry component is much more uniform spatially and temporally than the wet component. The dry component could therefore be modeled in the same manner as was described in Chapter 3 for the total atmospheric effect, while the wet component could be monitored through observations of the brightness temperature of the atmosphere near and at the 22 GHz water-vapor absorption band.

Another anticipated improvement in the VLBI equipment in the near future is the development of wide band (~50 MHz) tape recorder systems. (The tape recorders employed in the experi-

ments reported in this thesis are limited to a maximum bandwidth of 360 KHz.) This additional bandwidth could not only make possible the elimination of the group-delay ambiguity, as mentioned in Chapter 4, but will also allow the use of very much smaller antennas to achieve the same signal-to-noise ratio as is attainable with larger antennas employing the smaller bandwidth. The ability to employ smaller antennas is important, since the number of antennas the size of Goldstone or even Haystack is small, and observing time on such antennas is severely limited. There is, on the other hand, a substantial number of smaller antennas (10m to 25m in diameter) around the world. Also, the ability to use smaller antennas opens up the possibility of using small transportable antennas, thereby allowing VLBI stations to be set up nearly anywhere on the land surface of the Earth, as proposed in Reference 17. Recently, some experiments have been performed with a relatively large (≈10 m diameter) transportable antenna (Reference 11); however, use of the wider-band recording system will enable at least a threefold reduction in size while still yielding higher system sensitivity.

In addition to increasing the instantaneous, or recorded bandwidth, it should be possible to increase the synthesized bandwidth by employing wider band amplifiers, thereby reducing the uncertainty in the group-delay measurements.

Finally there is the problem of optimizing our observation schedules for the purpose of estimating baseline components (or whatever other parameters we wish to estimate from VLBI data). It should be possible to employ linear programming analysis to improve, if not optimize, our observation schedules.

TABLE 1

Station Parameters

	HAYSTACK	GOLDSTONE	ALASKA
Location	Westford, Mass	Mojave, Calif.	Gilmore Creek, Alaska
Organization	Northeast Radio Observatory Corp	Jet Propulsion Laboratory	National Oceanic Atmospheric Adm.
Antenna Diameter	120'	210'	85'
Configuration	Cassegrain	Cassegrain	Prime Focus
Mount	AZ/EL with intersecting axes	AZ/EL with intersecting axes	X/Y with Y axis offset 287"
Locations Initially Assumed (Geodetic, West Longitudes)	LON = 71 29 19.201 LAT = 42 37 23.00 ELEV = 145 m	LON = 116 53 19.150 LAT = 35 25 33.446 ELEV = 1030.85 m	LON = 147 29 41.955 LAT = 64 58 42.667 ELEV = 322 m
Low Noise Amplifier	Cooled Paramp	Maser	Uncooled Paramp
Approximate System Temperature	70°K	30°K	300°K
Number of Tape Drives Used During Most Experiments	2	2	1
Antenna Slew Rate	2°/sec	≈ 0.2°/sec	2°/sec

TABLE 1 (continued)

Station Parameters

	SWEDEN	NRAO
Location	Onsala, Sweden	Green Bank, W. Virginia
Organization	Chalmers University of Technology	National Radio Astronomy Observatory
Antenna Diameter	84'	140'
Configuration	Cassegrain	Prime focus
Mount	Equatorial with DEC axis offset 85"	Equatorial, with DEC axis offset 48'11".69
Locations Initially Assumed (Geodetic, West Longitudes)	LON = 348 4 47.2 LAT = 57 23 36.10 ELEV = 14 m	LON = 79 50 09.47 LAT = 38 26 15.54 ELEV = 816.9 m
Low Noise Amplifier	Maser	Cooled Paramp
Approximate System Temperature	50°K	120°
Number of Tape Drives Used During Most Experiments	1	1
Antenna Slew Rate	0.25°/sec	0.25°/sec

TABLE 2

Description of Experiments

DAY	STATIONS (See Appendix C)	SYNTHESIZED BANDWIDTH (MHz)	GROUP-DELAY AMBIGUITY (μsec)
1972			
Apr 14-15	H-G	39	1/3
May 9-10	H-G-A	39-69-39	1/3
May 29-30	H-G-A	39-69-39	1/3
June 3-4	H-A	69	1/3
June 6-7	H-G-A	39-69-39	1/3
June 27-28	H-G	39	1/3
Aug 29-	H-G	23	1
Nov 7	H-G	23	1
1973			
Feb 4-5	H-G	23	1
Mar 30-31	H-G	46	1/2
Apr 11-13	H-S	23	1
May 18-23	H-S	23	1
Aug 10-14	H-G-N-S	*	1/3
Oct 12-16	H-G-N-S	*	1/6
1974			
Jan 22-23	H-G-S	*	1/2
Mar 4 - 8	H-G-N-S	*	1/2
Apr 29-May 3	H-G-N-S	*	1/2
July 8-12	H-G-N-S	*	1/2
1975			
Jan 14 -17	H-G-N	*	1/2

*For these experiments the synthesized bandwidth was changed during the experiment. Full details are available in the Haystack archives.

TABLE 3

Auxiliary Information on Experiments

Nominal Center Frequency	7850 MHz
Polarization	Left Hand Circular (IEEE def.)
Recorder Bandwidth	720 K Bits/sec or 360 KHz
No. Tracks	6 Data plus 1 parity - 7
Density	800 characters per inch
Nominal Record Length	0.2 sec
Nominal Tape Length	3 minutes
Frequency Switching Period	0.2 sec
Maximum No. Frequencies	8

RUN	DATE M D Y	BASELINE	VALUE CM	DIFF CM	SIGMA CM	
75126- 21	4 11 73	HS LENGTH	559938598,0938	-164,7344	87,7759	*
75126- 18	5 18 73	HS LENGTH	559938733,3906	-29,4375	59,0161	*
75126- 3	8 10 73	HS LENGTH	559938792,7656	29,9375	29,8701	*
75126- 6	10 12 73	HS LENGTH	559938747,1406	-15,6875	49,6505	*
75126- 8	1 22 74	HS LENGTH	559938843,7500	80,9219	109,3671	*
75130- 19	3 4 74	HS LENGTH	559938760,7344	-2,0938	27,0566	*
75126- 10	4 29 74	HS LENGTH	559938745,9531	-16,8750	20,9536	*
75126- 13	7 8 74	HS LENGTH	559938862,7656	99,9375	51,8065	*
		HS LENGTH	559938762,8281		40,2671	

RUN	DATE M D Y	BASELINE	VALUE CM	DIFF CM	SIGMA CM	
75126- 21	4 11 73	HS X-COMP	187856081,8984	-18,0900	136,8134	*
75126- 18	5 18 73	HS X-COMP	187856176,3672	76,3794	124,0870	*
75126- 3	8 10 73	HS X-COMP	187856024,5000	-75,4879	38,8114	*
75126- 6	10 12 73	HS X-COMP	187855884,4609	-215,5274	93,6595	*
75126- 8	1 22 74	HS X-COMP	187856177,9453	77,9597	70,6074	*
75130- 19	3 4 74	HS X-COMP	187856177,6250	77,6386	44,8930	*
75126- 10	4 29 74	HS X-COMP	187856130,5469	30,5596	40,3455	*
75126- 13	7 8 74	HS X-COMP	187856075,5508	-24,4368	104,3269	*
		HS X-COMP	187856099,9883		78,9006	

TABLE 4. Baseline Results

RUN	DATE M D Y	BASELINE	VALUE CM	DIFF CM	SIGMA CM
75126- 21	4 11 73	HS Y-COMP	-516873261,1016	37,5211	75,2299 *
75126- 18	5 18 73	HS Y-COMP	-516873269,9844	28,6348	70,7155 *
75126- 3	8 10 73	HS Y-COMP	-516873349,1875	-50,5680	33,7073 *
75126- 6	10 12 73	HS Y-COMP	-516873488,4297	-189,8079	54,7814 *
75126- 8	1 22 74	HS Y-COMP	-516873351,5313	-52,9045	69,7287 *
75130- 19	3 4 74	HS Y-COMP	-516873242,2578	56,3639	30,3611 *
75126- 10	4 29 74	HS Y-COMP	-516873243,2813	55,3402	24,3166 *
75126- 13	7 8 74	HS Y-COMP	-516873409,3672	-110,7441	47,8060 *
		HS Y-COMP	-516873298,6250		76,3961

RUN	DATE M D Y	BASELINE	VALUE CM	DIFF CM	SIGMA CM
75126- 21	4 11 73	HS Z-COMP	105277528,9434	-681,3496	271,0302 *
75126- 18	5 18 73	HS Z-COMP	105278036,3184	-173,9744	175,3865 *
75126- 3	8 10 73	HS Z-COMP	105278234,3281	24,0363	83,5353 *
75126- 6	10 12 73	HS Z-COMP	105277557,8750	-652,4170	170,5898 *
75126- 8	1 22 74	HS Z-COMP	105278220,1465	9,8534	392,2742 *
75130- 19	3 4 74	HS Z-COMP	105278315,6836	105,3912	103,8412 *
75126- 10	4 29 74	HS Z-COMP	105278316,0176	105,7257	66,7923 *
75126- 13	7 8 74	HS Z-COMP	105278220,0488	9,7561	162,5737 *
		HS Z-COMP	105278210,2930		208,9957

Table 4 (continued)

RUN	DATE M	D	Y	BASELINE	VALUE CM	DIFF CM	SIGMA CM	
75125- 10	4	14	72	HG LENGTH	389999840,5938	-42,0078	12,9144	*
75125- 11	5	9	72	HG LENGTH	389999815,9063	-66,6953	9,7694	*
75125- 27	5	29	72	HG LENGTH	389999849,0156	-33,5859	11,5728	*
75125- 14	6	3	72	HG LENGTH	389999893,1094	10,5078	31,8757	*
75125- 16	6	27	72	HG LENGTH	389999919,1016	36,5000	17,8318	*
75125- 17	8	29	72	HG LENGTH	389999883,3984	,7969	4,9475	*
75125- 18	11	7	72	HG LENGTH	389999916,7500	34,1484	7,9550	*
75125- 19	2	4	73	HG LENGTH	389999885,0078	2,4063	7,6529	*
75125- 20	3	30	73	HG LENGTH	389999894,5625	11,9609	5,9143	*
75126- 3	8	10	73	HG LENGTH	389999881,6016	-1,0000	11,9714	*
75126- 6	10	12	73	HG LENGTH	389999874,9766	-7,6250	30,1437	*
75126- 8	1	22	74	HG LENGTH	389999833,1719	-49,4297	67,2919	*
75130- 19	3	4	74	HG LENGTH	389999992,3125	109,7109	43,3450	*
75126- 10	4	29	74	HG LENGTH	389999888,8047	6,2031	12,9638	*
75126- 13	7	8	74	HG LENGTH	389999917,6953	35,0938	38,6907	*
75130- 47	1	14	75	HG LENGTH	389999920,4219	37,8203	35,2825	*
				HG LENGTH	389999882,6016		26,3439	

Table 4. (continued)

RUN	DATE M D Y	BASELINE	VALUE CM	DIFF CM	SIGMA CM	
75125- 10	4 14 72	HG X-COMP	-384602678,6172	-33,7871	16,3282	*
75125- 11	5 9 72	HG X-COMP	-384602547,1719	97,6601	8,9741	*
75125- 27	5 29 72	HG X-COMP	-384602616,5391	28,2953	10,6412	*
75125- 14	6 3 72	HG X-COMP	-384602598,5156	46,3152	17,4718	*
75125- 16	6 27 72	HG X-COMP	-384602654,6250	-9,7935	9,2720	*
75125- 17	8 29 72	HG X-COMP	-384602649,8672	-5,0379	2,8461	*
75125- 18	11 7 72	HG X-COMP	-384602662,5781	-17,7483	3,2510	*
75125- 19	2 4 73	HG X-COMP	-384602651,7969	-6,9624	6,2418	*
75125- 20	3 30 73	HG X-COMP	-384602624,0938	20,7354	4,3221	*
75126- 5	8 10 73	HG X-COMP	-384602647,2813	-2,4524	8,9091	*
75126- 6	10 12 73	HG X-COMP	-384602668,3203	-23,4920	28,5254	*
75126- 8	1 22 74	HG X-COMP	-384602598,3438	46,4879	49,7592	*
75130- 19	3 4 74	HG X-COMP	-384602750,0703	-105,2372	39,3896	*
75126- 10	4 29 74	HG X-COMP	-384602629,7188	15,1089	10,5490	*
75126- 13	7 8 74	HG X-COMP	-384602665,6719	-20,8417	31,9294	*
75130- 47	1 14 75	HG X-COMP	-384602651,6484	-6,8165	25,8854	*
		HG X-COMP	-384602644,8281		23,8302	

Table 4 (continued)

RUN	DATE M D Y	BASELINE	VALUE CM	DIFF CM	SIGMA CM
75125- 10	4 14 72	HG Y-COMP	18407543,4482	5,1594	15,9550 *
75125- 11	5 9 72	HG Y-COMP	18407563,7256	25,4370	41,4665 *
75125- 27	5 29 72	HG Y-COMP	18407459,9810	-78.3078	17,4608 *
75125- 14	6 3 72	HG Y-COMP	18407551,2451	12.9566	27,1895 *
75125- 16	6 27 72	HG Y-COMP	18407137,3643	-400,9244	28,3924 *
75125- 17	8 29 72	HG Y-COMP	18407630,6108	92.3224	9,5536 *
75125- 18	11 7 72	HG Y-COMP	18407559,3120	21,0236	9,1859 *
75125- 19	2 4 73	HG Y-COMP	18407692,1924	153,9039	25,4748 *
75125- 20	3 30 73	HG Y-COMP	18407319,6226	-218,6658	13,6797 *
75126- 5	8 10 73	HG Y-COMP	18407735,1904	196,9016	24,9336 *
75126- 6	10 12 73	HG Y-COMP	18407543,2700	4,9815	57,4810 *
75126- 8	1 22 74	HG Y-COMP	18407460,0850	-78.2036	55,5982 *
75130- 19	3 4 74	HG Y-COMP	18407549,0117	10.7229	33,9297 *
75126- 10	4 29 74	HG Y-COMP	18407547,5723	9,2839	22,4395 *
75126- 13	7 8 74	HG Y-COMP	18407645,0869	106.7984	67,8022 *
75130- 47	1 14 75	HG Y-COMP	18407672,9839	134,6955	68,9151 *
		HG Y-COMP	18407538,2686		122,2850

Table 4 (continued)

RUN	DATE M D Y	BASELINE	VALUE CM	DIFF CM	SIGMA CM	
75125- 10	4 14 72	HG Z-COMP	-61982397,6191	512.5760	67,9121	*
75125- 11	5 9 72	HG Z-COMP	-61983051,8623	-141.6670	55,9939	*
75125- 27	5 29 72	HG Z-COMP	-61982860,5264	49,6690	24,4811	*
75125- 14	6 3 72	HG Z-COMP	-61983222,7451	-312,5498	101,7352	*
75125- 16	6 27 72	HG Z-COMP	-61983161,0684	-250,8731	66,3464	*
75125- 17	8 29 72	HG Z-COMP	-61982819,4092	90.7857	21,3948	*
75125- 18	11 7 72	HG Z-COMP	-61982971,5459	-61,3506	45,9399	*
75125- 19	2 4 73	HG Z-COMP	-61982799,2871	110.9081	22,4874	*
75125- 20	3 30 73	HG Z-COMP	-61983141,9336	-231,7387	22,9573	*
75126- 3	8 10 73	HG Z-COMP	-61982793,0986	117,0968	44,1472	*
75126- 6	10 12 73	HG Z-COMP	-61982677,8057	232,3899	73,9340	*
75126- 8	1 22 74	HG Z-COMP	-61982873,7012	36,4936	140,6824	*
75130- 19	3 4 74	HG Z-COMP	-61982907,2061	2,9888	49,4702	*
75126- 10	4 29 74	HG Z-COMP	-61983003,0459	-92,8509	31,2022	*
75126- 13	7 8 74	HG Z-COMP	-61982932,8662	-22,6711	75,2037	*
75130- 47	1 14 75	HG Z-COMP	-61983028,7422	-118,5470	83,9870	*
		HG Z-COMP	-61982910,1953		151,4348	

RUN	DATE M D Y	BASELINE	VALUE CM	DIFF CM	SIGMA CM	
75126- 3	8 10 73	HN LENGTH	84512988,3516	-9,5703	10,0449	*
75126- 6	10 12 73	HN LENGTH	84513007,0352	9,1133	21,2273	*
75130- 19	3 4 74	HN LENGTH	84513010,8711	12,9492	18,4292	*
75126- 10	4 29 74	HN LENGTH	84512999,1016	1,1797	7,2016	*
75126- 13	7 8 74	HN LENGTH	84513003,7754	5,8535	20,6654	*
		HN LENGTH	84512997,9219		6,7919	

Table 4 (continued)

RUN	DATE M D Y	BASELINE	VALUE CM	DIFF CM	SIGMA CM
75126- 3	8 10 73	HN X-COMP	-60952474,6836	-0,3753	6,7401 *
75126- 6	10 12 73	HN X-COMP	-60952490,5781	-16,2700	16,6035 *
75130- 19	3 4 74	HN X-COMP	-60952466,7939	7,5141	11,8205 *
75126- 10	4 29 74	HN X-COMP	-60952478,1943	-3,8859	4,5913 *
75126- 13	7 8 74	HN X-COMP	-60952448,5830	25,7255	11,4032 *
		HN X-COMP	-60952474,3086		9,0324

RUN	DATE M D Y	BASELINE	VALUE CM	DIFF CM	SIGMA CM
75126- 3	8 10 73	HN Y-COMP	46721618,8994	-18,7764	13,4023 *
75126- 6	10 12 73	HN Y-COMP	46721648,9727	11,2974	18,6097 *
75130- 19	3 4 74	HN Y-COMP	46721669,3398	31,6645	9,0557 *
75126- 10	4 29 74	HN Y-COMP	46721620,8369	-16,8389	5,9224 *
75126- 13	7 8 74	HN Y-COMP	46721662,5459	24,8705	12,2451 *
		HN Y-COMP	46721637,6758		21,8964

RUN	DATE M D Y	BASELINE	VALUE CM	DIFF CM	SIGMA CM
75126- 3	8 10 73	HN Z-COMP	-35275081,2568	8,8221	21,9591 *
75126- 6	10 12 73	HN Z-COMP	-35275058,7217	31,3569	34,4709 *
75130- 19	3 4 74	HN Z-COMP	-35275082,0264	8,0518	30,7542 *
75126- 10	4 29 74	HN Z-COMP	-35275098,3760	-8,2971	13,7667 *
75126- 13	7 8 74	HN Z-COMP	-35275105,4990	-15,4204	40,4621 *
		HN Z-COMP	-35275090,0781		12,6023

Table 4 (continued)

RUN	DATE M D Y	BASELINE	VALUE CM	DIFF CM	SIGMA CM
75125- 11	5 9 72	HA LENGTH	503948202,9609	95,7578	124,0440 *
75125- 27	5 29 72	HA LENGTH	503948145,6328	38,4297	26,2233 *
75125- 14	6 3 72	HA LENGTH	503947958,9609	-148,2422	48,8597 *
		HA LENGTH	503948107,2031		78,5198

RUN	DATE M D Y	BASELINE	VALUE CM	DIFF CM	SIGMA CM
75125- 11	5 9 72	HA X-COMP	-377395121,7813	66,1558	102,8700 *
75125- 27	5 29 72	HA X-COMP	-377395183,4844	4,4600	20,4095 *
75125- 14	6 3 72	HA X-COMP	-377395251,7266	-63,7826	61,3275 *
		HA X-COMP	-377395187,9375		23,6399

RUN	DATE M D Y	BASELINE	VALUE CM	DIFF CM	SIGMA CM
75125- 11	5 9 72	HA Y-COMP	-300362066,0781	66,5933	81,9875 *
75125- 27	5 29 72	HA Y-COMP	-300362130,0859	2,5822	34,8042 *
75125- 14	6 3 72	HA Y-COMP	-300362166,5313	-33,8584	53,0331 *
		HA Y-COMP	-300362132,6719		28,4030

RUN	DATE M D Y	BASELINE	VALUE CM	DIFF CM	SIGMA CM
75125- 11	5 9 72	HA Z-COMP	146011446,7539	576,5602	275,3582 *
75125- 27	5 29 72	HA Z-COMP	146010957,7695	87,5781	68,0187 *
75125- 14	6 3 72	HA Z-COMP	146010062,1445	-808,0465	174,2099 *
		HA Z-COMP	146010870,1914		323,7698

Table 4 (continued)

RUN	DATE M D Y	STAR		VALUE H M SEC	DIFF SEC	SIGMA SEC
75125- 11	5 9 72	7=3C84	RA	3 16 29,54911	-0,00049	,00121 *
75125- 27	5 29 72	7=3C84	RA	3 16 29,54745	-0,00216	,00096 *
75125- 14	6 3 72	7=3C84	RA	3 16 29,53966	-0,00994	,00973 *
75126- 21	4 11 73	7=3C84	RA	3 16 29,55026	,00066	,00307 *
75126- 18	5 18 73	7=3C84	RA	3 16 29,54694	-0,00267	,00287 *
75126- 3	8 10 73	7=3C84	RA	3 16 29,55254	,00293	,00073 *
75126- 6	10 12 73	7=3C84	RA	3 16 29,55495	,00534	,00231 *
75126- 8	1 22 74	7=3C84	RA	3 16 29,54985	,00024	,00199 *
75130- 19	3 4 74	7=3C84	RA	3 16 29,54646	-0,00314	,00117 *
75126- 10	4 29 74	7=3C84	RA	3 16 29,54832	-0,00129	,00102 *
75126- 13	7 8 74	7=3C84	RA	3 16 29,55137	,00176	,00255 *
75130- 47	1 14 75	7=3C84	RA	3 16 29,54804	-0,00157	,00232 *
		7=3C84	RA	3 16 29,54961		,00246

RUN	DATE M D Y	STAR		VALUE D M SEC	DIFF SEC	SIGMA SEC
75125- 11	5 9 72	7=3C84	DEC	41 19 51,60653	-0,08713	,00532 *
75125- 27	5 29 72	7=3C84	DEC	41 19 51,71338	,01973	,01463 *
75125- 14	6 3 72	7=3C84	DEC	41 19 51,69107	-0,00259	,18313 *
75126- 21	4 11 73	7=3C84	DEC	41 19 51,71736	,02371	,02271 *
75126- 18	5 18 73	7=3C84	DEC	41 19 51,71708	,02343	,01898 *
75126- 3	8 10 73	7=3C84	DEC	41 19 51,74206	,04840	,00780 *
75126- 6	10 12 73	7=3C84	DEC	41 19 51,76933	,07568	,01973 *
75126- 8	1 22 74	7=3C84	DEC	41 19 51,81960	,12595	,02712 *
75130- 19	3 4 74	7=3C84	DEC	41 19 51,77040	,07674	,01067 *
75126- 10	4 29 74	7=3C84	DEC	41 19 51,71965	,02600	,00794 *
75126- 13	7 8 74	7=3C84	DEC	41 19 51,75969	,06603	,01677 *
75130- 47	1 14 75	7=3C84	DEC	41 19 51,78749	,09383	,01541 *
		7=3C84	DEC	41 19 51,69366		,06887

Table 5. Source Coordinate Results

RUN	DATE M D Y	STAR		VALUE H M SEC	DIFF SEC	SIGMA SEC
75125- 11	5 9 72	9=NRAO140	RA	3 33 22,38833	,00281	,00129 *
75125- 18	11 7 72	9=NRAO140	RA	3 33 22,38333	-0,00219	,00114 *
		9=NRAO140	RA	3 33 22,38552		,00248

RUN	DATE M D Y	STAR		VALUE D M SEC	DIFF SEC	SIGMA SEC
75125- 11	5 9 72	9=NRAO140	DEC	32 8 36,31305	-0,06768	,01509 *
75125- 18	11 7 72	9=NRAO140	DEC	32 8 36,51837	,07598	,01599 *
		9=NRAO140	DEC	32 8 36,44239		,07171

RUN	DATE M D Y	STAR		VALUE H M SEC	DIFF SEC	SIGMA SEC
75125- 18	11 7 72	10=CTA26	RA	3 36 58,93725	-0,00000	,00126 *
		10=CTA26	RA	3 36 58,93725		,00000

RUN	DATE M D Y	STAR		VALUE D M SEC	DIFF SEC	SIGMA SEC
75125- 18	11 7 72	10=CTA26	DEC	-1 56 16,78680	,00000	,10499 *
		10=CTA26	DEC	-1 56 16,78680		,00000

Table 5 (continued)

RUN	DATE M D Y	STAR		VALUE H M SEC	DIFF SEC	SIGMA SEC
75125- 11	5 9 72	11=NRAO150	RA	3 55 45,23090	-0,00436	,00156 *
75126- 21	4 11 73	11=NRAO150	RA	3 55 45,23633	,00106	,00328 *
75126- 18	5 18 73	11=NRAO150	RA	3 55 45,23473	-0,00054	,00312 *
75126- 3	8 10 73	11=NRAO150	RA	3 55 45,23935	,00408	,00108 *
75126- 6	10 12 73	11=NRAO150	RA	3 55 45,23870	,00344	,00326 *
75126- 8	1 22 74	11=NRAO150	RA	3 55 45,24120	,00593	,00208 *
75130- 19	3 4 74	11=NRAO150	RA	3 55 45,23199	-0,00327	,00134 *
75126- 10	4 29 74	11=NRAO150	RA	3 55 45,23258	-0,00269	,00128 *
		11=NRAO150	RA	3 55 45,23526		,00376

RUN	DATE M D Y	STAR		VALUE D M SEC	DIFF SEC	SIGMA SEC
75125- 11	5 9 72	11=NRAO150	DEC	50 49 20,00872	-0,09912	,01031 *
75126- 21	4 11 73	11=NRAO150	DEC	50 49 20,10638	-0,00146	,01251 *
75126- 18	5 18 73	11=NRAO150	DEC	50 49 20,11485	,00701	,01262 *
75126- 3	8 10 73	11=NRAO150	DEC	50 49 20,13729	,02944	,00781 *
75126- 6	10 12 73	11=NRAO150	DEC	50 49 20,14862	,04077	,03331 *
75126- 8	1 22 74	11=NRAO150	DEC	50 49 20,14006	,03222	,01934 *
75130- 19	3 4 74	11=NRAO150	DEC	50 49 20,12524	,01739	,00895 *
75126- 10	4 29 74	11=NRAO150	DEC	50 49 20,11602	,00817	,01047 *
		11=NRAO150	DEC	50 49 20,10785		,04262

Table 5 (continued)

RUN	DATE M	D	Y	STAR		VALUE H	M	SEC	DIFF SEC	SIGMA SEC	
75125- 14	6	3	72	14=3C120	RA	4	30	31,59193	,00617	,00123	*
75125- 17	8	29	72	14=3C120	RA	4	30	31,58887	,00311	,00026	*
75125- 18	11	7	72	14=3C120	RA	4	30	31,58264	-0,00313	,00024	*
75125- 19	2	4	73	14=3C120	RA	4	30	31,59365	,00789	,00109	*
75125- 20	3	30	73	14=3C120	RA	4	30	31,58588	,00011	,00049	*
75126- 21	4	11	73	14=3C120	RA	4	30	31,58220	-0,00356	,00282	*
75126- 18	5	18	73	14=3C120	RA	4	30	31,58267	-0,00309	,00236	*
75126- 3	8	10	73	14=3C120	RA	4	30	31,58659	,00082	,00088	*
75126- 6	10	12	73	14=3C120	RA	4	30	31,58729	,00153	,00215	*
75126- 8	1	22	74	14=3C120	RA	4	30	31,58477	-0,00099	,00197	*
75130- 19	3	4	74	14=3C120	RA	4	30	31,58095	-0,00482	,00114	*
75126- 10	4	29	74	14=3C120	RA	4	30	31,58606	,00030	,00093	*
75126- 13	7	8	74	14=3C120	RA	4	30	31,58380	-0,00196	,00251	*
75130- 47	1	14	75	14=3C120	RA	4	30	31,58355	-0,00221	,00231	*
				14=3C120	RA	4	30	31,58577		,00313	

Table 5 (continued)

RUN	DATE M	D	Y	STAR		VALUE D	M	SEC	DIFF SEC	SIGMA SEC
75125- 14	6	3	72	14=3C120	DEC	5	14	59,24180	-0,24371	,04558 *
75125- 17	8	29	72	14=3C120	DEC	5	14	59,25383	-0,23168	,01957 *
75125- 18	11	7	72	14=3C120	DEC	5	14	59,66012	,17460	,01898 *
75125- 19	2	4	73	14=3C120	DEC	5	14	59,41724	-0,06828	,04624 *
75125- 20	3	30	73	14=3C120	DEC	5	14	59,59603	,11051	,02538 *
75126- 21	4	11	73	14=3C120	DEC	5	14	59,18298	-0,30254	,27259 *
75126- 18	5	18	73	14=3C120	DEC	5	14	59,38991	-0,09560	,19976 *
75126- 3	8	10	73	14=3C120	DEC	5	14	59,56670	,08119	,06969 *
75126- 6	10	12	73	14=3C120	DEC	5	14	59,55203	,06651	,12838 *
75126- 8	1	22	74	14=3C120	DEC	5	14	59,68550	,19999	,25396 *
75130- 19	3	4	74	14=3C120	DEC	5	14	59,82950	,34398	,09412 *
75126- 10	4	29	74	14=3C120	DEC	5	14	59,50523	,01971	,05342 *
75126- 13	7	8	74	14=3C120	DEC	5	14	59,84589	,36038	,14199 *
75130- 47	1	14	75	14=3C120	DEC	5	14	59,85191	,36640	,14871 *
				14=3C120	DEC	5	14	59,48552		,18627

Table 5 (continued)

RUN	DATE M	D	Y	STAR		VALUE H	M	SEC	DIFF SEC	SIGMA SEC
75125- 10	4	14	72	27=0J287	RA	8	51	57,24044	,00943	,00150 *
75125- 27	5	29	72	27=0J287	RA	8	51	57,23029	-0,00072	,00043 *
75125- 14	6	3	72	27=0J287	RA	8	51	57,22830	-0,00271	,00068 *
75125- 16	6	27	72	27=0J287	RA	8	51	57,22651	-0,00449	,00102 *
75125- 17	8	29	72	27=0J287	RA	8	51	57,23099	-0,00002	,00028 *
75125- 18	11	7	72	27=0J287	RA	8	51	57,22767	-0,00333	,00076 *
75125- 19	2	4	73	27=0J287	RA	8	51	57,23837	,00736	,00070 *
75125- 20	3	30	73	27=0J287	RA	8	51	57,22984	-0,00117	,00041 *
75126- 3	8	10	73	27=0J287	RA	8	51	57,23283	,00182	,00089 *
75126- 6	10	12	73	27=0J287	RA	8	51	57,23192	,00092	,00238 *
75126- 8	1	22	74	27=0J287	RA	8	51	57,23240	,00140	,00237 *
75130- 19	3	4	74	27=0J287	RA	8	51	57,23498	,00397	,00115 *
75126- 10	4	29	74	27=0J287	RA	8	51	57,23206	,00106	,00073 *
				27=0J287	RA	8	51	57,23100		,00257

Table 5 (continued)

RUN	DATE M	D	Y	STAR	VALUE D	M	SEC	DIFF SEC	SIGMA SEC
75125- 10	4	14	72	27=0J287	DEC	20	17 58,55286	.10073	.02745 *
75125- 27	5	29	72	27=0J287	DEC	20	17 58,45709	.00497	.01400 *
75125- 14	6	3	72	27=0J287	DEC	20	17 58,47216	.02004	.02213 *
75125- 16	6	27	72	27=0J287	DEC	20	17 58,60403	.15191	.04419 *
75125- 17	8	29	72	27=0J287	DEC	20	17 58,44059	-0.01153	.00877 *
75125- 18	11	7	72	27=0J287	DEC	20	17 58,64713	.19501	.03966 *
75[illegible]- 19	2	4	73	27=0J287	DEC	20	17 58,24669	-0.20543	.02034 *
75125- 20	3	30	73	27=0J287	DEC	20	17 58,45290	.00078	.00991 *
75126- 3	8	10	73	27=0J287	DEC	20	17 58,50186	.04973	.03984 *
75126- 6	10	12	73	27=0J287	DEC	20	17 58,62187	.16975	.07334 *
75126- 8	1	22	74	27=0J287	DEC	20	17 58,50800	.05588	.08695 *
75130- 19	3	4	74	27=0J287	DEC	20	17 58,59744	.14532	.04393 *
75126- 10	4	29	74	27=0J287	DEC	20	17 58,48537	.03325	.01911 *
				27=0J287	DEC	20	17 58,45212		.06671

Table 5 (continued)

RUN		DATE M	D	Y	STAR		VALUE H	M	SEC	DIFF SEC	SIGMA SEC	
75125-	10	4	14	72	28=4C39,25	RA	9	23	55,31510	,01769	,00245	*
75125-	11	5	9	72	28=4C39,25	RA	9	23	55,29349	-0,00393	,00427	*
75125-	27	5	29	72	28=4C39,25	RA	9	23	55,29563	-0,00179	,00054	*
75125-	14	6	3	72	28=4C39,25	RA	9	23	55,29427	-0,00314	,00872	*
75125-	16	6	27	72	28=4C39,25	RA	9	23	55,29268	-0,00473	,00131	*
75125-	17	8	29	72	28=4C39,25	RA	9	23	55,29677	-0,00065	,00049	*
75125-	19	2	4	73	28=4C39,25	RA	9	23	55,30317	,00576	,00073	*
75125-	20	3	30	73	28=4C39,25	RA	9	23	55,29357	-0,00384	,00060	*
75126-	21	4	11	73	28=4C39,25	RA	9	23	55,29829	,00087	,00306	*
75126-	18	5	18	73	28=4C39,25	RA	9	23	55,29644	-0,00097	,00286	*
75126-	5	8	10	73	28=4C39,25	RA	9	23	55,30087	,00346	,00069	*
75126-	6	10	12	73	28=4C39,25	RA	9	23	55,30253	,00512	,00260	*
75126-	8	1	22	74	28=4C39,25	RA	9	23	55,29990	,00249	,00205	*
75130-	19	3	4	74	28=4C39,25	RA	9	23	55,29831	,00090	,00122	*
75126-	10	4	29	74	28=4C39,25	RA	9	23	55,29635	-0,00107	,00105	*
75126-	13	7	8	74	28=4C39,25	RA	9	23	55,30065	,00324	,00236	*
					28=4C39,25	RA	9	23	55,29741		,00351	

Table 5 (continued)

RUN	DATE M	D	Y	STAR		VALUE D	M	SEC	DIFF SEC	SIGMA SEC
75125- 10	4	14	72	28=4C39,25	DEC	39	15	23,70697	-0,02675	,02147 *
75125- 11	5	9	72	28=4C39,25	DEC	39	15	23,62621	-0,10751	,43316 *
75125- 27	5	29	72	28=4C39,25	DEC	39	15	23,72858	-0,00514	,00722 *
75125- 14	6	3	72	28=4C39,25	DEC	39	15	23,80443	,07071	,11024 *
75125- 16	6	27	72	28=4C39,25	DEC	39	15	23,75362	,01990	,01609 *
75125- 17	8	29	72	28=4C39,25	DEC	39	15	23,72820	-0,00552	,00434 *
75125- 19	2	4	73	28=4C39,25	DEC	39	15	23,60366	-0,13005	,01080 *
75125- 20	3	30	73	28=4C39,25	DEC	39	15	23,75012	,01641	,00396 *
75126- 21	4	11	73	28=4C39,25	DEC	39	15	23,73975	,00604	,02251 *
75126- 18	5	18	73	28=4C39,25	DEC	39	15	23,79022	,05651	,01859 *
75126- 5	8	10	73	28=4C39,25	DEC	39	15	23,72097	-0,01275	,00869 *
75126- 6	10	12	73	28=4C39,25	DEC	39	15	23,78625	,05253	,02896 *
75126- 8	1	22	74	28=4C39,25	DEC	39	15	23,74523	,01152	,03186 *
75130- 19	3	4	74	28=4C39,25	DEC	39	15	23,78186	,04814	,01643 *
75126- 10	4	29	74	28=4C39,25	DEC	39	15	23,73406	,00034	,01102 *
75126- 13	7	8	74	28=4C39,25	DEC	39	15	23,81136	,07765	,02123 *
				28=4C39,25	DEC	39	15	23,73371		,03326

Table 5 (continued)

RUN	DATE M	D	Y	STAR		VALUE D	M	SEC	DIFF SEC	SIGMA SEC	
75125- 10	4	14	72	33=3C273B	DEC	2	19	43,57861	,26853	,04318	*
75125- 11	5	9	72	33=3C273B	DEC	2	19	43,49699	,18691	,05514	*
75125- 27	5	29	72	33=3C273B	DEC	2	19	43,14650	-0,16359	,03852	*
75125- 14	6	3	72	33=3C273B	DEC	2	19	43,20546	-0,10463	,03528	*
75125- 16	6	27	72	33=3C273B	DEC	2	19	43,28166	-0,02842	,10702	*
75125- 17	8	29	72	33=3C273B	DEC	2	19	43,20376	-0,10632	,02559	*
75125- 18	11	7	72	33=3C273B	DEC	2	19	43,30270	-0,00739	,02638	*
75125- 19	2	4	73	33=3C273B	DEC	2	19	43,36660	,05652	,04387	*
75125- 20	3	30	73	33=3C273B	DEC	2	19	43,39604	,08596	,03294	*
75126- 21	4	11	73	33=3C273B	DEC	2	19	42,60881	-0,70128	,38408	*
75126- 18	5	18	73	33=3C273B	DEC	2	19	43,14643	-0,16365	,26552	*
75126- 3	8	10	73	33=3C273B	DEC	2	19	43,36296	,05287	,07432	*
75126- 6	10	12	73	33=3C273B	DEC	2	19	43,01935	-0,29073	,07787	*
75126- 8	1	22	74	33=3C273B	DEC	2	19	43,47625	,16616	,46834	*
75130- 19	3	4	74	33=3C273B	DEC	2	19	43,36350	,05341	,06523	*
75126- 10	4	29	74	33=3C273B	DEC	2	19	43,36503	,05494	,04486	*
75126- 13	7	8	74	33=3C273B	DEC	2	19	43,61664	,30655	,06923	*
75130- 47	1	14	75	33=3C273B	DEC	2	19	43,31765	,00757	,17131	*
				33=3C273B	DEC	2	19	43,31008		,13214	

Table 5 (continued)

RUN	DATE M	D	Y	STAR		VALUE H	M	SEC	DIFF SEC	SIGMA SEC
75125- 10	4	14	72	35=30279	RA	12	53	35,83685	,00286	,00082 *
75125- 11	5	9	72	35=30279	RA	12	53	35,83336	-0,00063	,00145 *
75125- 14	6	3	72	35=30279	RA	12	53	35,83586	,00187	,00052 *
75125- 17	8	29	72	35=30279	RA	12	53	35,83016	-0,00382	,00072 *
75125- 18	11	7	72	35=30279	RA	12	53	35,83184	-0,00215	,00069 *
75125- 19	2	4	73	35=30279	RA	12	53	35,83491	,00093	,00129 *
75125- 20	3	30	73	35=30279	RA	12	53	35,83483	,00084	,00105 *
75126- 3	8	10	73	35=30279	RA	12	53	35,83449	,00051	,00159 *
75126- 6	10	12	73	35=30279	RA	12	53	35,82851	-0,00548	,00109 *
75130- 19	3	4	74	35=30279	RA	12	53	35,83291	-0.00107	,00062 *
75126- 10	4	29	74	35=30279	RA	12	53	35,83520	,00122	,00078 *
75126- 13	7	8	74	35=30279	RA	12	53	35,83779	,00381	,00091 *
75130- 47	1	14	75	35=30279	RA	12	53	35,83508	,00109	,00158 *
				35=30279	RA	12	53	35,83398		,00249

Table 5 (continued)

RUN	DATE M	D	Y	STAR		VALUE D	M	SEC	DIFF SEC	SIGMA SEC
75125- 10	4	14	72	35=3C279	DEC	-5	31	8,16230	-0.17147	,03766 *
75125- 11	5	9	72	35=3C279	DEC	-5	31	7,69309	,29774	,08543 *
75125- 14	6	3	72	35=3C279	DEC	-5	31	8,13761	-0.14677	,04828 *
75125- 17	8	29	72	35=3C279	DEC	-5	31	7,83385	,15699	,04424 *
75125- 18	11	7	72	35=3C279	DEC	-5	31	7,83526	,15558	,03742 *
75125- 19	2	4	73	35=3C279	DEC	-5	31	8,06927	-0.07843	,07356 *
75125- 20	3	30	73	35=3C279	DEC	-5	31	7,94662	,04421	,06351 *
75126- 3	8	10	73	35=3C279	DEC	-5	31	8,05257	-0.06173	,12670 *
75126- 6	10	12	73	35=3C279	DEC	-5	31	8,40817	-0.41734	,12300 *
75130- 19	3	4	74	35=3C279	DEC	-5	31	8,00805	-0.01721	,05498 *
75126- 10	4	29	74	35=3C279	DEC	-5	31	7,98635	,00449	,05958 *
75126- 13	7	8	74	35=3C279	DEC	-5	31	8,07090	-0.08006	,07699 *
75130- 47	1	14	75	35=3C279	DEC	-5	31	7,97611	,01472	,05598 *
				35=3C279	DEC	-5	31	7,99084		,14434

RUN	DATE M	D	Y	STAR		VALUE H	M	SEC	DIFF SEC	SIGMA SEC
75125- 16	6	27	72	36=0Q208	RA	14	4	45,62320	-0.00221	,00121 *
75125- 17	8	29	72	36=0Q208	RA	14	4	45,62572	,00030	,00058 *
75125- 18	11	7	72	36=0Q208	RA	14	4	45,62302	-0.00240	,00552 *
75125- 19	2	4	73	36=0Q208	RA	14	4	45,62699	,00158	,00076 *
75125- 20	3	30	73	36=0Q208	RA	14	4	45,62453	-0.00089	,00064 *
75126- 10	4	29	74	36=0Q208	RA	14	4	45,62706	,00164	,00308 *
				36=0Q208	RA	14	4	45,62542		,00114

Table 5 (continued)

RUN	DATE M	D	Y	STAR		VALUE D	M	SEC	DIFF SEC	SIGMA SEC
75125- 14	6	3	72	36=0Q208	DEC	28	41	29,41693	.00578	0 *
75125- 16	6	27	72	36=0Q208	DEC	28	41	29,36272	-0.04843	.03975 *
75125- 17	8	29	72	36=0Q208	DEC	28	41	29,41719	.00604	.02119 *
75125- 18	11	7	72	36=0Q208	DEC	28	41	29,44966	.03853	.08157 *
75125- 19	2	4	73	36=0Q208	DEC	28	41	29,53530	.12415	.04289 *
75125- 20	3	30	73	36=0Q208	DEC	28	41	29,38050	-0.03065	.02191 *
75126- 10	4	29	74	36=0Q208	DEC	28	41	29,43541	.02426	.05586 *
				36=0Q208	DEC	28	41	29,41115		.04546

RUN	DATE M	D	Y	STAR		VALUE H	M	SEC	DIFF SEC	SIGMA SEC
75125- 11	5	9	72	43=3C345	RA	16	41	17,63709	.00216	.00123 *
75125- 27	5	29	72	43=3C345	RA	16	41	17,63482	-0.00011	.00098 *
75125- 16	6	27	72	43=3C345	RA	16	41	17,62852	-0.00641	.00165 *
75125- 17	8	29	72	43=3C345	RA	16	41	17,63526	.00033	.00064 *
75125- 19	2	4	73	43=3C345	RA	16	41	17,63611	.00117	.00093 *
75125- 20	3	30	73	43=3C345	RA	16	41	17,63335	-0.00158	.00082 *
75126- 21	4	11	73	43=3C345	RA	16	41	17,63620	.00127	.00304 *
75126- 18	5	18	73	43=3C345	RA	16	41	17,63621	.00128	.00278 *
75126- 3	8	10	73	43=3C345	RA	16	41	17,63585	.00091	.00083 *
75126- 6	10	12	73	43=3C345	RA	16	41	17,64251	.00758	.00253 *
75126- 8	1	22	74	43=3C345	RA	16	41	17,63613	.00120	.00201 *
75130- 19	3	4	74	43=3C345	RA	16	41	17,63065	-0.00428	.00177 *
75126- 10	4	29	74	43=3C345	RA	16	41	17,63477	-0.00016	.00099 *
75126- 13	7	8	74	43=3C345	RA	16	41	17,63736	.00243	.00243 *
75130- 47	1	14	75	43=3C345	RA	16	41	17,63101	-0.00392	.00252 *
				43=3C345	RA	16	41	17,63493		.00202

Table 5 (continued)

RUN	DATE M D Y	STAR		VALUE D M SEC	DIFF SEC	SIGMA SEC
75125- 11	5 9 72	43=3C345	DEC	39 54 10,92444	-0,03245	,00708 *
75125- 27	5 29 72	43=3C345	DEC	39 54 10,96223	,00533	,01657 *
75125- 16	6 27 72	43=3C345	DEC	39 54 10,83464	-0,12226	,01806 *
75125- 17	8 29 72	43=3C345	DEC	39 54 10,95385	-0,00304	,00646 *
75125- 19	2 4 73	43=3C345	DEC	39 54 11,02827	,07137	,01256 *
75125- 20	3 30 73	43=3C345	DEC	39 54 10,97278	,01589	,01022 *
75126- 21	4 11 73	43=3C345	DEC	39 54 10,94990	-0,00700	,02309 *
75126- 16	5 18 73	43=3C345	DEC	39 54 10,95641	-0,00048	,02008 *
75126- 3	8 10 73	43=3C345	DEC	39 54 10,96510	,00821	,00770 *
75126- 6	10 12 73	43=3C345	DEC	39 54 10,97014	,01324	,02785 *
75126- 8	1 22 74	43=3C345	DEC	39 54 11,03254	,07564	,03141 *
75130- 19	3 4 74	43=3C345	DEC	39 54 10,87900	-0,07783	,02068 *
75126- 10	4 29 74	43=3C345	DEC	39 54 10,98638	,02949	,00940 *
75126- 13	7 8 74	43=3C345	DEC	39 54 11,03842	,08152	,02147 *
75130- 47	1 14 75	43=3C345	DEC	39 54 10,93332	-0,02358	,01768 *
		43=3C345	DEC	39 54 10,95690		,03699

RUN	DATE M D Y	STAR		VALUE H M SEC	DIFF SEC	SIGMA SEC
75125- 18	11 7 72	56=3C418	RA	20 37 7,49008	,00024	,00209 *
75125- 19	2 4 73	56=3C418	RA	20 37 7,49622	,00638	,00133 *
75125- 20	3 30 73	56=3C418	RA	20 37 7,48277	-0,00707	,00090 *
75126- 21	4 11 73	56=3C418	RA	20 37 7,49844	,00859	,00357 *
75126- 16	5 18 73	56=3C418	RA	20 37 7,49535	,00551	,00321 *
75126- 3	8 10 73	56=3C418	RA	20 37 7,49606	,00622	,00126 *
		56=3C418	RA	20 37 7,48984		,00645

Table 5 (continued)

RUN	DATE M	D	Y	STAR		VALUE D	M	SEC	DIFF SEC	SIGMA SEC
75125- 18	11	7	72	56=3C418	DEC	51	8	35,63900	-0,01832	,09962 *
75125- 19	2	4	73	56=3C418	DEC	51	8	35,67990	,02258	,00870 *
75125- 20	3	30	73	56=3C418	DEC	51	8	35,65238	-0,00494	,01104 *
75126- 21	4	11	73	56=3C418	DEC	51	8	35,62777	-0,02955	,02429 *
75126- 18	5	18	73	56=3C418	DEC	51	8	35,59177	-0,06555	,02125 *
75126- 3	8	10	73	56=3C418	DEC	51	8	35,63777	-0,01955	,01795 *
				56=3C418	DEC	51	8	35,65732		,02591

RUN	DATE M	D	Y	STAR		VALUE H	M	SEC	DIFF SEC	SIGMA SEC
75125- 10	4	14	72	59=2134+00	RA	21	34	5,23340	,00759	,00130 *
75125- 27	5	29	72	59=2134+00	RA	21	34	5,22671	,00090	,00058 *
75125- 16	6	27	72	59=2134+00	RA	21	34	5,21457	-0,01124	,00153 *
75125- 17	8	29	72	59=2134+00	RA	21	34	5,22595	,00014	,00034 *
75125- 18	11	7	72	59=2134+00	RA	21	34	5,22582	,00001	,00117 *
75125- 19	2	4	73	59=2134+00	RA	21	34	5,23340	,00759	,00095 *
75125- 20	3	30	73	59=2134+00	RA	21	34	5,22329	-0,00252	,00043 *
75126- 21	4	11	73	59=2134+00	RA	21	34	5,25456	,02875	,02774 *
75126- 18	5	18	73	59=2134+00	RA	21	34	5,21539	-0,01042	,00468 *
75126- 3	8	10	73	59=2134+00	RA	21	34	5,22735	,00154	,00090 *
75126- 6	10	12	73	59=2134+00	RA	21	34	5,21328	-0,01253	,00232 *
75126- 8	1	22	74	59=2134+0	RA	21	34	5,22629	,00047	,00229 *
75130- 19	3	4	74	59=2134+00	RA	21	34	5,22382	-0,00199	,00178 *
75126- 10	4	29	74	59=2134+00	RA	21	34	5,22870	,00289	,00102 *
				59=2134+00	RA	21	34	5,22581		,00321

Table 5 (continued)

RUN	DATE M D Y	STAR		VALUE D M SEC	DIFF SEC	SIGMA SEC
75125- 10	4 14 72	59=2134+00	DEC	N 28 23,98358	-1,05083	,13717 *
75125- 27	5 29 72	59=2134+00	DEC	N 28 24,82392	-0,21049	,04505 *
75125- 16	6 27 72	59=2134+00	DEC	N 28 25,09436	,05996	,13325 *
75125- 17	8 29 72	59=2134+00	DEC	N 28 25,14545	,11104	,03761 *
75125- 18	11 7 72	59=2134+00	DEC	N 28 24,91358	-0,12082	,09609 *
75125- 19	2 4 73	59=2134+00	DEC	N 28 24,83681	-0,19759	,05736 *
75125- 20	3 30 73	59=2134+00	DEC	N 28 25,25139	,21698	,04316 *
75126- 21	4 11 73	59=2134+00	DEC	N 28 22,32050	-2,71390	2,12687 *
75126- 18	5 18 73	59=2134+00	DEC	N 28 25,47512	,44072	,47832 *
75126- 3	8 10 73	59=2134+00	DEC	N 28 25,04716	,01275	,09514 *
75126- 6	10 12 73	59=2134+00	DEC	N 28 25,64731	,61290	,14664 *
75126- 8	1 22 74	59=2134+00	DEC	N 28 25,20214	,16774	,62922 *
75130- 19	3 4 74	59=2134+00	DEC	N 28 25,15790	,12350	,15431 *
75126- 10	4 29 74	59=2134+00	DEC	N 28 25,02373	-0,01068	,06501 *
		59=2134+00	DEC	N 28 25,03440		,23476

Table 5 (continued)

RUN	DATE M	D	Y	STAR	VALUE H	M	SEC	DIFF SEC	SIGMA SEC
75125- 10	4	14	72	63=VR422201 RA	22	0	39,39675	,01131	,00170 *
75125- 27	5	29	72	63=VR422201 RA	22	0	39,38689	,00146	,00090 *
75125- 14	6	3	72	63=VR422201 RA	22	0	39,38823	,00280	,00078 *
75125- 15	6	27	72	63=VR422201 RA	22	0	39,37016	-0,01527	,00163 *
75125- 17	8	29	72	63=VR422201 RA	22	0	39,38718	,00175	,00053 *
75125- 18	11	7	72	63=VR422201 RA	22	0	39,38161	-0,00383	,00155 *
75125- 19	2	4	73	63=VR422201 RA	22	0	39,38998	,00454	,00118 *
75125- 20	3	30	73	63=VR422201 RA	22	0	39,37700	-0,00844	,00069 *
75126- 21	4	11	73	63=VR422201 RA	22	0	39,38965	,00420	,00309 *
75126- 18	5	18	73	63=VR422201 RA	22	0	39,38595	,00052	,00276 *
75126- 3	8	10	73	63=VR422201 RA	22	0	39,38832	,00288	,00073 *
75126- 6	10	12	73	63=VR422201 RA	22	0	39,38864	,00321	,00260 *
75126- 6	1	22	74	63=VR422201 RA	22	0	39,38393	-0,00150	,00247 *
75130- 19	3	4	74	63=VR422201 RA	22	0	39,38164	-0,00379	,00192 *
75126- 13	7	8	74	63=VR422201 RA	22	0	39,38874	,00330	,00251 *
75130- 47	1	14	75	63=VR422201 RA	22	0	39,38290	-0,00253	,00263 *
				63=VR422201 RA	22	0	39,38543		,00515

Table 5 (continued)

RUN	DATE M D Y	STAR		VALUE D M	SEC	DIFF SEC	SIGMA SEC
75125- 10	4 14 72	63=VR422201	DEC	42 2	8,22872	-0.17076	,01724 *
75125- 27	5 29 72	63=VR422201	DEC	42 2	8,39276	-0.00672	,00608 *
75125- 14	6 3 72	63=VR422201	DEC	42 2	8,30723	-0.09225	,00772 *
75125- 16	6 27 72	63=VR422201	DEC	42 2	8,40433	,00485	,01533 *
75125- 17	8 29 72	63=VR422201	DEC	42 2	8,41048	,01100	,00470 *
75125- 18	11 7 72	63=VR422201	DEC	42 2	8,39487	-0.00461	,01022 *
75125- 19	2 4 73	63=VR422201	DEC	42 2	8,43536	,03588	,00750 *
75125- 20	3 30 73	63=VR422201	DEC	42 2	8,42218	,02270	,00615 *
75126- 21	4 11 73	63=VR422201	DEC	42 2	8,41598	,01650	,02397 *
75126- 18	5 18 73	63=VR422201	DEC	42 2	8,37709	-0.02239	,01818 *
75126- 3	8 10 73	63=VR422201	DEC	42 2	8,41879	,01931	,00821 *
75126- 6	10 12 73	63=VR422201	DEC	42 2	8,39828	-0.00120	,01795 *
75126- 8	1 22 74	63=VR422201	DEC	42 2	8,46946	,06998	,02930 *
75130- 19	3 4 74	63=VR422201	DEC	42 2	8,41731	,01783	,01369 *
75126- 13	7 8 74	63=VR422201	DEC	42 2	8,46360	,06413	,02136 *
75130- 47	1 14 75	63=VR422201	DEC	42 2	8,42437	,02489	,02955 *
		63=VR422201	DEC	42 2	8,39948		,04109

RUN	DATE M D Y	STAR		VALUE H M	SEC	DIFF SEC	SIGMA SEC
75125- 14	6 3 72	66=CTA102	RA	22 30	7,82732	,00000	,00327 *
		66=CTA102	RA	22 30	7,82732		,00000

RUN	DATE M D Y	STAR		VALUE D M	SEC	DIFF SEC	SIGMA SEC
75125- 14	6 3 72	66=CTA102	DEC	11 28	22,49229	-0.00000	,28474 *
		66=CTA102	DEC	11 28	22,49229		,00000

Table 5 (continued)

RUN	DATE M D Y	STAR		VALUE H M	SEC	DIFF SEC	SIGMA SEC
75125- 10	4 14 72	67=30454,3	RA	22 51	29,53479	,00169	,00122 *
75125- 27	5 29 72	67=30454,3	RA	22 51	29,53364	,00053	,00064 *
75125- 14	6 3 72	67=30454,3	RA	22 51	29,53876	,00565	,00816 *
75125- 16	6 27 72	67=30454,3	RA	22 51	29,51954	-0,01356	,00115 *
75125- 17	8 29 72	67=30454,3	RA	22 51	29,53460	,00149	,00024 *
75125- 18	11 7 72	67=30454,3	RA	22 51	29,53101	-0,00210	,00056 *
75125- 19	2 4 73	67=30454,3	RA	22 51	29,53786	,00476	,00091 *
75125- 20	3 30 73	67=30454,3	RA	22 51	29,52997	-0,00313	,00039 *
75126- 21	4 11 73	67=30454,3	RA	22 51	29,52929	-0,00382	,00368 *
75126- 18	5 18 73	67=30454,3	RA	22 51	29,52908	-0,00403	,00277 *
75126- 3	8 10 73	67=30454,3	RA	22 51	29,53440	,00129	,00064 *
75126- 6	10 12 73	67=30454,3	RA	22 51	29,53204	-0,00106	,00199 *
75126- 8	1 22 74	67=30454,3	RA	22 51	29,53210	-0,00101	,00374 *
75126- 10	4 29 74	67=30454,3	RA	22 51	29,53421	,00110	,00081 *
		67=30454,3	RA	22 51	29,53311		,00284

Table 5 (continued)

RUN	DATE M D Y	STAR		VALUE D M SEC	DIFF SEC	SIGMA SEC
75125- 10	4 14 72	67=3C454,3	DEC	15 52 54,06890	-0,17057	,02334 *
75125- 27	5 29 72	67=3C454,3	DEC	15 52 54,10867	-0,13079	,01903 *
75125- 14	6 3 72	67=3C454,3	DEC	15 52 54,23783	-0,00164	,46421 *
75125- 16	6 27 72	67=3C454,3	DEC	15 52 54,40508	,16561	,02024 *
75125- 17	8 29 72	67=3C454,3	DEC	15 52 54,24007	,00061	,00565 *
75125- 18	11 7 72	67=3C454,3	DEC	15 52 54,18121	-0,05826	,01143 *
75125- 19	2 4 73	67=3C454,3	DEC	15 52 54,27305	,03358	,01049 *
75125- 20	3 30 73	67=3C454,3	DEC	15 52 54,25912	,01966	,00770 *
75126- 21	4 11 73	67=3C454,3	DEC	15 52 54,53711	,29765	,17058 *
75126- 18	5 18 73	67=3C454,3	DEC	15 52 54,32150	,08204	,07454 *
75126- 3	8 10 73	67=3C454,3	DEC	15 52 54,29982	,06036	,03267 *
75126- 6	10 12 73	67=3C454,3	DEC	15 52 54,15545	-0,08301	,04320 *
75126- 8	1 22 74	67=3C454,3	DEC	15 52 54,43924	,19977	,13341 *
75126- 10	4 29 74	67=3C454,3	DEC	15 52 54,24534	,00587	,02407 *
		67=3C454,3	DEC	15 52 54,23946		,05367

RUN	DATE M D Y	STAR		VALUE H M SEC	DIFF SEC	SIGMA SEC
75125- 11	5 9 72	75=NRAO512	RA	16 38 48,20011	,00121	,00131 *
75126- 8	1 22 74	75=NRAO512	RA	16 38 48,19806	-0,00084	,00503 *
75130- 19	3 4 74	75=NRAO512	RA	16 38 48,19449	-0,00441	,01438 *
75126- 10	4 29 74	75=NRAO512	RA	16 38 48,19796	-0,00094	,00120 *
		75=NRAO512	RA	16 38 48,19890		,00110

Table 5 (continued)

RUN	DATE M D Y	STAR		VALUE D M SEC	DIFF SEC	SIGMA SEC
75125- 11	5 9 72	75=NRA0512	DEC	39 52 30,22601	-0,00387	,00782 *
75126- 8	1 22 74	75=NRA0512	DEC	39 52 30,24900	,01912	,05838 *
75130- 19	3 4 74	75=NRA0512	DEC	39 52 30,11481	-0,11507	,11390 *
75126- 10	4 29 74	75=NRA0512	DEC	39 52 30,25221	,02233	,01830 *
		75=NRA0512	DEC	39 52 30,22988		,01205

RUN	DATE M D Y	STAR		VALUE H M SEC	DIFF SEC	SIGMA SEC
75130- 19	3 4 74	80=0Q172	RA	14 42 50,49610	0	,01018 *
		80=0Q172	RA	14 42 50,49610		0

RUN	DATE M D Y	STAR		VALUE D M SEC	DIFF SEC	SIGMA SEC
75130- 19	3 4 74	80=0Q172	DEC	10 11 12,52911	,00000	,67897 *
		80=0Q172	DEC	10 11 12,52911		,00000

Table 5 (continued)

TRPLET	DATA	X CM	SIGMA CM	Y CM	SIGMA CM	Z CM	SIGMA CM
H-G-A	111	60,86	67,0	119,33	97,8	-186,21	132,7

TRPLET	DATA	X CM	SIGMA CM	Y CM	SIGMA CM	Z CM	SIGMA CM
H-N-S	222	24,31	104,5	42,55	107,8	-217,20	158,5
H-N-S	333	-16,25	43,9	-59,14	44,3	-62,59	69,9
H-N-S	555	130,07	47,8	-98,53	30,3	-45,09	102,0
H-N-S	666	56,70	21,4	-18,92	22,5	-119,20	49,4
H-N-S	777	57,50	20,6	-82,17	28,0	130,93	65,8

TRPLET	DATA	X CM	SIGMA CM	Y CM	SIGMA CM	Z CM	SIGMA CM
H-N-G	222	-25,68	33,8	71,63	100,0	51,62	65,6
H-N-G	333	-30,23	120,9	255,95	117,9	174,01	151,9
H-N-G	555	10,35	48,1	80,03	54,3	32,27	103,5
H-N-G	666	-27,03	25,7	134,18	39,6	65,53	52,6
H-N-G	777	-27,95	38,2	64,40	51,8	18,81	65,2
H-N-G	888	3,16	9,8	69,43	19,7	20,24	21,0

TRPLET	DATA	X CM	SIGMA CM	Y CM	SIGMA CM	Z CM	SIGMA CM
H-S-G	222	-3,52	43,8	71,62	76,3	151,79	93,2
H-S-G	333	21,31	247,5	448,64	174,3	351,93	254,2
H-S-G	444	11,64	72,0	-81,82	78,7	-1323,44	1445,8
H-S-G	555	-151,06	86,5	311,09	125,2	104,84	197,6
H-S-G	666	328,23	73,4	113,10	73,7	364,42	176,9
H-S-G	777	-66,81	44,8	131,81	56,5	30,79	175,1

TRPLET	DATA	X CM	SIGMA CM	Y CM	SIGMA CM	Z CM	SIGMA CM

Table 6. Baseline Closure Errors

TRPLET	DATA	X CM	SIGMA CM	Y CM	SIGMA CM	Z CM	SIGMA CM
G-N-S	222	46,47	110,6	42,53	150,6	-117,03	180,9
G-N-S	333	35,28	249,7	133,55	176,3	115,33	258,3
G-N-S	555	-31,34	96,5	132,53	125,3	27,48	208,8
G-N-S	666	411,95	74,6	-40,00	76,9	179,69	180,0
G-N-S	777	16,64	45,4	-14,77	59,3	142,90	177,9

Table 6 (continued)

TRPLET	DATA	X CM	SIGMA CM	Y CM	SIGMA CM	Z CM	SIGMA CM
H-N-S	223	-28,06	102,4	-31,55	104,2	-187,28	155,2
H-N-S	224	-110,56	102,5	-117,30	104,3	-318,51	177,8
H-N-S	225	70,36	102,4	-126,81	103,9	-182,47	161,2
H-N-S	226	-5,77	102,0	-87,00	104,2	-231,95	154,5
H-N-S	227	-21,73	101,7	-102,95	104,1	-150,06	154,7
H-N-S	232	50,95	47,7	-14,73	51,0	-106,27	75,6
H-N-S	233	-1,42	42,8	-88,83	42,9	-76,35	68,5
H-N-S	234	-83,92	43,2	-174,58	43,0	-207,58	110,6
H-N-S	235	97,50	42,9	-184,09	42,1	-71,54	81,2
H-N-S	236	20,85	41,8	-144,28	42,8	-121,02	66,8
H-N-S	237	4,91	41,3	-160,23	42,5	-39,13	67,4
H-N-S	252	40,85	49,3	-41,89	40,3	-140,92	88,9
H-N-S	253	-11,52	44,6	-115,98	29,4	-111,00	82,9
H-N-S	254	-94,02	44,9	-201,73	29,6	-242,23	120,0
H-N-S	255	87,40	44,7	-211,25	28,1	-106,19	93,7
H-N-S	256	10,75	43,7	-171,44	29,2	-155,67	81,5
H-N-S	257	-5,20	43,2	-187,39	28,8	-73,78	61,9
H-N-S	262	68,26	31,1	53,73	35,6	-127,48	60,1
H-N-S	263	15,88	23,0	-20,36	22,6	-97,56	50,9
H-N-S	264	-66,62	23,7	-106,11	22,8	-228,79	100,6
H-N-S	265	114,80	23,1	-115,63	20,9	-92,75	67,0
H-N-S	266	38,16	21,1	-75,81	22,3	-142,23	48,6
H-N-S	267	22,21	20,1	-91,77	21,8	-60,34	49,3
H-N-S	272	60,77	31,2	30,86	39,6	48,37	71,7
H-N-S	273	8,40	24,1	-43,23	28,4	78,29	64,1
H-N-S	274	-74,10	23,8	-128,98	28,5	-52,94	107,9
H-N-S	275	107,32	23,3	-138,50	27,0	83,10	77,5
H-N-S	276	30,67	21,3	-98,69	28,2	33,62	62,3
H-N-S	277	14,73	20,3	-114,64	27,7	115,51	62,9
H-N-S	322	9,48	104,9	72,23	108,4	-203,44	159,1
H-N-S	323	-42,69	102,8	-1,86	104,8	-173,52	155,8
H-N-S	324	-125,39	103,0	-87,61	104,9	-304,75	178,4
H-N-S	325	56,03	102,8	-97,13	104,5	-168,71	161,8

Table 7. Baseline Closure Errors

TRPLET	DATA	X CM	SIGMA CM	Y CM	SIGMA CM	Z CM	SIGMA CM
H-N-G	223	148,15	91,4	301,37	125,8	163,52	124,0
H-N-G	224	-115,15	45,8	104,35	97,6	239,83	184,9
H-N-G	225	121,07	42,4	-21,55	101,2	63,09	86,2
H-N-G	226	4,40	35,3	116,14	95,7	204,35	69,6
H-N-G	227	-30,59	41,7	202,12	99,8	206,52	78,8
H-N-G	228	14,73	31,4	-75,84	94,0	21,37	61,7
H-N-G	232	-169,23	85,4	-5,48	89,1	48,35	108,7
H-N-G	233	-15,40	120,5	226,26	117,4	160,25	151,3
H-N-G	234	-278,70	90,9	27,24	86,5	236,56	204,2
H-N-G	235	-42,48	89,2	-98,66	90,5	59,82	122,2
H-N-G	236	-159,15	86,1	39,03	84,4	201,08	111,1
H-N-G	237	-194,13	88,9	125,01	89,0	203,25	117,1
H-N-G	238	-148,82	84,5	-152,95	82,4	18,10	106,4
H-N-G	252	-179,07	36,9	60,50	50,7	-40,30	77,3
H-N-G	253	-5,24	92,6	292,24	91,7	71,60	130,6
H-N-G	254	-268,54	48,2	93,22	45,8	147,91	189,4
H-N-G	255	-32,32	45,7	-32,68	53,1	-28,83	95,4
H-N-G	256	-148,99	38,4	163,01	41,8	112,43	80,7
H-N-G	257	-183,98	44,3	190,99	50,4	114,60	88,8
H-N-G	258	-138,66	34,8	-86,97	37,5	-70,55	74,0
H-N-G	262	-75,65	23,3	32,78	48,8	-110,23	46,3
H-N-G	263	98,18	86,1	264,52	90,7	1,67	115,0
H-N-G	264	-165,12	38,8	65,50	43,7	77,98	179,0
H-N-G	265	71,10	34,7	-60,40	51,3	-98,76	72,6
H-N-G	266	-45,57	25,5	77,29	39,5	42,50	51,8
H-N-G	267	-60,55	33,6	163,27	48,5	44,67	63,7
H-N-G	268	-35,24	19,8	-114,69	34,9	-140,48	40,6
H-N-G	272	-65,62	29,1	-98,55	52,0	-151,51	44,3
H-N-G	273	198,01	89,5	133,19	92,5	-39,61	114,2
H-N-G	274	-155,29	42,5	-65,83	47,3	36,70	178,5
H-N-G	275	80,93	38,8	-191,73	54,4	-140,04	71,3
H-N-G	276	-35,74	30,9	-54,04	43,4	1,22	50,0
H-N-G	277	-70,73	38,0	31,94	51,7	3,39	62,2

Table 7 (continued)

TRPLET	DATA	X CM	SIGMA CM	Y CM	SIGMA CM	Z CM	SIGMA CM
H-S-G	223	170,31	95,6	303,36	108,0	263,69	140,6
H-S-G	224	-92,98	53,6	104,34	73,1	340,00	196,4
H-S-G	225	143,23	50,7	-21,56	77,9	163,26	108,7
H-S-G	226	26,56	45,0	116,13	70,7	304,52	96,1
H-S-G	227	-8,42	50,2	202,11	76,1	306,69	102,9
H-S-G	228	36,89	42,0	-75,85	68,2	121,54	90,5
H-S-G	232	-204,89	233,4	142,80	159,0	269,95	233,6
H-S-G	233	-31,06	248,4	374,54	176,5	381,85	256,2
H-S-G	234	-294,36	235,5	175,52	157,6	458,15	290,6
H-S-G	235	-58,14	234,8	40,62	159,8	281,42	240,2
H-S-G	236	-174,81	233,7	187,31	156,4	422,68	234,8
H-S-G	237	-209,80	234,7	273,29	159,0	424,85	237,7
H-S-G	238	-154,48	233,1	-4,67	155,4	239,70	232,5
H-S-G	242	-33,77	68,1	-274,38	86,1	-1612,96	1433,1
H-S-G	243	140,06	106,9	-42,64	115,1	-1501,06	1437,0
H-S-G	244	-123,23	74,8	-241,66	83,3	-1424,75	1443,5
H-S-G	245	112,98	72,8	-367,56	87,6	-1601,49	1434,2
H-S-G	246	-3,69	68,9	-229,87	81,2	-1460,23	1433,3
H-S-G	247	-38,67	72,4	-143,89	85,9	-1458,06	1433,8
H-S-G	248	6,64	66,9	-421,85	79,1	-1643,21	1432,9
H-S-G	252	-251,27	85,2	234,91	127,5	128,10	187,4
H-S-G	253	-77,44	120,3	466,65	148,7	240,00	214,9
H-S-G	254	-340,73	90,6	267,63	125,7	316,31	254,9
H-S-G	255	-104,52	88,9	141,73	128,5	139,57	195,5
H-S-G	256	-221,19	85,8	279,42	124,3	280,83	188,8
H-S-G	257	-256,17	88,6	365,40	127,4	283,00	192,4
H-S-G	258	-210,66	84,3	87,44	122,9	97,85	186,0
H-S-G	262	268,05	70,1	-60,96	83,8	196,94	178,9
H-S-G	263	441,88	114,1	170,78	113,4	308,84	207,6
H-S-G	264	178,56	82,2	-28,24	80,9	385,15	248,8
H-S-G	265	414,80	80,3	-154,14	85,3	208,41	187,4
H-S-G	266	298,13	76,8	-16,43	78,7	349,67	180,4
H-S-G	267	263,14	80,0	69,53	83,6	351,84	184,2

Table 7 (continued)

TRPLET	DATA	X CM	SIGMA CM	Y CM	SIGMA CM	Z CM	SIGMA CM
G-N-S	223	-154,91	254,6	113,72	205,3	1,13	280,4
G-N-S	224	16,22	122,3	-303,47	155,8	-1881,78	1441,5
G-N-S	225	-201,28	132,6	205,83	182,0	-140,72	243,2
G-N-S	226	318,03	126,9	-90,05	154,5	-71,88	236,8
G-N-S	227	-57,97	110,9	-173,27	144,4	-325,80	232,3
G-N-S	232	73,11	59,9	-14,75	116,8	-6,10	115,5
G-N-S	233	-128,27	237,0	56,44	182,0	112,06	243,4
G-N-S	234	42,86	79,4	-360,75	123,5	-1770,85	1434,7
G-N-S	235	-174,64	94,5	148,55	155,2	-29,79	199,4
G-N-S	236	344,67	86,4	-147,33	121,9	39,05	191,5
G-N-S	237	-31,33	60,4	-230,55	108,8	-214,87	186,0
G-N-S	252	63,02	61,2	-41,91	112,6	-40,75	124,6
G-N-S	253	-138,36	237,3	20,23	179,3	77,41	247,8
G-N-S	254	32,77	80,4	-387,91	119,4	-1805,50	1435,5
G-N-S	255	-184,73	95,3	121,39	152,0	-64,44	204,8
G-N-S	256	334,58	87,3	-174,48	117,8	4,40	197,1
G-N-S	257	-41,42	61,7	-257,70	104,2	-249,52	191,7
G-N-S	262	90,42	47,8	53,72	111,0	-27,31	106,0
G-N-S	263	-110,95	234,2	124,91	178,3	90,85	239,0
G-N-S	264	60,17	70,8	-292,28	117,9	-1792,06	1434,0
G-N-S	265	-157,33	87,3	217,02	150,9	-51,00	194,0
G-N-S	266	361,98	78,5	-78,86	116,3	17,84	185,9
G-N-S	267	-14,02	48,5	-158,08	102,5	-236,08	180,2
G-N-S	272	82,94	47,9	30,84	112,3	148,54	112,9
G-N-S	273	-118,44	234,2	102,03	179,1	266,70	242,1
G-N-S	274	52,69	70,8	-311,16	119,2	-1616,21	1434,5
G-N-S	275	-164,81	87,4	194,14	151,8	124,85	197,9
G-N-S	276	354,50	78,6	-101,73	117,5	193,69	189,9
G-N-S	277	-21,50	48,5	-184,95	103,9	-60,23	184,4
G-N-S	322	210,02	135,6	119,64	143,6	-113,76	200,6
G-N-S	323	8,64	265,4	190,83	200,2	4,40	293,5
G-N-S	324	179,77	145,3	-224,36	149,0	-1878,51	1444,1
G-N-S	325	-47,73	154,1	281,94	176,3	-137,45	258,2

Table 7 (continued)

TABLE 8

Antenna Axis Offset Results*

Station	Data**	Axis Offset Measured-VLBI Estimate
Alaska	1	-0.55 ± 0.46 m
NRAO	2	-0.03 ± 0.29
	3	0.34 ± 0.67
	5	0.18 ± 0.55
	6	-0.11 ± 0.29
	7	-0.39 ± 0.34
Onsala	2	-2. ± 3.
	3	5. ± 5.
	4	11 ± 6.
	5	11. ± 7.
	6	-10. ± 3.
	7	6. ±10.

*The measured axis offset values are given in Section 4.5.5.

**The "data" codes are given in Section 4.5.4.

TABLE 9

Estimates of Corrections to BIH Values for Polar Motion and A1-UT1

Date	Polar Motion		
	ΔX Comp.* (0".01)	ΔY Comp.* (0".01)	Δ(A1-UT1) msec
Phase I			
Apr 14-15 1972	- 7.0±0.7	---	- 1.1±0.7
May 9-10 1972	3.8±1.6	- 15.5±10.	1.1±1.5
May 29-30 1972	2.0±0.9	- 12.7± 9.	2.9±1.2
June 6-7 1972	5.0±1.8	---	1.2±1.4
Aug 29-30 1972	---	---	---
Nov 7 1972	- 1.1±0.8	---	1.2±0.8
Feb 4-5 1973	- 3.2±0.9	---	- 1.2±0.8
Mar 30-31 1973	4.4±0.7	---	5.7±0.6
Jan 16-17 1975	0.6±2.2	---	5.4±1.3
Weighted mean and rms scatter about weighted mean	- 0.6±4.3	- 14.0± 1.4	2.0±2.8
Phase II			
Aug 10-14 1973	3.3±9.6	4.1±16.2	- 5.1±6.4
Oct 12-16 1973	- 8.2±6.0	5.6± 8.1	- 2.5±1.4
Jan 22-23 1974	---	---	---
Mar 4-8 1974	- 7.7±3.1	- 3.8± 4.1	- 4.2±0.8
Apr 29-May 3 1974	- 2.9±4.4	1.1± 6.4	- 2.6±1.7
July 8-12 1974	1.2±3.1	6.1± 5.5	- 2.2±1.1
Weighted mean and rms scatter about weighted mean	- 3.4±4.2	0.8± 4.4	- 3.3±0.9

*To convert these angular measurements into meters at the surface of the Earth, note that 0".01~0.3 m, and 1 msec ~ 0.5 m.

TABLE 10

Comparison of the Mean and Scatter About the Mean from Table 9 with the Results from Reference 16

	Polar Motion		(A1-UT1)
	X Component	Y Component	
	Mean	Mean	Mean
From Table 9 Phase I	-0.2±1.3 m	-4.2±0.3 m	2.0±2.8 msec
From Table 9 Phase II	-1.0±1.3	0.2±1.3	-3.3±0.9
From Reference 18	0.2±1.3	---	2.8±2.9

APPENDIX A

USE OF DIFFERENCED OBSERVABLES

In Chapter 2 the use of differenced observations to eliminate systematic clock errors is discussed. Here we wish to analyze in detail the problem of the determination of baselines and source coordinates from differenced observations.

Let us suppose that our receiver stations are capable of making simultaneous observations on two separate sources and that the observations we wish to deal with will be the difference between the delay for one source and the delay for the other. (We will discuss the use of differences of non-simultaneous observations later.) Following the discussion in Chapter 2, we notice that the delays from observations of a given source follow a diurnal sinusoid, therefore the differenced observations also follow a diurnal sinusoid, and can be characterized by three independent parameters, e.g. phase, amplitude and offset from zero. (The frequency is assumed to be known.) Each source pair therefore contributes three independent observations. There are six parameters that we wish to determine from these data: three components of the baseline, and two coordinates for each source, less the right ascension of one source. If we try to improve the solution by adding a new pair of sources, we add four unknown parameters and only three independent observations for each new pair. If, instead, we keep one source the same

and only add one new source, we add only two unknown parameters, but still we get three new independent observations. It is easy to show that with a single reference source and four other sources paired with it the number of unknowns is equal to the number of independent observations.

For comparison purposes, we should note that with undifferenced observations, three sources were sufficient to determine the baseline and source coordinates. The fact that five are needed now is a measure of the real information that is lost along with the clock effects in the process of forming differenced observations.

For real observations it is possible, of course, to observe a reference source continuously only if the stations are all located on the same side of the equator and the magnitude of the declination of the reference source is greater than the co-latitude of the station furthest from the pole. Since it is not always possible to meet such conditions, it is necessary to investigate the conditions under which more than one reference source can be employed. Each new reference star adds two unknowns. Each new non-reference star adds two unknowns. The baseline has three unknowns. The number of independent observations is three times the number of non-reference stars. The necessary condition for a unique solution is that the number of independent observations be greater than or equal to the number of unknowns; in other words:

$$3N_S \geq 3 + (2N_{RS} - 1) + 2N_S \qquad \text{(A-1)}$$

or

$$N_S \geq 2 + 2N_{RS} \qquad \text{(A-2)}$$

where

N_{RS} = number of reference stars

N_S = number of non-reference stars

Thus if three reference sources are required, at least eleven sources must be observed in all. Eleven sources is only the minimum number required to determine the baseline and source coordinates. Again, in actual practice, it is highly desirable to far exceed the minimum number of sources required in order to provide redundancy and internal consistency checks. None of the observation schedules that we have employed have called for observation on a number of sources far in excess of eleven.

Up to this point we have considered only the case of pairs of simultaneous observations. If the observations being differenced are not exactly simultaneous, then we must consider the problem of clock errors again. If we write the delay as the sum of the geometric delay plus a polynomial for the difference in clock errors for the two sites,

$$\tau_i = \tau_{Gi} + \alpha + \beta t_i + \gamma t_i^2 + \ldots \qquad \text{(A-3)}$$

then the differenced observable can be written as

$$\tau_2 - \tau_1 = \tau_{G2} - \tau_{G1} + \beta (t_2 - t_1) + \gamma (t_2^2 - t_1^2) + \ldots \qquad \text{(A-4)}$$

If the magnitudes of the high order derivatives of the clock error are not negligible, it is a simple matter to add the appropriate polynomial coefficients to the set of parameters to be estimated. In order to be able to estimate these additional parameters, it is necessary to add to the above minimum criteria a single observation for each clock term required in the solution. Again, as always, a large surplus of observations beyond the theoretical minimum is desirable.

APPENDIX B

EXPRESSION OF ATOMIC TIME AS FUNCTION OF COORDINATE TIME*

B.1 INTRODUCTION

In this Appendix we derive a simple expression for the readings of atomic clocks in terms of our choice of coordinate time (see Section 3.2). As stated, our context is the solar system whose dynamics can be described utilizing the weak-field solution to Einstein's field equations. The equations of motion so derived can be cribed in terms of harmonic coordinates (see Reference 20, p. 162), with origin at the solar-system barycenter. As with any choice of coordinates, these are not "observables" (i.e., they are not directly measurable in actual experiments). Since all of our calculations are carried out with coordinates, we must derive convenient expressions for the observables in terms of the coordinates. We restrict ourselves here to the coordinate expression for the readings of Earth-based atomic clocks such as those utilized in our very-long-baseline-interferometry (VLBI) experiments.

---

*This work was carried out in collaboration with R. D. Reasenberg.

As it will be necessary in the following analysis to distinguish among many apparently similar quantities, the following conventions will be employed

$t \equiv$ coordinate time

$AT \equiv$ time kept by an atomic clock on the Earth

$r_i \equiv$ displacement of the center of mass of a gravitating body, i, from the center of mass of the Earth

$\vec{x} \equiv$ three-vector displacements not covered by other conventions; defined in diagrams as used

$\dot{\vec{x}} \equiv$ derivative of $\vec{x}$ with respect to t

$\vec{v} \equiv$ three-velocity of a body with respect to the solar-system barycenter

B.2 ANALYSIS

B.2.1 General Formulation

In the post-Newtonian approximation to the solution of the Einstein field equations, the assumption is made that one is dealing with a system of slow-moving particles ($v << c$) bound together by their mutual weak gravitational interactions, a system

like our solar system (see Reference 20, p. 212). In this approximation, the relation between time kept by an arbitrarily moving atomic clock and coordinate time, t, is given by

$$AT - t \simeq \int(\phi - \frac{v^2}{2})dt \qquad \text{(B.1)}$$

where terms of order v^4 and higher have been neglected [see Reference 20, p. 221, Equations (9.2.2 and 9.2.3)]. Note that in the system of units used here, c = 1. In other words, the unit of length is the light-second, as in Section 2.3.1.

We can write

$$AT - t = \alpha t + \varepsilon_{per} + k \qquad \text{(B.2)}$$

where ε_{per} represents the periodic terms in the solution. In this Appendix we will be concerned solely with the ε_{per} portion of this solution. Constant terms in the integrand and in the integral will be neglected as they arise. Treating the rate in this manner neglects a constant factor of order $(1 + v^2)$ in the amplitude of the periodic terms. The deviation from unity of this factor is the same order as other terms which will be neglected.

B.2.2 Separation into Diurnal and Non-diurnal Terms

In order to integrate Equation (B.1) for clocks associated with earth observatories, it has been found useful to separate the integrand into two

types of time-varying terms. The first type depends on the displacement of the atomic clock from the center of the Earth. These terms tend to have diurnal periodicity, and will be referred to as diurnal terms. The second type depends on the displacement of the center of the Earth from the solar system barycenter and will be referred to as non-diurnal terms.

In order to separate the velocity terms, we write (Figure B.1)

$$\vec{v} = \vec{v}_{ec} + \dot{\vec{x}}_r \tag{B.3}$$

where $\vec{v}_{ec}$ is the velocity of the center of mass of the Earth, and where, in this weak-field approximation, we make the further approximation that these vectors can be added in a Euclidean manner. Then,

$$\frac{v^2}{2} = \frac{v_{ec}^2}{2} + \frac{\dot{x}_r^2}{2} + \vec{v}_{ec} \cdot \dot{\vec{x}}_r \tag{B.4}$$

Of these three terms, the first is a non-diurnal term, the second is, for all practical purposes, a constant, and the third is a diurnal term.

In order to separate the potential terms we make a Taylor expansion about the center of mass of the Earth (Figure B.1)

$$\phi_i = -\frac{GM_i}{(r_i^2 + x_r^2 - 2\vec{r}_i \cdot \vec{x}_r)^{1/2}}$$

where ϕ_i is the contribution of body i to the potential, M_i is the mass of body i, and G is the gravitational constant.

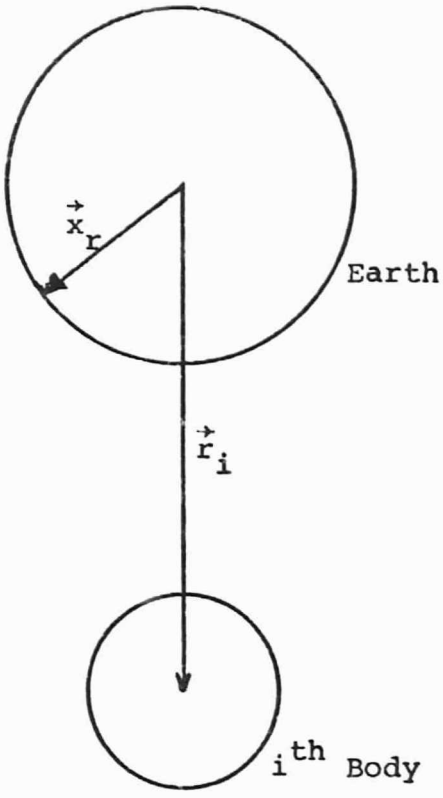

Figure B.1

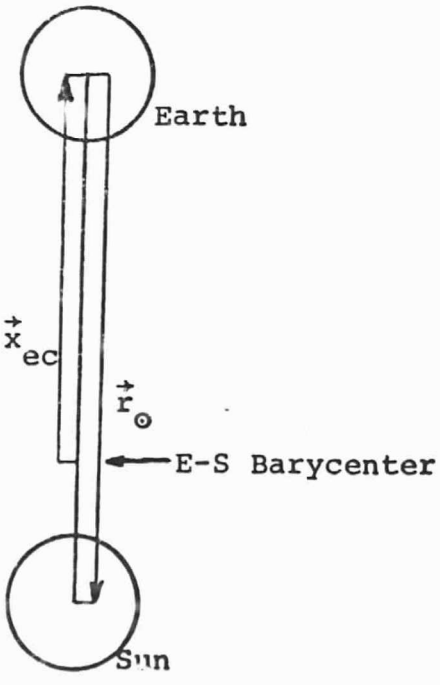

Figure B.2

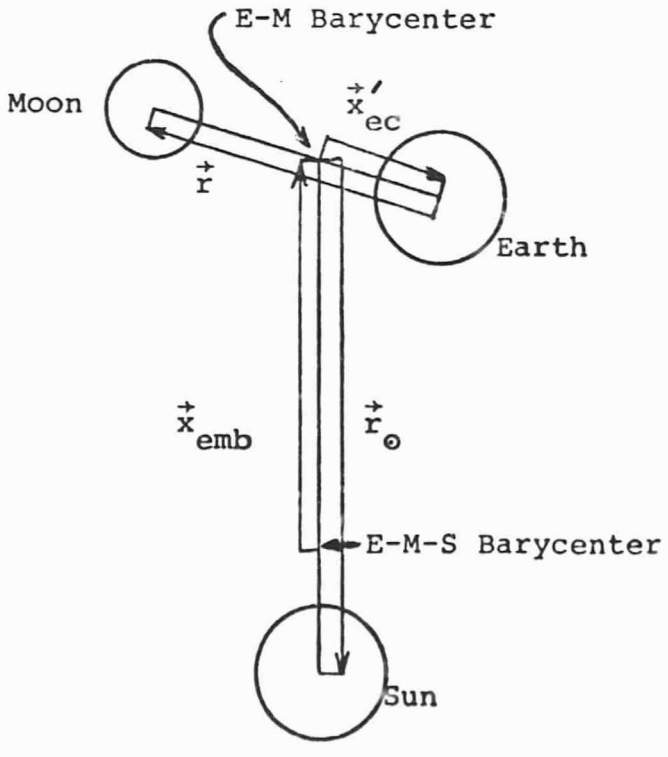

Figure B.3

$$= - \frac{GM_i}{|\vec{r}_i|} \left[1 + \frac{\vec{r}_i \cdot \vec{x}_r}{\vec{r}_i^2} - \frac{1}{2} \frac{x_r^2}{r_i^2}\right.$$

$$\left. + \frac{3}{8} \frac{x_r^4 - 4x_r^2(\vec{r}_i \cdot \vec{x}_r) + 4(\vec{r}_i \cdot \vec{x}_r)^2}{|\vec{r}_i|^4} + \ldots\right] \qquad \text{(B.5)}$$

Keeping terms to order $\frac{1}{r_i^3}$

$$\phi_i = - \frac{GM_i}{|\vec{r}_i|} - \frac{GM_i \vec{r}_i \cdot \vec{x}_r}{|\vec{r}_i|^3} + \frac{GM_i x_r^2}{2|\vec{r}_i|^3}$$

$$- \frac{3}{2} \frac{GM_i(\vec{r}_i \cdot \vec{x}_r)^2}{|\vec{r}_i|^5} \qquad \text{(B.6)}$$

Only the second term has a diurnal signature.

B.2.3 Integration of the Diurnal Terms

If we collect diurnal terms from Equations (B.4) and (B.6), and substitute into Equation (B.1), we obtain

$$(AT - t)_{diurnal} = \int [-\vec{v}_{ec} \cdot \dot{\vec{x}}_r$$

$$- \sum_i \frac{GM_i \vec{x}_r \cdot \vec{r}_i}{|\vec{r}_i|^3}] dt \qquad \text{(B.7)}$$

If the laws of motion are taken to be approximately Newtonian

$$\dot{\vec{v}}_{ec} \simeq \sum_i \frac{GM_i}{|\vec{r}_i|^3} \vec{r}_i \tag{B.8}$$

which is sufficiently accurate for the correction terms, then the integral takes the simple form*

$$(AT - t)_{diurnal} = -\vec{v}_{ec} \cdot \vec{x}_r \tag{B.9}$$

Before analyzing the approximations employed in deriving Equation (B.9), we consider the approximation involved in Equation (B.1). As can be seen from Reference 20, p. 221, Equation (9.2.3), the largest terms omitted from Equation (B.1) are smaller than the terms kept by $v^2 \sim 10^{-8}$. Since the expression in Equation (B.9) represents a near-sinusoid with amplitude of 1.5 μsec, the diurnal terms neglected in Equation (B.1) should have an effect on the order of 1.5×10^{-14} sec.

Turning to the approximations made in Equation (B.7), we see that the largest short-period (semi-diurnal) term neglected is contained in

$$\epsilon = \frac{3}{2} GM_i \frac{(\vec{r}_i \cdot \vec{x}_r)^2}{|\vec{r}_i|^5} \tag{B.10}$$

*This result was observed independently by Thomas (Reference 19).

If we expand, integrate and evaluate using $GM_{\odot} \sim 5 \times 10^{-6}$ sec, $|\vec{r}_i| \sim 5 \times 10^{2}$ sec, $|\vec{x}_r| \sim 2 \times 10^{-2}$ sec, the amplitude of the semi-diurnal term is seen to be 7×10^{-14} sec, so Equation (B.9) should be accurate to a fraction of a picosecond.

There is another assumption hidden in Equation (B.9). We have considered the gravity field of all the bodies in the solar system external to the Earth. To be more accurate, the gravitational potential of Equation (B.7) should have contained a term of the form

$$\phi_{\oplus} = -\frac{GM_{\oplus}}{|\vec{x}_r|} \tag{B.11}$$

For a rigid, spherical Earth, this term can be neglected as it is constant. However, the Earth tides cause an effect of the order of

$$\Delta|\vec{x}_r| \sim 30 \text{ cm} \sim 10^{-9} \text{ sec} \tag{B.12}$$

and thus a variation in potential of magnitude

$$\Delta\phi = \frac{GM_{\oplus}}{|\vec{x}_r|^2} \Delta|\vec{x}_r| \sim 4 \times 10^{-17} \tag{B.13}$$

which is of the same order as the error represented by Equation (B.10).

Another question which needs to be considered is the effect of the non-sphericity of the Earth. This introduces a position-dependent variation in the Earth's potential, which, because it is constant on a short time scale ($<< 10^6$ years) will not be treated further here.

B.2.4 Integration of the Non-diurnal Terms

The terms of Equation (B.1) which are neither diurnal, semidiurnal, nor constant are

$$(AT - t)_{\text{non-diurnal}} = \int [- \frac{v_{ec}^2}{2} - \sum_i \frac{GM_i}{|\vec{r}_i|}]dt \qquad (B.14)$$

There is, at present, no known simple expression for this integral for the general case of N gravitating bodies. There are, however, some interesting and useful special cases which can be handled. For the two-body, Earth-Sun case (Figure B.2)

$$AT - t = \int [- \frac{v_{ec}^2}{2} - \frac{GM_\oplus}{|\vec{r}_\odot|}]dt \qquad (B.15)$$

With the diurnal result in mind, we seek a solution of the form:

$$AT - t = P_1 \vec{v}_{ec} \cdot \vec{x}_{ec} \qquad (B.16)$$

where P_1 is a constant to be determined. If we differentiate Equation (B.16)

$$\frac{d}{dt}(AT - t) = P_1 v_{ec}^2 + P_1 \vec{x}_{ec} \cdot \dot{\vec{v}}_{ec} \tag{B.17}$$

and again take the Newtonian laws of motion [Equation (B.8)]

$$\frac{d}{dt}(AT - t) = P_1 v_{ec}^2 + P_1 \vec{x}_{ec} \cdot \frac{GM_\odot}{|\vec{v}_\odot|^3} \vec{r}_\odot \tag{B.18}$$

and since

$$\vec{x}_{ec} = - \frac{M_\odot}{M_\oplus + M_\odot} \vec{r}_\odot = -K\vec{r}_\odot \tag{B.19}$$

we find

$$\frac{d}{dt}(AT - t) = P_1 v_{ec}^2 - P_1 K \frac{GM_\odot}{|\vec{r}_\odot|} \tag{B.20}$$

Now for the case of a two-body orbit, Newtonian conservation of energy requires

$$\frac{M_\odot M_\oplus}{M_\odot + M_\oplus} \left(\frac{\dot{r}_\odot^2}{2} - \frac{G(M_\odot + M_\oplus)}{|\vec{r}_\odot|} \right) = E_t \tag{B.21}$$

or

$$\frac{v_{ec}^2}{2K^2} - \frac{G(M_\odot + M_\oplus)}{|r_\odot|} = E_t' \tag{B.22}$$

Where E_t and E_t' are constant. Combining Equations (B.20) and (B.22)

$$\frac{d}{dt}(AT - t) + P_2 E_t' = P_1 v_{ec}^2 - P_1 K \frac{GM_\odot}{|r_\odot|} + \frac{P_2 v_{ec}^2}{2K^2} - \frac{P_2 G(M_\odot + M_\oplus)}{|r_\odot|}$$

$$= (P_1 + \frac{P_2}{2K^2}) v_{ec}^2 + [-P_1 K M_\odot - P_2(M_\odot + M_\oplus)] \frac{G}{|r_\odot|} \tag{B.23}$$

Now by equating the coefficients of the v_{ec}^2 and the $\frac{G}{|r_\odot|}$ terms with the respective coefficients of the integrand of Equation (B.15), we are able to determine P_1.

$$P_1 = - \frac{2M_\odot + M_\oplus}{M_\odot} \tag{B.24}$$

and thus

$$(AT - t)_{\text{two body}} = - \frac{2M_\odot + M_\oplus}{M_\odot} \vec{v}_{ec} \cdot \vec{x}_{ec} - \int P_2 E_t' \, dt \tag{B.25}$$

and since we have defined t in such a way as to eliminate linear terms like the second term on the right-hand side

$$(AT - t)_{\text{two body}} = -K_{\odot\,\oplus}\,\vec{v}_{ec} \cdot \vec{x}_{ec} \tag{B.26}$$

with

$$K_{\odot\,\oplus} = \frac{2M_{\odot} + M_{\oplus}}{M_{\odot}} = (1 + \frac{1}{K}) \tag{B.27}$$

Another interesting case which we can try to handle is the Earth-Moon-Sun system. The geometry of the situation suggests that we resolve the problem into two two-body problems and perhaps a cross-term. We write Equation (B.1) as (see Figure B.3)

$$(AT - t)_{e\text{-}m\text{-}s} = \int[-\frac{GM_{\odot}}{|\vec{r}_{\odot} - \vec{x}'_{ec}|} - \frac{GM_{\leftmoon}}{|\vec{r}_{\leftmoon}|}$$

$$- \frac{(\dot{x}_{emb} + \dot{x}'_{ec})^2}{2}]dt \tag{B.28}$$

If we break up the first potential term as before, and expand the velocity term, we arrive at

$$AT - t = \int[-\frac{GM_{\odot}}{|\vec{r}_{\odot}|} - \frac{(\dot{x}_{emb})^2}{2}]dt$$

$$+ \int[-\frac{GM}{|\vec{r}|} - \frac{(\dot{x}'_{ec})^2}{2}]dt + \int[-\frac{GM_{\odot}}{|\vec{r}_{\odot}|^3}\,\vec{r}_{\odot}\cdot\vec{x}'_{ec}$$

$$- \dot{\vec{x}}_{emb} \cdot \dot{\vec{x}}'_{ec}]dt \tag{B.29}$$

The third term has exactly the form of the diurnal problem [Equation (B.8)], and has a solution $-\dot{\vec{x}}_{emb} \cdot \vec{x}'_{ec}$. The first and second terms have the form of the problem in Equation (B.15). The solution to Equation (B.15), however, cannot be directly applied in this case because the conservation of energy equation [Equation (B.21)] doesn't apply to a three-body situation. That is to say, the energy interactions are too complicated to be expressed in simple closed form as in Equation (B.21). However, we can ignore this problem and treat the Moon's orbit and the Earth-Moon barycenter orbit as though they were separate two-body orbits, and then estimate the error introduced by neglecting the energy interaction. We then arrive at

$$(AT - t)_{e\text{-}m\text{-}s} = -\dot{\vec{x}}_{emb} \cdot \vec{x}_{emb} \cdot K_{\odot\oplus} - \dot{\vec{x}}'_{ec} \cdot \vec{x}'_{ec} \cdot K_{\odot\oplus} - \dot{\vec{x}}_{emb} \cdot \vec{x}'_{ec} \qquad \text{(B.30)}$$

We will consider the errors in this expression term by term. The error in the third term [See Equation (B.9)] has an amplitude of 2.7×10^{-12} sec. The error in the second term is associated with the

assumption of constant energy for the Earth-Moon orbit. However, the amplitude of this term is only about 3.6×10^{-11} seconds. An error in this term of less than ten percent will be less than the error in the third term, and thus we can neglect errors in term 2. In order to estimate the errors in the first term, we need to estimate the energy interaction between the Earth/Moon system and the Earth-Moon-barycenter/Sun system. If we calculate the magnitude of the quadrupole component of the potential of the Earth-Moon system at the position of the Sun, and compare it with the monopole component of the potential, we find that the quadrupole term is smaller by a factor of 10^7. This would indicate that errors in the first term of Equation (B.25) caused by the quadrupole interaction of the Earth-Moon system are of the order of 3×10^{-10} sec. However, in order to use Equation (B.25) for a clock on the real Earth, some attention must be paid to the perturbations of the Earth's orbit by other planets. According to I. I. Shapiro (private communication, 1973), studies by numerical integration indicate that the short term variations in the energy of the Earth's orbit are no more than a part in 10^5. This would indicate that the first term in Equation (B.25) is accurate to only 3×10^{-9} sec.

B.3 CONCLUSION

If we collect the terms of Equations (B.9) and (B.29), we arrive at

$$(AT - t)_{periodic} = -\dot{\vec{x}}_{emb} \cdot \vec{x}_{emb} \cdot K_{\odot\oplus} - \dot{\vec{x}}'_{ec} \cdot \vec{x}'_{ec} \cdot K_{\oplus)} - \dot{\vec{x}}_{emb} \cdot \vec{x}'_{ec} - \vec{v}_{ec} \cdot \vec{x}_r \qquad \text{(B.30)}$$

The first term, an annual sinusoid, should be accurate to 3×10^{-9} sec. The second and third terms, monthly sinusoids, should be accurate to 3×10^{-12} sec. The fourth term, a diurnal sinusoid, should be accurate to 2×10^{-13} sec.

It may well be asked why there is any use in having error limits on the short-period terms which are orders of magnitude smaller than the errors in the longer period terms. The answer is that for some types of observations, smaller error limits are needed only for the shorter period terms. In VLBI work, for example, everything but the longitude-dependent diurnal term cancels out of the observations to very high accuracy.

It is hoped that Equation (B.30) will be of some use in processing various types of astronomical observations.

APPENDIX C

ORGANIZATION AND PRESENTATION OF RESULTS

The results quoted in this thesis represent the quintessence of the results from a very large number of computer runs. Ideally, the entire print-out from each run should be included in this thesis, so that interested readers would be able to investigate such things as what combination of clock and atmosphere parameters were employed and what the parameter correlation matrix looked like. Unfortunately the sheer volume of this print-out (several thousand pages) precludes its being included in this thesis. In order to make this information as available as possible, the computer print-outs are being kept on file at the Haystack Observatory, and the results reported here are catalogued so as to unambiguously identify the computer run which produced each result. Each computer run is assigned a unique run code which identifies it by date and sequence number. Thus, for example, number 75095-32 is the run code for the 32nd run processed on the 95th day of 1975 (April 5).

The baseline results reported in this thesis are summarized in Table 4. The first entry in each line of these tables is the run code, as explained above. The next entry further identifies the run by giving the date of the first observations in the data set. The next entry identifies the baseline according to the following codes:

H - Haystack (Tyngsboro, Mass.)

G - Goldstone (Mohave, California)

N - NRAO (Green Bank, W. Virginia)

S - Onsala (Sweden)

A - Alaska (Gilmore Creek, Alaska)

The next entry in each line is the baseline component, in centimeters. This value is followed by the difference of that baseline component value from the weighted mean value (see below), and finally by the formal standard error (sigma) for that component from that particular run. The bottom line of each section of the table gives the weighted mean and standard deviation of the solutions tabulated above, where the weighted mean is defined as

$$M = (\sum_i P_i/w_i^2)/\sum_i (1/w_i^2)$$

and the standard deviation* is defined as

$$S = [(\sum_i D_i^2/w_i^2)/\sum_i (1/w_i^2)]^{1/2}$$

where P_i is the estimated value of the parameter being displayed, w_i is the formal error for that estimate, and

$$D_i = P_i - M$$

This last line, of course, does not list a run code or date. One final note -- it is possible to display in this table a value which one does not wish included in the weighted mean value, either because it is not independent of the other results, or because something else is wrong with the result. The asterisks

---

*The standard deviation of the mean is smaller by a factor of the square root of the number of independent measurements, of course.

on the far right-hand side of the table indicate which values have been included in the weighted mean.

The source coordinate results reported in this thesis are summarized in Table 5. The entries in this table parallel the entries in the baseline table. The values for right ascension are given in hours, minutes, and seconds of time, and the differences and formal errors are given in seconds of time. The values for declination are given in degrees, minutes, and seconds of arc, and the differences and formal errors are given in seconds of arc.

In addition to the solution values, the residuals from some of these computer runs are plotted in Figures 3 to 23. The heading at the top of each figure gives the baseline according to the above codes. The heading then gives the type of residual (delay or delay rate) being plotted, and the horizontal scale units (nanoseconds for delay, picoseconds per second for delay rates). Finally, the heading gives the date and run code. The plots show the delays or rates on the horizontal axis. The vertical direction is the time of the observation, in days starting with 0:00 UTC on the date of the first observation in the data set. Individual observations are plotted with letters, the letters indicating the source under observation according to the following code:

a = 7* = 3C84

b = 9 = NRAO140

c = 10 = CTA26

d = 11 = NRAO150

e = 14 = 3C120

f = 27 = OJ287

g = 28 = 4C39.25

h = 29 = OK290

j = 33 = 3C273B

k = 34 = 3C274

l = 35 = 3C275

m = 36 = OQ208

n = 41 = CTD93

o = 43 = 3C345

p = 53 = OV080

p = 56 = 3C418

r = 59 = 2134+00

s = 60 = Ox161

t = 63 = VR422201 (= BL LAC)

u = 66 = CTA102

v = 67 = 3C454.3

w = 74 = OR103

x = 75 = NRAO512

y = 77 = 3C390.3

z = 78 = 2048+31

α = 79 = OH471

β = 80 = OQ172

γ = 81 = 4C11.50

δ = 82 = CTD135

ε = 83 = 2344+09A

ζ = 84 = 2344+09B

In addition, data points which have been edited out of the solution (see Chapter 4) are indicated by a single dot, and points which are off scale are indicated by a ⊙ symbol at the edge of the plot. (Note: many of these sources were not observed, and some were observed only a very few times.)

---

*The numbers in this column are sequence numbers in our computerized tables of source coordinates.

REFERENCES

1. Ash, M. E., Determination of Earth Satellite Orbits, M.I.T. Lincoln Lab Tech. Note 1972-5 (1972).

2. Chao, C. C., A Preliminary Estimation of Tropospheric Influence on the Range and Range Rate Data During the Closest Approach of the MM71 Mars Mission, JPL Tech. Memo. 391-129 (1970).

3. Counselman, C. C., Kent, S. M., Knight, C. A., Shapiro, I. I., Clark, T. A., Hinteregger, H. F., Rogers, A. E. E., and Whitney, A. R., Phys. Rev. Letts. 33, 1621 (1974).

4. Explanatory Supplement to the Astronomical Ephemeris and the American Ephemeris and Nautical Almanac, H.M. Nautical Almanac Office (1961).

5. Hinteregger, H. F., Ph.D. Thesis, M.I.T. (1972).

6. Hinteregger, H. F., Shapiro, I. I., Robertson, D. S., Knight, C. A., Ergas, R. A., Whitney, A. R., Rogers, A. E. E., Moran, J. M., Clark, T. A., and Burke, B. F., Science 178, 396 (1972).

7. Knight, C. A., Ph.D. Thesis, M.I.T. (in preparation)

8. McClure, P., Diurnal Polar Motion, Goddard Space Flight Center, X-592-73-259 (1973).

9. Melchior, P., The Earth Tides, Pergamon Press (1966).

10. Preston, R. A., Ph.D. Thesis, M.I.T. (1972).

11. Ong, K. M., MacDoran, P. F., Thomas, J. B., Fliegel, H. F., Skjerve, L. J., Spitzmesser, D. J., Batelaan, P. D., Paine, S. T., and Newsted, M. G., in The Deep Space Network Progress Report 42-26, Jet Propulsion Laboratory (1975).

12. Rogers, A. E. E., private communication.

13. Rogers, A. E. E., Counselman, C. C., Hinteregger, H. F., Knight, C. A., Robertson, D. S., Shapiro, I. I., Whitney, A. R., and Clark, T. A., Ap. J. 186, 801 (1973).

14. Shapiro, I. I., private communication.

15. Shapiro, I. I., The Prediction of Ballistic Missile Trajectories from Radar Observations, McGraw-Hill (1958).

16. Shapiro, I. I., Hinteregger, H. F., Knight, C. A., Punsky, J. J., Robertson, D. S., Rogers, A. E. E., Whitney, A. R., Clark, T. A., Marandino, G. E., Goldstein, R. M., and Spitzmesser, D. J., Ap. J. 183, L47 (1973).

17. Shapiro, I. I. and Knight, C. A., in Earthquake Displacement Fields and the Rotation of the Earth, Reidel (1970), p. 285.

18. Shapiro, I. I., Robertson, D. S., Knight, C. A., Counselman, C. C., Rogers, A. E. E., Hinteregger, H. F., Lippincott, S., Whitney, A. R., Clark, T. A., Niell, A. E. and Spitzmesser, D. J., Science 186, 920 (1974).

19. Thomas, J. B., Astronomical Journal 80, 405 (1975).

20. Weinberg, S., Gravitational and Cosmology, Principles and Applications of the General Theory of Relativity, John Wiley and Sons (1972).

21. Whitney, A. R., Ph.D. Thesis, M.I.T. (1974).

22. Whitney, A. R., Rogers, A. E. E., Knight, C. A., Hinteregger, H. F., Lippincott, S., Levine, J. L., Clark, T. A., Shapiro, I. I. and Robertson, D. S., in preparation.

23. Wittels, J. J., Ph.D. Thesis, M.I.T. (1975).

24. Woolard, E. W., and Clemence, G. M., Spherical Astronomy, Academic Press (1966).

BIOGRAPHICAL NOTE

Douglas Scott Robertson was born in [redacted], [redacted] on [redacted] He attended schools in Cincinnati, Ohio and St. Louis, Missouri, and received a Bachelor of Science degree in Physics with honors from Principia College (1968). Studies for his doctorate at M.I.T. have been with the Department of Earth and Planetary Sciences. Mr. Robertson's primary interests have been in the fields of geology, astrometry and geophysics. He is a member of Sigma Xi.

Mr. Robertson married Joan [redacted] in May, 1972. In [redacted] his daughter, Carolyn, was born.

Among his major interests are scuba diving, skiing and photography.